NOAA OAR Special Report

PMEL Tsunami Forecast Series: Vol. 64
A Tsunami Forecast Model for Key West, Florida

(Draft)

Liujuan Tang
Christopher Moore

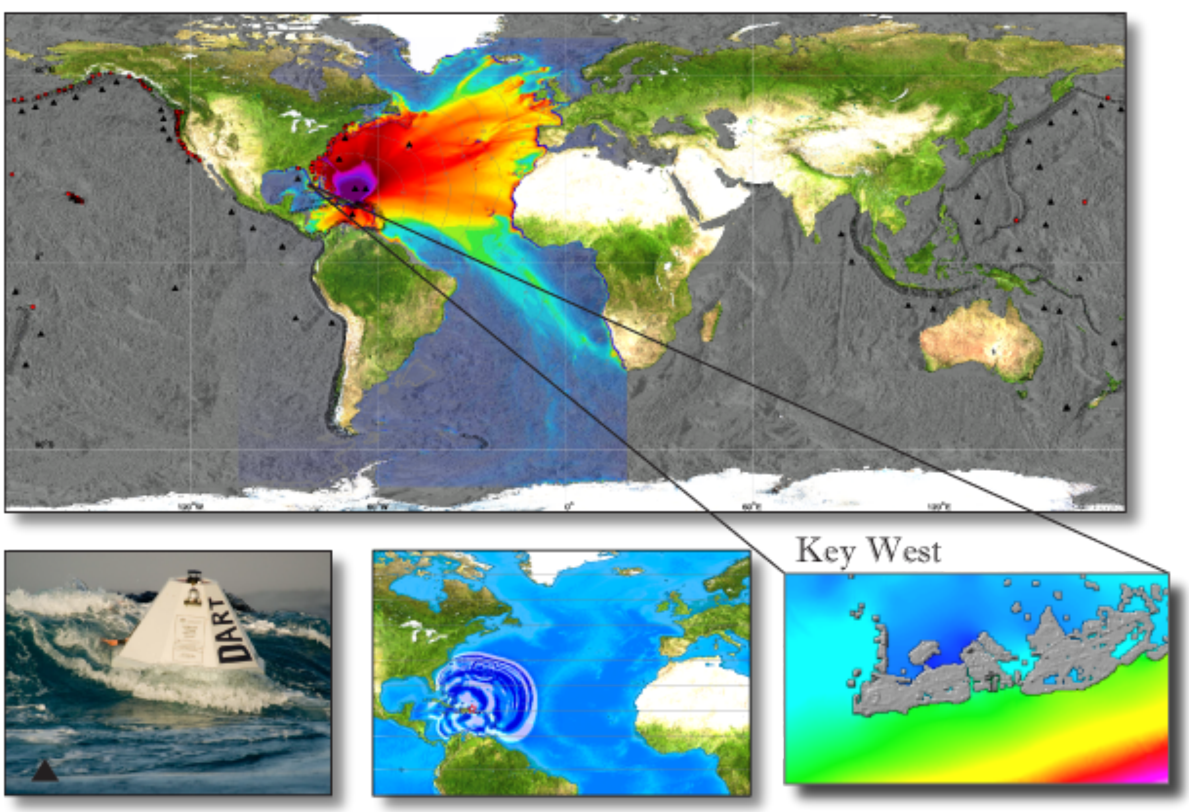

April 2014

NOAA Center for Tsunami Research (NCTR)
Pacific Marine Environmental Laboratory

Contents

List of Tables

PMEL Tsunami Forecast Series: Vol. 64
A Tsunami Forecast Model for Key West, Florida

Liujuan Tang and Christopher Moore

Abstract

This report documents the development and testing of a tsunami forecast model for Key West, Florida. Based on the Method of Splitting Tsunami (MOST) model, the forecast model is capable of simulating four hours of tsunami wave dynamics at a resolution of 3 arc sec in minutes of computational time. A higher resolution reference inundation model of 1/3 arc sec was developed in parallel to provide modeling references for the forecast model. Both models were tested for nine simulated mega-tsunami events with a magnitude (Mw) of 9.3. The modeled amplitude, current, and inundation limits agree well between the forecast and reference models.

The study shows that a mega-tsunami originating from the Gulf of Honduras can cause severe inundation at Key West. The shallow Great Bahama Bank can protect Key West from tsunamis approaching from the east. Large waves can arrive 12–22 hours after the first wave for far-field tsunamis, which may require longer warning duration for such events. Wavelet analyses show relatively long resonant periods from 66 to 256 minutes at the site. The modeled current at the shallow depth and inundation on the flat area can be sensitive to the Manning friction coefficient for large tsunamis, and as a result of this sensitivity, inundation extents may be subject to uncertainty in low-lying flat areas near the coast.

The southern coast of Key West can experience waves 3-4 times larger than those at the northern coast. The simulated Mw 9.3 tsunamis show an impressive local variability of tsunami amplitudes at Key West, and indicate the complexity of forecasting tsunami amplitudes at a coastal location. It is essential to use high-resolution models to provide the accuracy useful for coastal tsunami forecasts and practical guidance.

1 Introduction

The National Oceanic and Atmospheric Administration (NOAA) Center for Tsunami Research (NCTR), located at NOAA's Pacific Marine Environmental Laboratory (PMEL), has developed a tsunami forecasting system for operational use by NOAA's two Tsunami Warning Centers located in Hawaii and Alaska (Titov *et al.*, 2005; Titov, 2009). The forecast system combines real-time deep-ocean tsunami measurements from tsunameters (González *et al*., 2005; Meinig *et al*., 2005, Bernard *et al.*, 2006; Bernard and Titov, 2007) and the Method of Splitting Tsunami (MOST) model, a suite of finite difference numerical codes based on the nonlinear shallow water wave equations (Titov and Synolakis, 1998; Titov and González, 1997; Synolakis *et al*., 2008; Titov *et al*., 2011) to produce real-time forecasts of tsunami arrival time, heights, periods, and inundation. To achieve accurate and detailed forecasts of tsunami impact for specific sites, high-resolution tsunami forecast models are under development for U.S. coastal communities at risk (Tang *et al.*, 2008a, 2009, 2010; Arcas and Uslu, 2010; Righi and Arcas, 2010; Uslu *et al*., 2010; Wei and Arcas, 2010). The resolution of these models has to be high enough to resolve the dynamics of a tsunami inside a particular harbor, including influences of major harbor structures such as breakwaters and seawalls. These models have been integrated as crucial components into the tsunami forecast system.

As of March 2013, the forecast system real-time measurements come from a network of 62 tsunameter stations deployed at optimal locations in the Pacific, Atlantic, and Indian oceans, the Caribbean Sea, the Gulf of Mexico, and the South China Sea (e.g., Spillane *et al*., 2008). While the buoy array is owned and maintained by nine different nations (the U.S., Australia, Chile, China, Japan, India, Indonesia, Thailand, and Russia), the data from the entire array are made publicly available in real time via the Global Telecommunications System. The data from the tsunameters are used to provide guidance by comparing them to pre-computed open ocean model results. These pre-computed propagation models currently cover all three ocean basins (Pacific, Atlantic, and Indian), and are comprised of 1725 different tsunami scenarios with initial deformations covering the major tsunamigenic subduction zones throughout the world (Figure 1; Table 1). The fully implemented system uses real-time data from the tsunameter network to provide high-resolution tsunami forecasts for 75 U.S. coastal communities (e.g., Figure 1), with additional models envisioned for smaller communities in the future. Since its first testing in the 17 November 2003 Rat Island tsunami, the forecast system has produced experimental real-time forecasts for more than 20 tsunamis in the Pacific and Indian oceans (Titov *et al*., 2005; Wei *et al*., 2008; Titov, 2009; Titov and Tang, 2011; Tang *et al*., 2012; http://nctr.pmel.noaa.gov/database_devel.html). The forecast method has also been tested with data from nine additional events, including several near-field tsunamis, that produced deep-ocean tsunameter data (http://nctr.pmel.noaa.gov/database_devel.html; Titov *et a*l., 2005; Tang *et al*., 2008b; Wei *et al*., 2013).

This report describes the development and testing of the Key West forecast model. In 2012, NCTR developed the first version of a Key West forecast model, which was incorporated into the tsunami forecast system. The first version of the model grid was developed by Paul Chamberlain. As new bathymetric/topographic and tsunami data were obtained and the model development technique progressed further, the model was updated and re-tested here. The primary objective in developing this model is to provide NOAA's Tsunami Warning Centers the ability to assess danger posed to Key West following tsunami generation in the Atlantic Ocean Basin with a goal to provide accurate and timely forecasts that will enable the community to respond appropriately. A secondary objective of the report is to explore the potential tsunami impact from earthquakes at major subduction zones in the Atlantic Ocean to the city by using the developed forecast model. Wavelet analysis was applied to investigate the local responses to tsunami waves.

The report is organized as follows. Section 2 briefly introduces NOAA's tsunami forecast method. Section 3 describes the model development. Section 4 presents the results and discussion, which includes a study of the model's sensitivity to the friction coefficient, model validation, and testing for simulated tsunamis. A summary and conclusion are provided in Section 5.

2 Forecast Method

NOAA's real-time tsunami forecasting scheme is a process that comprises two steps: (1) construction of a propagation scenario via inversion of deep-ocean tsunameter measurements with pre-computed tsunami source functions; and (2) development of coastal predictions by running high-resolution forecast models in real time (Titov *et al*., 1999, 2005; Titov, 2009; Tang *et al*., 2009, 2012). The tsunameter-constrained tsunami source, the corresponding offshore scenario from the tsunami source function database, and high-resolution forecast models cover the entire evolution of earthquake-induced tsunamis, generation, propagation, and coastal inundation, providing a complete tsunami forecast capability.

2.1 Construction of a propagation scenario based on deep-ocean tsunameter measurements and pre-computed tsunami source functions

Several real-time data sources, including seismic, coastal tide gauge, and deep-ocean data have been used for tsunami warning and forecasting (Satake *et al*., 2008; Whitmore, 2003; Titov, 2009). NOAA's strategy for real-time forecasting of tsunamis is to use deep-ocean measurements at tsunameter stations, also known as DART (Deep-ocean Assessment and Reporting of Tsunami) buoys, as the primary data source. The DART buoys offer several key advantages: (1) unlike seismic data, which are an indirect measure of tsunamis, tsunameters provide a direct measure of tsunami waves; (2) deep ocean tsunami measurements are, in general, the earliest tsunami information available because tsunamis propagate much faster in deep ocean than in shallow coastal areas where coastal tide gauges are located; (3) compared to coastal tide gauges, tsunameter data, with a high signal-to-noise ratio, can be obtained without interference from harbor and local shelf effects; and (4) wave dynamics of tsunami propagation in deep water is assumed to be linear (Kânoğlu and Synolakis, 2006; Liu, 2009). This linear process allows application of efficient inversion schemes.

Time series of tsunami observations in deep water (depths << wave length) can be decomposed into a linear combination of a set of tsunami source functions in the time domain by a linear least squares method (Percival *et al*., 2011). The coefficients obtained through this inversion process are called *tsunami source coefficients*. During real-time tsunami forecasting, seismic waves propagate much faster than tsunami waves so the initial seismic magnitude can be estimated before the tsunameter data are available. Since time is of the essence, this initial tsunami forecast is based on the seismic magnitude only. An updated forecast will be made via the inversion method when tsunameter data are available.

Titov *et al*. (1999, 2001) conducted sensitivity studies on far-field, deep-water tsunamis with different parameters of an elastic deformation model described in Gusiakov (1978) and Okada (1985). The results showed source magnitude and location essentially define far-field tsunami signals for a wide range of subduction zone earthquakes. Other parameters have a secondary influence and can be predefined during the forecast. Based on these results, tsunami source function databases for the Pacific, Atlantic, and Indian oceans have been built using the following predefined source parameters: length = 100 km, width = 50 km, slip = 1 m, rake = 90 or -90, and rigidity = 4.5×10^{10} N/m^2. The other parameters (strike, dip, and depth) are location-specific and are based on the subduction zone source. Details of the propagation database are described in Gica *et al*. (2008). Each tsunami source function models a tsunami generated by a typical Mw 7.5 earthquake with predefined source parameters mentioned above. Figure 1 shows the locations of tsunami source functions. Figure 2 shows the maximum amplitudes at Key West offshore from the tsunami source functions in the Atlantic Ocean.

The tsunami source functions in the database are computed with a time step of 10 sec and a spatial resolution of 4 arc min (approximately 7.4 km along the north–south direction). The output (offshore wave height and depth-averaged velocities of the entire domain) are then compressed and saved every 1 min in time and 16 arc min in space (Tolkova, 2007). As inundation is calculated by the high-resolution forecast models, the propagation scenarios do not include inundation, a reflection boundary condition is enforced at 20 m water depth (Gica *et al*., 2008), and friction is assumed to be negligible.

The percentage of energy released from an earthquake that is transferred into the water column during tsunami generation is difficult to accurately model using seismic methods. However, the goal of tsunameter inversion is not to quantify the energy at the initial stage of tsunami generation, but to quantify the amount of wave energy that propagates outside the source area in the form of surface long gravity waves, which can be well measured by the tsunameter stations. Since it is this propagating energy that results in impact at the coast, an estimation of the tsunami source (the propagation scenario) is made by directly measuring the deep-ocean tsunami data. Regardless of the details of earthquake processes for tsunami generation at the initial stage, the inversion can ensure that the propagation scenario gives the best approximation to the tsunami measurements, and, therefore, the best estimation of the total energy transferred to the tsunami waves. Once the inversion is complete, the database can provide immediate offshore forecasts of tsunami amplitudes and all other wave parameters. The tsunami source, constrained by real-time tsunami measurements, provides an accurate offshore tsunami scenario without additional time-consuming deep-water model runs.

When tsunami waves propagate into shallow water, the steady-state assumption requires no net energy losses or gains. The decrease in transport speed must be offset with an increase in energy density in order to maintain a constant energy flux. The low spatial resolution and simplified boundary conditions of the propagation model result in inaccuracies in nearshore dynamics. As a consequence, the numerical dissipation (due to low spatial resolution) will cause energy decay in the propagation modeling (Tang *et al*., 2012). For the purpose of energy conservation, high-resolution, site-specific inundation forecast models were developed using MOST to more accurately simulate nearshore wave dynamics.

2.2 Coastal predictions by using high-resolution forecast models in real time

High-resolution forecast models are designed for the final stage of tsunami wave evolution: coastal runup and inundation. Once the tsunameter-constrained tsunami source is obtained (as a linear combination of tsunami source functions), the pre-computed time series of offshore wave height and depth-averaged velocity from the model propagation scenario are applied as the dynamic boundary conditions for the forecast models. This saves the simulation time of basin-wide tsunami propagation. Tsunami inundation and nearshore currents are highly nonlinear processes; therefore, a linear combination would not provide an accurate solution. A high-resolution model is also required to resolve shorter tsunami wavelengths nearshore with accurate bathymetric/topographic data. Using the MOST model, the forecast models each contain three telescoping computational grids with increasing resolution, covering regional, intermediate, and nearshore areas. Runup and inundation are computed at the coastline. The highest resolution grid includes the population center and coastal water-level stations for forecast verification. The grids are derived from the best available bathymetric/topographic data at the time of development, and will be updated as new survey data become available.

The forecast models are optimized for speed and accuracy. By reducing the computational areas and grid resolutions, each model is optimized to provide 4-hr event forecasting results in a maximum of 10 min of computational time using a single processor, while still providing enough accuracy for forecasting. To ensure forecast accuracy at every step of the process, the model output is validated with historical tsunami records when available and compared to numerical results from the original full-resolution, full-extent “reference” inundation model. In order to provide warning guidance for the duration of a tsunami event, each forecast model has been developed to provide simulation output for up to 24 hr (30 hr for Atlantic sites) from the time of tsunami generation.

3 Model Development

3.1 Forecast area

Key West is located at the southernmost tip of an archipelago of lowland islands in southern Florida, known as the Keys (Figure 4). The Keys are a chain of oolite and limestone islands formed during the last ice age when sea levels dropped and fossilized ancient coral reefs. Key West is located ~ 208 km (129 mi) southwest of Miami and is the southernmost point of the continental U.S.

Known as the Gibraltar of the West, Key West has always held a strategic interest for the U.S. The U.S. Military maintains a strong presence there, currently occupying 3000 acres, including a Naval Air Station, Coast Guard facilities, and surface warship piers. Historically specializing in fishing and wreck salvaging, Key West has long been one of the most prosperous cities in Florida. Its relative isolation, ideal climate, and setting have fostered a unique culture. Tourism continues to be a vitally important part of the Key West economy. In 2011 alone, over 1.2 million tourists visited Key West, and $1.1 billion in U.S. dollars were spent on tourism and recreation (http://www.keywestchamber.org/PDF/trends.PDF). The city of Key West is the county seat of Monroe County and encompasses the island of Key West, a portion of Stock Island, Sigsbee Park, Fleming Key, and Sunset Key. The city comprises a total area of 11.9 sq km (7.4 sq mi), of which 75% is land, approximately half of which lies at a maximum elevation of ~5.5 m (18 ft). The 2010 Census reported a resident population of 24,649, with 8925 households in the town (http://quickfacts.census.gov/qfd/states/12/1236550.html).

Figure 5 shows area photos of Key West. The deepest charted depths in the approaches to Key West are 194 m. The continental shelf extends east 5–8 km offshore. NOAA's National Ocean Service (NOS) has operated a tide gauge (station ID 8724580) at Key West since January 1913. The tide gauge is located on the concrete sea wall near the north property line of the Naval Air Station (at 24.5549°N, 278.1914°E). The mean tidal range is 0.390 m. Mean high water (MHW) is 1.853 m above station datum. Water depth at the tide station, according to the source bathymetry grid (Grothe *et al.*, 2011), is approximately 11.5 m below MHW.

Figure 3 shows historical tsunamis in the Caribbean Sea and the Atlantic Ocean, as documented in the National Geophysical Data Center (NGDC) database. Although no tsunami runup data were found for Key West in the NGDC database, its low-lying coastal area, high coastal population density, and potential tsunami hazard from Caribbean Sea subduction zone earthquakes necessitate a Key West forecast model to aid the community in site-specific evacuation decisions.

3.2 Bathymetry and topography

In September of 2011, the NGDC developed a 1/3 arc sec digital elevation model (DEM) covering the Key West region (Grothe *et al.*, 2011). At the latitude of Key West, (24°33'19"N, 81°46'58"W) 1/3 arc sec of latitude is equal to 10.25 m, and 1/3 arc sec of longitude is equal to 9.38 m. The details of the DEM development can be found in Grothe *et al*. (2011).

The DEM were generated from diverse digital datasets in the region (sources shown in Figure 6) and were designed to represent modern morphology. The digital data were obtained from several U.S. federal, state, and local agencies, including:

(1) Bathymetry data from

- NOS hydrographic survey data (1852–2003)
- NGDC multibeam swath sonar surveys (1995–2004)
- NOAA's Office of Coast Survey Electronic Navigational Charts soundings (2002–2008)
- U.S. Army Corps of Engineers (USACE) hydrographic channel/harbor surveys (2009)

(2) Topography datasets from:

- South Florida Water Management District bare-earth lidar DEM with 3 m spatial resolution (2007–2008)
- U.S. Geological Survey 2009 National Elevation Dataset 1/3 arc sec data.

All datasets were shifted to the World Geodetic System 1984 (WGS84) horizontal datum and transferred to NAVD 88MHW vertical datum. The MHW DEM was created by adding a "NAVD 88 to MHW" conversion grid to the NAVD 88 DEM.

The grid generator at NCTR's Atlas (http://nctr.pmel.noaa.gov/education/science/modeling.html) was used to generate a 6 arc sec DEM covering the Straits of Florida, Great Bahama Bank, and Cuba. Data sources include:

- Key West VA 1/3″
- Palm Beach 1/3″
- U.S. Virgin Islands 1″
- Gulf Coast/Caribbean 9″
- Atlantic Test 1′ (ETOPO1 from NGDC)

The bathymetry and topography of Key West used in the development of this forecast model were based on the 1/3 arc sec DEM provided by the NGDC.As new DEMs become available, the forecast model will be updated and report updates will be posted at http://nctr.pmel.noaa.gov/forecast_reports/.

3.3 Model setup

By sub-sampling the DEMs described in Section 3.2, two sets of computational grids were derived for Key West: the reference inundation model and the optimized forecast model.

The reference grids consist of three levels of telescoping grids with increasing resolution (Figure 7). The A grid covers the Straits of Florida and Bahamas in 30 arc sec. The B grid covers Key West and its offshore area in 6 arc sec. Runup and inundation simulations are computed at the coastline in the C grid at 1/3 arc sec.

To improve the computational speed for operational purpose, the forecast model must include fewer node numbers, while still providing accurate modeling. The Key West forecast model also has three levels of telescoping grids (Figure 8). Resolutions of 120 arc sec and 12 arc sec were used for the forecast model's A and B grids, respectively. Runup and inundation simulations are computed at the coastline in the forecast model's C grid at 3 arc sec. Figure 8c shows the Key West warning point (at 278.1914°E , 24.5549°N) in 11.5 m of water depth. Two synthetic tide gauges were placed at nearshore locations in the south and the north.

Grid details at each level and input parameters are summarized in Table 2. A vertical wall was placed at 0.5 m water depth for the A and B grids. Due to the shallow, wide Great Bahama Bank at the entrance of the Straits of Florida, a 0.5 m water depth was necessary to propagate the wave over the shallow areas.

All model runs were tested on a DELL PowerEdge R510 computer equipped with two Xeon E5670 processors at 2.93 Ghz, each with 12 MBytes of cache and 32 GB of memory. The processors are hex core and support hyperthreading, resulting in the computer performing as a 24 processor core machine. Additionally, the testing computer supports 10 Gigabit Ethernet for fast network connections. This computer configuration is similar to or the same as those installed at the Tsunami Warning Centers, so the compute times should only vary slightly. For a 4-hr event simulation, it takes eight processors 2 hr to produce the reference model, whereas a single processor can produce the forecast model in just 3 min.

4 Results and Discussion

4.1 Sensitivity of modeled sea surface elevation, current, and inundation to friction coefficients

Accurate simulation of tsunami-induced current, runup, and inundation requires high-resolution bathymetry and topography data in the runup area and good tsunami source and model parameters. Titov *et al*. (2005) have shown that, under these conditions, the MOST runup and inundation results agree quite well with the stereoscopic aerial photography and field survey data on Okushiri Island generated by the 12 July 1993 Hokkaido-Nansei-Oki Mw 7.8 earthquake. Wei *et al*. (2013) have also shown excellent agreements between the modeled near-field runup and inundation and the survey data for the 11 March 2011 Japan tsunami.

At present, one major difficulty is the lack of high-quality inundation/runup and current measurements to verify the accuracy of topography and to calibrate the Manning friction coefficient. In this section, we tested the Key West forecast model for a Mw 9.3 tsunami from the Gulf of Honduras (Scenario #7 in Table 3) with five different Manning coefficients (n = 0–0.04).

Figure 9 shows amplitude time series at the Key West tide gauge computed with the five different Manning coefficients. The maximum amplitude, η_{max} decreases from 1.2 m to 0.9 m, a 0.4 m (33%) difference, when the Manning coefficient n increases from 0.0 to 0.4. With n = 0.00, the model was self-terminated following the large wave around 4.5 hr due to instability. Figure 10 shows the maximum surface elevation in the A, B, and C grids, and the maximum current in the C grid with n = 0.01–0.04. In deep water (500 m or greater), friction has little effect on the maximum amplitude. However, at shallow depth (100 m or less), small roughness coefficients produce larger amplitude and current. This effect is more distinct at water depth less than 5 m. Figure 11 shows the inundations in the forecast C grid with four different Manning coefficients (n = 0.01–0.04). The black line indicates the zero contour line. Small roughness coefficients can produce greater inundation in flat areas.

The above results indicate friction does influence the results, and it is very difficult (if not impossible) to provide the friction coefficient that is "reasonable," or reflects reality. This is due to many factors beyond the roughness itself, such as the exact approximation of the shear stress of the flow and numerical approximation. The Manning formula used in the MOST model is an empirical engineering formulation. Use of any specific number cannot be validated in any real sense for tsunamis (and may be impossible to validate), so the choice of a specific coefficient for a specific site is somewhat arbitrary. The goal is to account for friction that is known and to improve the stability of the runs for a particular site. The best way to validate the friction is with observational data, but such data are rarely available, especially for inundation. For this application, the coefficient chosen is a conservative one.

For Key West, with large, very shallow areas in its A, B, and C grids, and the requirement of an offshore water depth of 0.5 m, the smallest possible friction value that produces consistent stable computations for all tested scenarios (n=0.03) is used. Due to the model's sensitivity to the Manning coefficient, inundation extents may be subject to uncertainty in low-lying flat areas near the coast.

It should be noted, for MOST version 4, that n can be set to different values for different grids. For example, a small n can be used for the A and B grids with a relatively large n for the C grid to stabilize the model for large runup/run-down.

4.2 Model validation and stability testing

Figures 2a and 2b show the maximum amplitudes at Key West offshore points west and east from the 214 scenarios in the propagation database. Each scenario represents a tsunami generated by a Mw 7.5 earthquake. The results indicate:

(1) The Great Bahama Bank may serve as a protective barrier for Key West from tsunamis propagating from the east. The unit sources along Dominica and Puerto Rico produce large amplitude waves at the offshore east point (Figure 2b). However, the amplitudes become very small after they propagate through the Great Bahama Bank and reach the offshore west point (Figure 2a).

(2) Tsunamis originating from the Gulf of Honduras can approach Key West from the west through the Yucatan Channel. Due to the relatively deep water along the path, the tsunami waves can reach Key West with less loss in energy.

A set of nine simulated Mw 9.3 tsunamis was selected here for further examination (Table 3). Each simulated earthquake involves 20 tsunami source functions (10 pairs) and a uniform 25 m coefficient. Both the Key West reference and forecast models were tested with the nine scenarios.

Figure 12 shows the amplitude (η) time series at the Key West tide gauge for the nine Mw 9.3 scenarios. Figure 13 show the result for a micro Mw 6.8 tsunami. Figure 14 shows the wavelet analysis of the time series. Table 3 summarizes the $\eta_{\max}$ and uncertainty due to model setup differences. The uncertainty is computed as:

$$uncertainty = \frac{|\eta_{\max 2} - \eta_{\max 1}|}{\eta_{\max 1}} \times 100$$

where $\eta_{\max1}$ and $\eta_{\max2}$ are the maximum water surface elevation computed by the reference and forecast models, respectively.

The forecast model shows good consistency in the time series with those of the reference model. The larger the η_{max}, the smaller the discrepancy (Figure 15a). The uncertainty in the largest η_{max} of 1.0 m at the Key West tide gauge computed by the forecast model is within 2%. The arrivals of the maximum amplitudes can be 12–22 hr after the first wave. The forecast model was tested for running up to 30 hr after the earthquake. Figure 13 shows the model is also stable for a micro-tsunami (about 0.03 mm in amplitude) generated by a Mw 6.8 earthquake at the South Sandwich Islands subduction zone.

Wavelet analyses were performed for the scenarios to explore peak resonant periods, T_P, at the Key West tide gauge. Figure 14 shows the amplitude spectrograms. The site shows relatively long and broad resonant periods from 66 to 256 min (Figure 15b). The most common peak period is near 140 min.

Figures 16 and 17 show the modeled amplitude time series at two virtual gauges, one at the south shore and the other at the north shore. The south shore point can experience waves up to 3–4 times greater than those at the north shore point. It should be noted that the wide, shallow coral reefs along the north shore play an important role in dissipating wave energy.

Figure 18 shows that both the reference and forecast models produce similar maximum water elevation, maximum current, and inundation limit in the study area. Large maximum currents can be seen in both the reference and forecast models for many of the scenarios, especially over shallow areas.

Tsunami waves in the study area vary significantly for the nine Mw 9.3 scenarios. The Gulf of Honduras scenario (#7 in Table 3), produces waves near 1 m at the Key West tide gauge. The inundations are significant. These results show the complexity and high nonlinearity of nearshore tsunami waves, which again demonstrate the value of a high-resolution forecast model for providing accurate site-specific forecast details.

5 Summary and Conclusions

A tsunami forecast model was developed for Key West, Florida. The computational grids for the Key West forecast model were derived from the best available bathymetric and topographic data sources. The forecast model is optimally constructed at 3 arc sec resolution, to enable a 4-hr inundation simulation within minutes of computational time using a single processor. A higher resolution reference inundation model of 1/3 arc sec was also developed in parallel, to provide modeling references for the forecast model. Both models were tested for a set of nine simulated Mw 9.3 tsunamis. The Key West tide gauge was chosen as the warning point for the site.

The modeled amplitude, inundation, and current are sensitive to the friction coefficient at shallow water depth. Due to the lack of data for calibration of the friction coefficient and the shallow offshore water depth of 0.5 m for Key West, the smallest possible friction value (n=0.03) that produces consistently stable computations for the forecast model is used.

The tsunami amplitude time series at the Key West tide gauge show excellent agreement between the forecast and reference models. The modeled inundation limits and currents agree reasonably well between the two models.

This study highlights that (a) a mega-tsunami from the Gulf of Honduras could cause several inundations at Key West; (b) the south shore is more susceptible to larger waves than the north shore; (c) the Great Bahama Bank may protect Key West from tsunamis propagating from the east; and (d) maximum waves can arrive 12–22 hours after the first wave, requiring longer periods of warning guidance for the duration of such events. The simulated Mw 9.3 tsunamis show an impressive local variability of tsunami amplitudes at Key West, demonstrating the complexity of forecasting tsunami amplitudes at a coastal location and the need to use high-resolution models in order to provide enough accuracy to be useful for coastal tsunami forecasts and practical guidance.

Acknowledgments

The authors thank Paul Chamberlain for developing the first version of the Key West grid; Vasily V. Titov for discussion; Hongqiang Zhou for comments; Jean C. Newman for assistance and preparing the cover image; Lindsey Wright for SIFT testing; David. R. Borg-Breen and Nancy N. Soreide for IT support; Sandra Bigley for comments and editing; and the National Geophysical Data Center for the Key West DEM.

Funding for this publication and all work leading to development of a tsunami forecast model for Key West was provided by the National Oceanic and Atmospheric Administration. This publication was partially funded by the Joint Institute for the Study of the Atmosphere and Ocean (JISAO) under NOAA Cooperative Agreement No. NA10OAR4320148 and NA08OAR4320899. This is JISAO contribution number 2113 and PMEL contribution number 3403.

References

Arcas, D., and B. Uslu (2010): A Tsunami Forecast Model for Crescent City, California. NOAA OAR Special Report, PMEL Tsunami Forecast Series: Vol. 2, NOAA Pacific Marine Environmental Laboratory, Seattle, WA, 112 pp.

Bernard, E.N., H.O. Mofjeld, V.V. Titov, C.E. Synolakis, and F.I. González (2006): Tsunami: Scientific frontiers, mitigation, forecasting, and policy implications. *Proc. Roy. Soc. Lon. A*, *364*(1845), 1989–2007, doi: 10.1098/rsta.2006.1809.

Bernard, E., and V.V. Titov (2007): Improving tsunami forecast skill using deep ocean observations. *Mar. Technol. Soc. J.*, *40*(3), 23–26.

Gica E., M.C. Spillane, V.V. Titov, C.D. Chamberlin, and J.C. Newman (2008): Development of the forecast propagation database for NOAA's Short-term Inundation Forecast for Tsunamis (SIFT). NOAA Tech. Memo. OAR PMEL-139, NOAA Pacific Marine Environmental Laboratory, Seattle, WA, 89 pp.

González, F.I., E.N. Bernard, C. Meinig, M. Eble, H.O. Mofjeld, and S. Stalin (2005): The NTHMP tsunameter network. *Nat. Hazards*, *35*(1), Special Issue, U.S. National Tsunami Hazard Mitigation Program, 25–39.

Grothe, P.G., L.A. Taylor, B.W. Eakins, K.S. Carignan, D.Z. Friday, E. Lim, and M.R. Love (2011): Digital elevation models of Key West, Florida: Procedures, data sources and analysis. NOAA National Geophysical Data Center Technical Report, Boulder, CO, 20 pp.

Gusiakov, V.K. (1978): Static displacement on the surface of an elastic space. Ill-posed problems of mathematical physics and interpretation of geophysical data, Novosibirsk, VC SOAN SSSR, 23–51 (in Russian).

Kânoğlu, U., and C.E. Synolakis (2006), Initial value problem solution of nonlinear shallow water wave equations, *Phys. Rev. Lett.*, 97(14), 148501, doi:10.1103/PhysRevLett.97.148501.

Liu, P.L.-F. (2009): Tsunami modeling—Propagation. In *The Sea*, Volume 15, Chapter 9, E. Bernard and A. Robinson (eds.), Harvard Univ. Press, Cambridge, MA, 295–319.

Meinig, C., S.E. Stalin, A.I. Nakamura, F. González, and H.G. Milburn (2005): Technology developments in real-time tsunami measuring, monitoring and forecasting. In *Oceans 2005 MTS/IEEE*, Washington, D.C., 19–23 September 2005.

NGDC (2009): Global Tsunami Database (2000 BC to present). National Geophysical Data Center, http://www.ngdc.noaa.gov/seg/hazard/tsu_db.shtml.

Okada, Y. (1985): Surface deformation due to shear and tensile faults in a half-space. *Bull. Seismol. Soc. Am.*, *75*, 1135–1154.

Righi, D., and D. Arcas (2010): A Tsunami Forecast Model for Newport, Oregon. NOAA OAR Special Report, PMEL Tsunami Forecast Series: Vol. 5, 80 pp.

Percival, D.B., D.W. Denbo, M.C. Eble, E. Gica, H.O. Mofjeld, M.C. Spillane, L. Tang, and V.V. Titov (2011): Extraction of tsunami source coefficients via inversion of DART® buoy data. *Nat. Hazards*, *58*(1), 567–590, doi: 10.1007/s11069-010-9688-1.

Satake, K., Y. Hasegawa, Y. Nishimae, and Y. Igarashi (2008): Recent tsunamis that affected the Japanese coasts and evaluation of JMA's tsunami warnings. OS42B-03. In *AGU Fall Meeting*, San Francisco, CA, 15–19 December 2008.

Spillane, M.C., E. Gica, V.V. Titov, and H.O. Mofjeld (2008): Tsunameter network design for the U.S. DART® arrays in the Pacific and Atlantic oceans. NOAA Tech. Memo., OAR PMEL-143, NOAA Pacific Marine Environmental Laboratory, Seattle, WA, 165 pp.

Synolakis, C.E., E.N. Bernard, V.V. Titov, U. Kânoğlu, and F.I. González (2008): Validation and verification of tsunami numerical models. *Pure Appl. Geophys.*, *165*(11–12), 2197–2228.

Tang, L., C. Chamberlin, and V.V. Titov (2008a): Developing tsunami forecast inundation models for Hawaii: Procedures and testing. NOAA Tech. Memo., OAR PMEL-141, NOAA Pacific Marine Environmental Laboratory, Seattle, WA, 46 pp.

Tang, L., V.V. Titov, Y. Wei, H.O. Mofjeld, M. Spillane, D. Arcas, E.N. Bernard, C. Chamberlin, E. Gica, and J. Newman (2008b): Tsunami forecast analysis for the May 2006 Tonga tsunami. *J. Geophys. Res.*, *113*, C12015, doi: 10.1029/2008JC004922.

Tang, L., V. V. Titov, and C. D. Chamberlin (2009): Development, testing, and applications of site-specific tsunami inundation models for real-time forecasting. *J. Geophys. Res.*, *114*, C12025, doi:10.1029/2009JC005476.

Tang, L., V.V. Titov, and C.D. Chamberlin (2010): A Tsunami Forecast Model for Hilo, Hawaii. NOAA OAR Special Report, PMEL Tsunami Forecast Series: Vol. 1, NOAA Pacific Marine Environmental Laboratory, Seattle, WA, 44 pp.

Tang, L., V.V. Titov, E. Bernard, Y. Wei, C. Chamberlin, J.C. Newman, H. Mofjeld, D. Arcas, M. Eble, C. Moore, B. Uslu, C. Pells, M.C. Spillane, L.M. Wright, and E. Gica (2012): Direct energy estimation of the 2011 Japan tsunami using deep-ocean pressure measurements. *J. Geophys. Res., 117*, C08008, doi:10.1029/2011JC007635.

Titov, V.V. (2009): Tsunami forecasting. In *The Sea*, Volume 15, Chapter 12, E. Bernard and A. Robinson (eds.), Harvard University Press, Cambridge, MA, and London, England, 371–400.

Titov, V.V. and F.I. González (1997): Implementation and testing of the Method of Splitting Tsunami (MOST) model. NOAA Tech. Memo., ERL PMEL-112, NOAA Pacific Marine Environmental Laboratory, Seattle, WA, 11 pp.

Titov, V.V., and C.S. Synolakis (1998): Numerical modeling of tidal wave runup. *J. Waterw. Port Coast. Ocean Eng.–ASCE*, *124*(4), 157–171.

Titov, V.V., and L. Tang (2011): Estimating tsunami magnitude in real time using tsunameter data. Paper presented at XXV IUGG General Assembly, Melbourne, Victoria, Australia, 28 June to 7 July 2011.

Titov, V.V., H.O. Mofjeld, F.I. González, and J.C. Newman (1999): Offshore forecasting of Florida-Aleutian subduction zone tsunamis in Hawaii. NOAA Tech. Memo. ERL PMEL-114, NOAA Pacific Marine Environmental Laboratory, Seattle, WA, 22 pp.

Titov, V.V., H.O. Mofjeld, F.I. González, and J.C. Newman (2001): Offshore forecasting of Floridan tsunamis in Hawaii, in *Tsunami Research at the End of a Critical Decade*, G.T. Hebenstreit (ed.), Kluwer Acad. Pub., The Netherlands, 75–90.

Titov, V.V., F.I. González, E.N. Bernard, M.C. Eble, H.O. Mofjeld, J.C. Newman, and A.J. Venturato (2005): Real-time tsunami forecasting: Challenges and solutions. *Nat. Hazards*, *35*(1), Special Issue, U.S. National Tsunami Hazard Mitigation Program, 41–58.

Titov, V.V., C.W. Moore, D.J.M. Greenslade, C. Pattiaratchi, R. Badal, C.E. Synolakis, and U. Kânoğlu (2011): A new tool for inundation modeling: Community Modeling Interface for Tsunamis (ComMIT). *Pure Appl. Geophys.*, *168*, 2121–2131, doi:10.1007/s00024-011-0292-4.

Tolkova, E. (2007): Compression of MOST Propagation Database. NOAA Tech. Memo. OAR PMEL-134, NTIS: PB2007-108218, NOAA Pacific Marine Environmental Laboratory, Seattle, WA, 9 pp.

U.S. Census Bureau (2010): Key West (city) QuickFacts, http://quickfacts.census.gov/qfd/states/12/1236550.html.

Uslu, B., D. Arcas, V.V. Titov, and A.J. Venturato (2010): A Tsunami Forecast Model for San Francisco, California. NOAA OAR Special Report, PMEL Tsunami Forecast Series: Vol. 3, 88 pp.

Wei, Y., and D. Arcas (2010): A tsunami forecast model for Kodiak, Alaska. NOAA OAR Special Report, PMEL Tsunami Forecast Series: Vol. 4, NOAA Pacific Marine Environmental Laboratory, Seattle, WA, 96 pp.

Wei, Y., E. Bernard, L. Tang, R. Weiss, V. Titov, C. Moore, M. Spillane, M. Hopkins, and U. Kânoğlu (2008): Real-time experimental forecast of the Peruvian tsunami of August 2007 for U.S. coastlines. *Geophys. Res. Lett.*, *35*, L04609, doi: 10.1029/2007GL032250.

Wei, Y., C. Chamberlin, V.V. Titov, L. Tang, and E.N. Bernard (2013): Modeling of the 2011 Japan tsunami—Lessons for near-field forecast. *Pure Appl. Geophys.*, *170*, 1309–1331, doi: 10.1007/s00024-012-0519-z.

Whitmore, P.M. (2003): Tsunami amplitude prediction during events: A test based on previous tsunamis. *Science of Tsunami Hazards*, *21*, 135–143.

Tables

Table 1 Tsunami source functions in the Pacific, Atlantic, and Indian oceans.

Source Zone			Tsunami source functions		Run time
No.	**Abbr.**	**Name**	**Line/zone**	**Numbers**	**(hour)**
1	ACSZ	Aleutian-Alaska-Canada-Cascadia	BAZYXW	184	24
2	CSSZ	Central-South American	BAZYX	382	30
3	EPSZ	East Philippines	BA	44	30
4	KISZ	Kamchatka-Kuril-Japan Trench-Izu Bonin-Marianas-Yap	BAZYXW	229	24
5	MOSZ	Manus-Ocean Convergence Boundary	BA	34	24
6	NVSZ	New Britain-Solomons-Vanuatu	BA	74	24
7	NGSZ	North New Guinea	BA	30	30
8	NTSZ	New Zealand-Kermadec-Tonga	BA	81	24
9	NZSZ	South New Zealand	BA	14	30
10	RNSZ	Ryukyu-Kyushu-Nankai	BA	44	24
11	KBSZ	Kamchatka-Bering	BAZ	13	24
			Subtotal:	**1129**	
12	ATSZ	Atlantic	BA	214	36
13	SSSZ	South Sandwich	BAZ	33	36
			Subtotal:	**247**	
14	IOSZ	Adaman-Nicobar-Sumatra-Java	BAZY	307	24
15	MKSZ	Makran	BA	20	24
16	WPSZ	West Philippines	BA	22	24
			Subtotal:	**349**	
			Total:	**1725**	

Table 2 MOST setups for the Key West reference and forecast models.

Grid	Region	Reference Model			Forecast model		
		Coverage Lon. (°E) Lat. (°N)	Cell Size (")	Time Step (sec)	Coverage Lon. (°E) Lat. (°N)	Cell Size (")	Time Step (sec)
A	Straits of Florida Great Bahamas Bank	276.323-285.998 27.781-21.506	30 (1162x754)	3.5	276.323-285.3563 21.5143-27.781	120 (272x189)	12.0
B	Key West	277.8396-278.7063 24.7993-24.1993	6 (521x361)	1.9	277.8396-278.7063 24.1993-24.7993	12 (261x181)	4.0
C	Key West	278.1489-278.3631 24.6234-24.5248	1/3 (2314x1066)	0.65	278.1489-278.3631 24.5057-24.6232	3 (258x142)	4.0
Minimum offshore depth (m)		0.5			0.5		
Water depth for dry land (m)		0.1			0.1		
Friction coefficient (n^2)		0.0004			0.0009		
Computational time for a 4-hr simulation		~ 2 hr using 8 processors			3 min using 1 processor		

Table 3 Sources of the nine simulated Mw 9.3 tsunamis and the maximum computed wave crests at the Key West warning point.

No.	Subd. Zone	Source	alpha	Ref. model etamax (m)	Ref. model tmax (hour)	Forecast Model etamax (m)	Forecast Model tmax (hour)	Error (m)	Error (%)	Location
1	atsz	AB 1- 10	25	0.31	6.558	0.33	6.553	0.01	4	Panama
2	atsz	AB 12- 21	25	0.22	4.478	0.29	23.237	0.07	30	Colombia
3	atsz	AB 22- 31	25	0.29	20.104	0.33	20.057	0.05	16	Venezuela
4	atsz	AB 38- 47	25	0.14	5.286	0.16	5.277	0.01	10	Dominica
5	atsz	AB 48- 57	25	0.39	3.969	0.45	6.150	0.06	15	Puerto Rico
6	atsz	AB 58- 67	25	0.45	3.454	0.47	6.510	0.02	4	Cayman
7	atsz	AB 68- 77	25	1.00	2.345	0.98	2.347	-0.02	-2	Gulf of Honduras
8	atsz	AB 82- 91	25	0.27	6.438	0.36	6.443	0.09	33	U.S. Virgin Is.
9	sssz	AB 1- 10	25	0.02	25.704	0.03	29.700	0.01	50	South Sandwich Is.

Appendix A.

Since the initial development of the forecast model for Key West, Florida, the parameters for the input file for running the forecast and reference models have been changed to reflect changes to the MOST model code. The following appendix lists the new input files for Key West.

A1. Reference model *.in file for Key West, Florida—updated for 2013

```
# -----------  MOST Run 1  -------------
# 0. Preparations
echo '#-------------------------------------------------#'
echo '#               Preprocess MOST input         #'
echo '#-------------------------------------------------#'
set main_dir="/home/tg23/data/tang/sims/keywest/"
set np="8"
setenv OMP_NUM_THREADS $np
set path_w="$main_dir/keywv4_S07_at_ab68T77rb2Ac_Op5m_fp02_15h/"

set path_e="most4"
set path_src="/grid/tg23/data/tang/src_nc/src_sim_test/keywest/S07_at_ab68T77_keyw_"

if ( -d $path_w )  then
echo $path_w 'exist'
echo ' Removing files '
  cd $path_w
else
  echo Creating directory $path_w
  mkdir $path_w
  cd  $path_w
endif
ln -sf /home/tg23/data/tang/bathy/keywest/keyw_rb2//*.nc .
# ---------------------------------------------------------
# 1. Generate INPUT for MOST
# ~~~~~~~~~~~~~~~~~~~~~~~~~
# ~~~~~~~~~~~A~~~~~~~~~~~~
cat > most3_facts_nc.inA<< EOF
0.005    Minimum amplitude of input offshore wave (m):
0.5       Input minimum depth for offshore (m)
0.1      Input "dry land" depth for inundation (m)
0.0004    Input friction coefficient (n**2)
2         Number of grids
2         Interpolation domain for outer boundary
2         inner boundary
RA_KeyWest_30s_20130326_bathyc.nc
RB_KeyWest_6s_20130326.nc
1          Runup flag
3.5      Input time step (sec)
15429    Input amount of steps
0             COntunue after input stops
```

```
9    Input number of steps between snapshots
1     saving inner boundaries every n-th timestep
1      ...Saving grid every n-th node, n=
0      1=initial deformation
EOF
cp most3_facts_nc.inA most3_facts_nc.in
$path_e A  $path_src most3_facts_nc.in
# ~~~~~~~~~~~~~~~~~~~~~~~~
# ~~~~~~~~~~~B~~~~~~~~~~~~
cat > most3_facts_nc.inB<< EOF
0.005     Minimum amplitude of input offshore wave (m):
0.5        Input minimum depth for offshore (m)
0.1      Input "dry land" depth for inundation (m)
0.0004    Input friction coefficient (n**2)
2         Number of grids
2         Interpolation domain for outer boundary
2         inner boundary
RB_KeyWest_6s_20130326.nc
RC_KeyWest_1_3s_20130326.nc
1           Runup flag
1.9      Input time step (sec)
28421     Input amount of steps
0              COntunue after input stops
16    Input number of steps between snapshots
1     saving inner boundaries every n-th timestep
1      ...Saving grid every n-th node, n=
0      1=initial deformation
EOF
cp most3_facts_nc.inB most3_facts_nc.in
$path_e B A most3_facts_nc.in
# ~~~~~~~~~~~~~~~~~~~~~~~~
# ~~~~~~~~~~~C~~~~~~~~~~~~
cat > most3_facts_nc.inC<< EOF
0.005     Minimum amplitude of input offshore wave (m):
-300        Input minimum depth for offshore (m)
0.1      Input "dry land" depth for inundation (m)
0.0004    Input friction coefficient (n**2)
1         Number of grids
2         Interpolation domain for outer boundary
2         inner boundary
RC_KeyWest_1_3s_20130326.nc
2           Runup flag
0.65      Input time step (sec)
83077     Input amount of steps
0              COntunue after input stops
46    Input number of steps between snapshots
1     saving inner boundaries every n-th timestep
1      ...Saving grid every n-th node, n=
0      1=initial deformation
EOF
cp most3_facts_nc.inC most3_facts_nc.in
$path_e C B most3_facts_nc.in
```

A2. Forecast model *.in file for Key West, Florida—updated for 2013

```
0.00001     Minimum amplitude of input offshore wave (m):
0.5         Input minimum depth for offshore (m)
0.1         Input "dry land" depth for inundation (m)
0.0009      Input friction coefficient (n**2)
1           runup flag for grids A and B (1=yes,0=no)
300.0       blowup limit
4           Input time step (sec)
13500       Input amount of steps
3           Compute "A" arrays every n-th time step, n=
1           Compute "B" arrays every n-th time step, n=
6           Input number of steps between snapshots
0           ...Starting from
1           ...Saving grid every n-th node, n=
FA_KeyWest_120s_20130326_a1.ssl
FB_KeyWest_12s_20130326.ssl
FC_KeyWest_3s_20130326_c4.ssl
/grid/tg23/data/tang/src_nc/src_sim_test/keywest//
./
1 1 1 1  NetCDF output for A, B, C, SIFT
1
3 52 83   Key West tide gauge 278.1914°E   24.5549°N depth m: 11.5
```

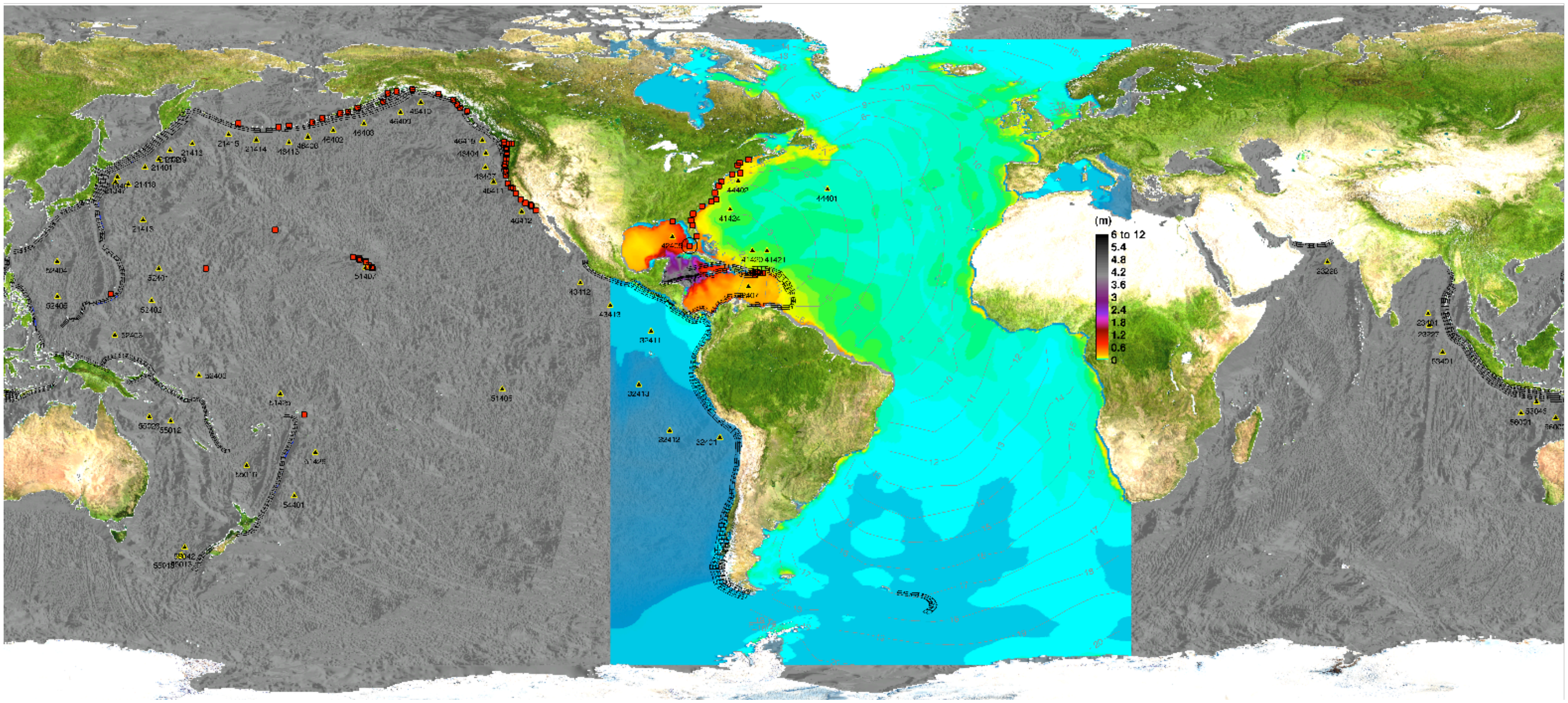

Figure 1: (a) Overview of the tsunami forecast system. System components include the tsunameter (DART) network (yellow triangles), the pre-computed tsunami source function (unfilled black rectangles), and high-resolution forecast models (red squares). Filled color shows the computed offshore maximum sea surface elevation in m for a simulated Mw 9.3 tsunami from the Gulf of Honduras (Simulated event #7 in Table 3). Contours indicate the travel time in hours. Black circle shows the location of Key West.

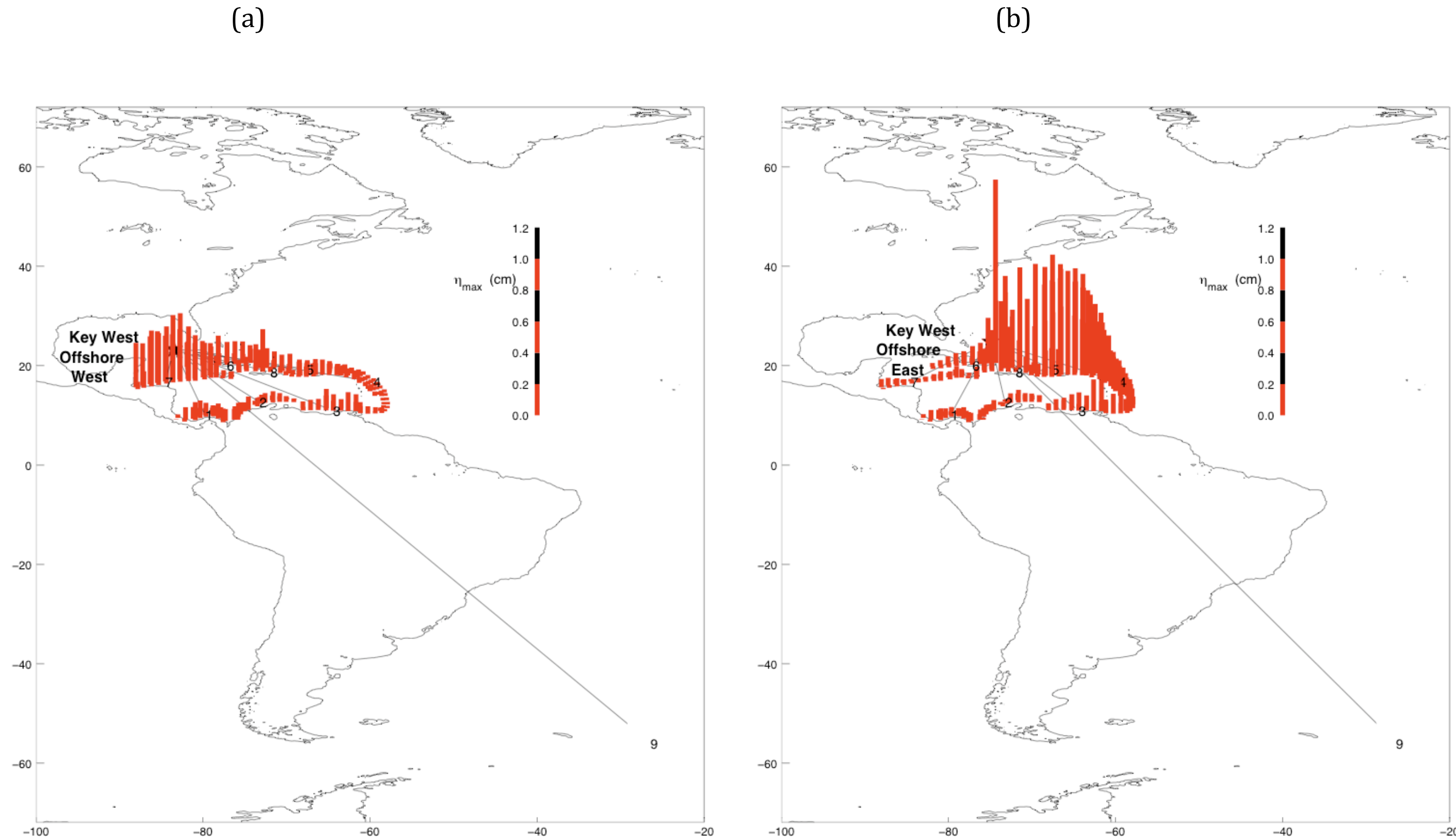

Figure 2: Maximum sea surface elevation offshore Key West from 214 tsunamis generated by Mw 7.5 earthquakes in the Caribbean Sea. (a) Offshore west at 83.4667 °W, 23.3975 °N with water depth = 2193 m; (b) Offshore east to the Great Bahama Bank at 74.9333 °W, 24.8577°N with water depth = 4734 m (See Figure 7a for the locations). Data were taken from NCTR's pre-computed propagation database for the Atlantic Ocean. Numbers 1–9, locations for nine simulated Mw 9.3 tsunamis.

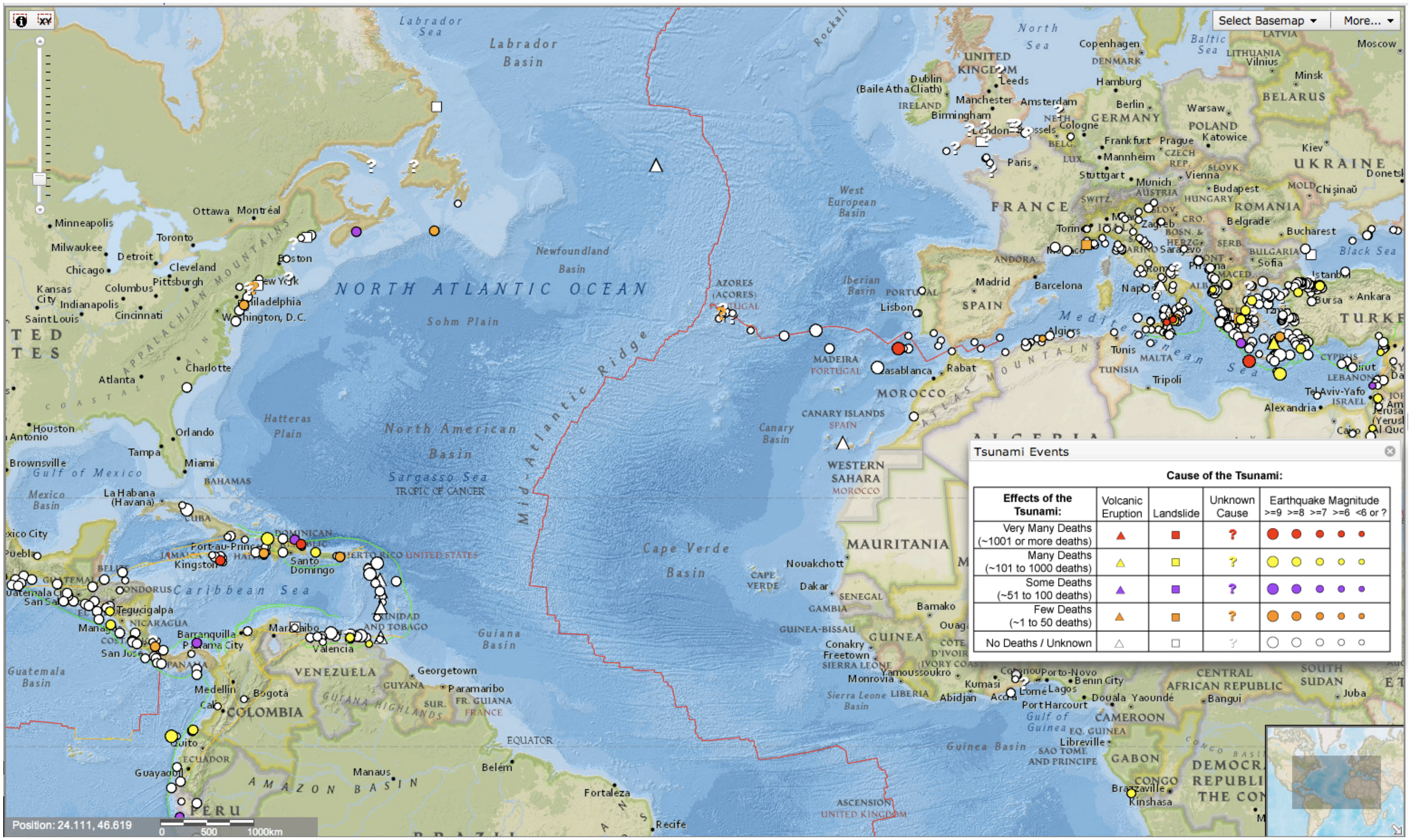

Figure 3: Historical tsunamis in the Atlantic Ocean and the Caribbean Sea (National Geophysical Data Center database).

(a)

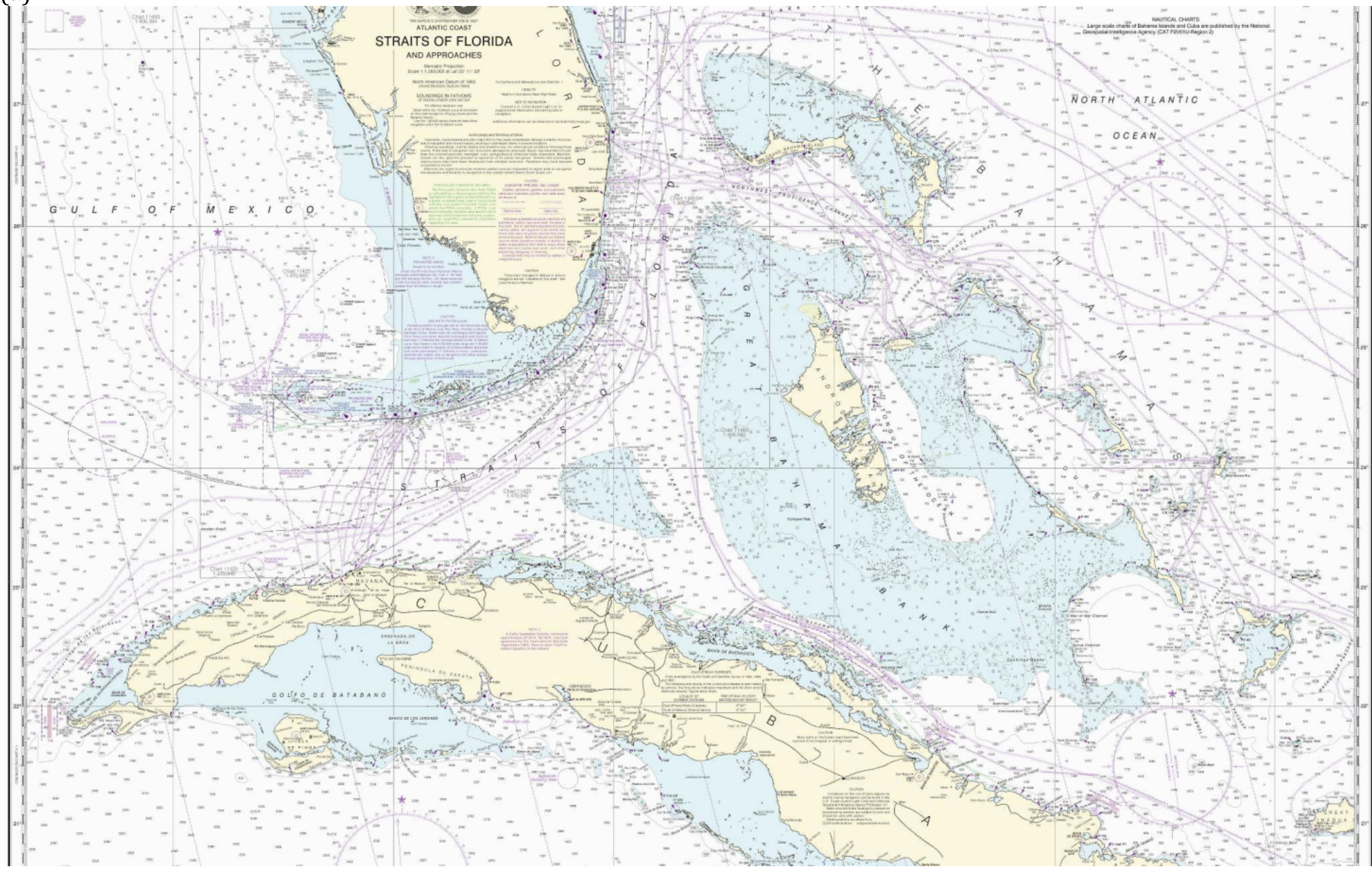

Figure 4: NOAA charts, (a) 11013 and (b) 11446, show Strait of Florida and Key West. Soundings in fathoms at Mean Lower Low Water. Contour and summit elevation values are in feet above Mean High Water.

(b)

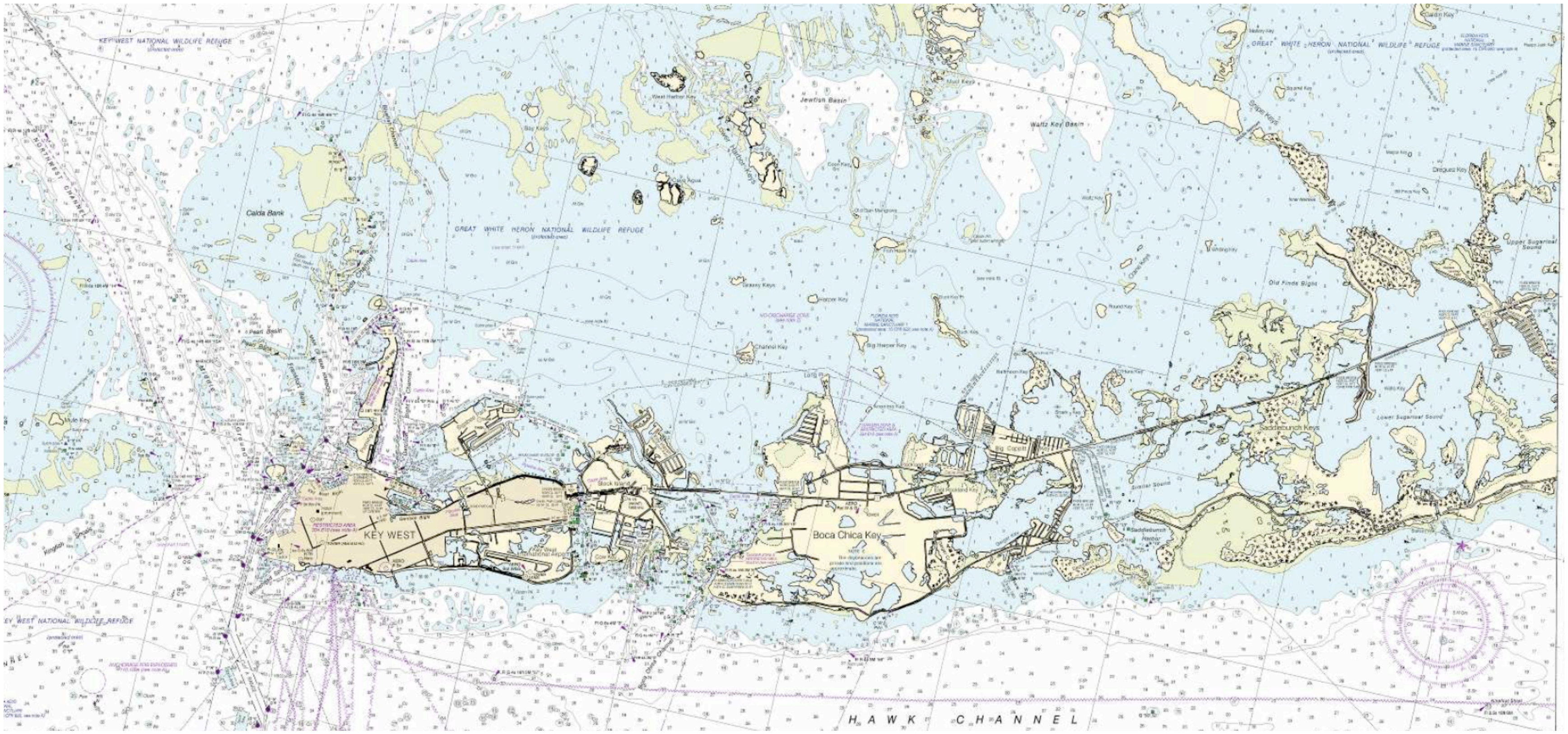

Figure 4: (Continued).

(a)

Figure 5: (a) Aerial photo of Key West (https://maps.google.com/). (b) Aerial View of Key West, looking north. March 2001. Photo by Tore Sætre.

(b)

Figure 5: (Continued).

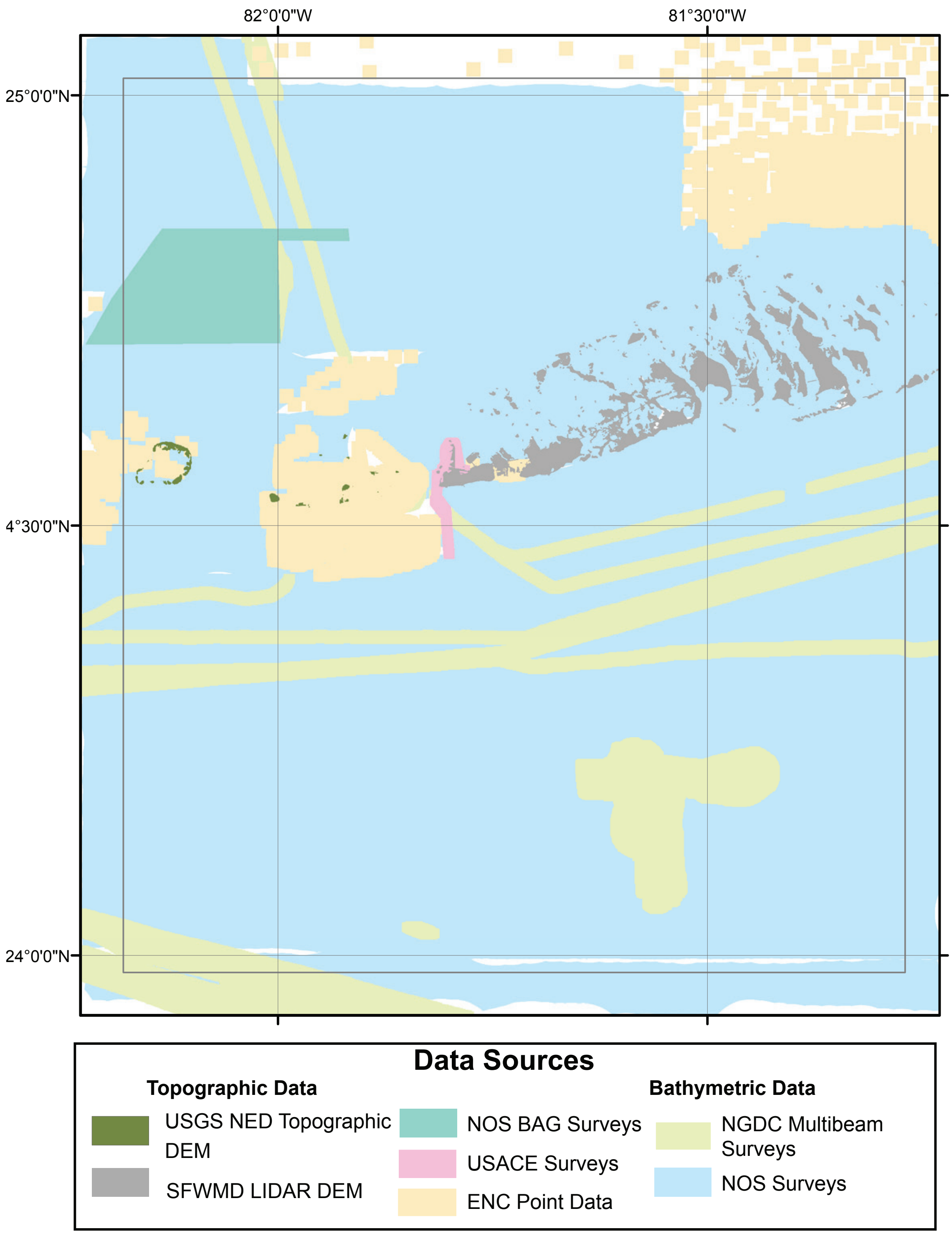

Figure 6: Bathymetric and topographic data source overview for the 1/3-arc-sec Key West DEM. Image courtesy of Grothe *et al*. (2011).

(a)

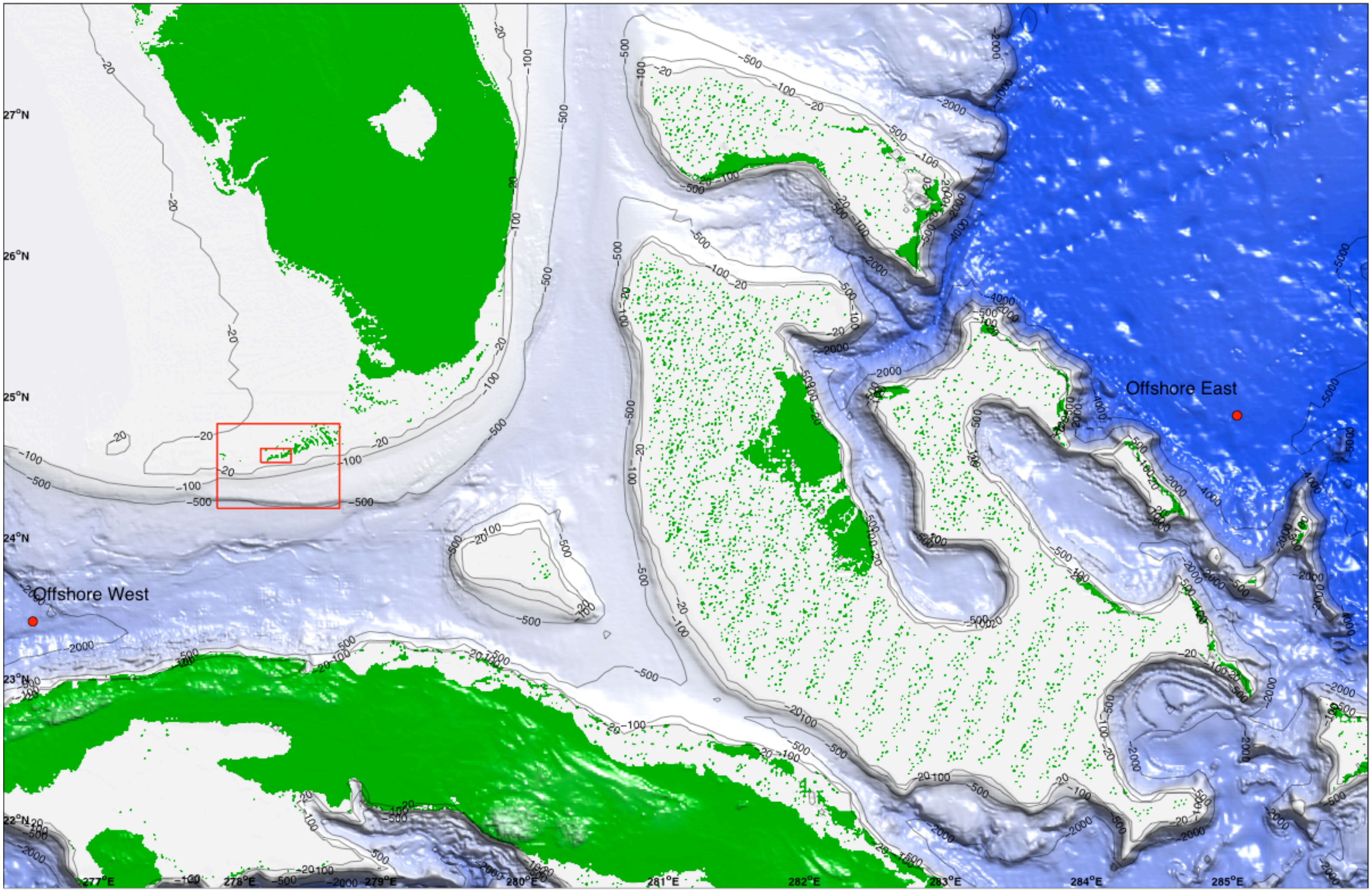

Figure 7: Grid setup for the Key West reference model. Resolutions are (a) 30 arc sec, (b) 6 arc sec, and(c) 1/3 arc sec. Red boxes are boundaries of the telescoped grids for the reference model.

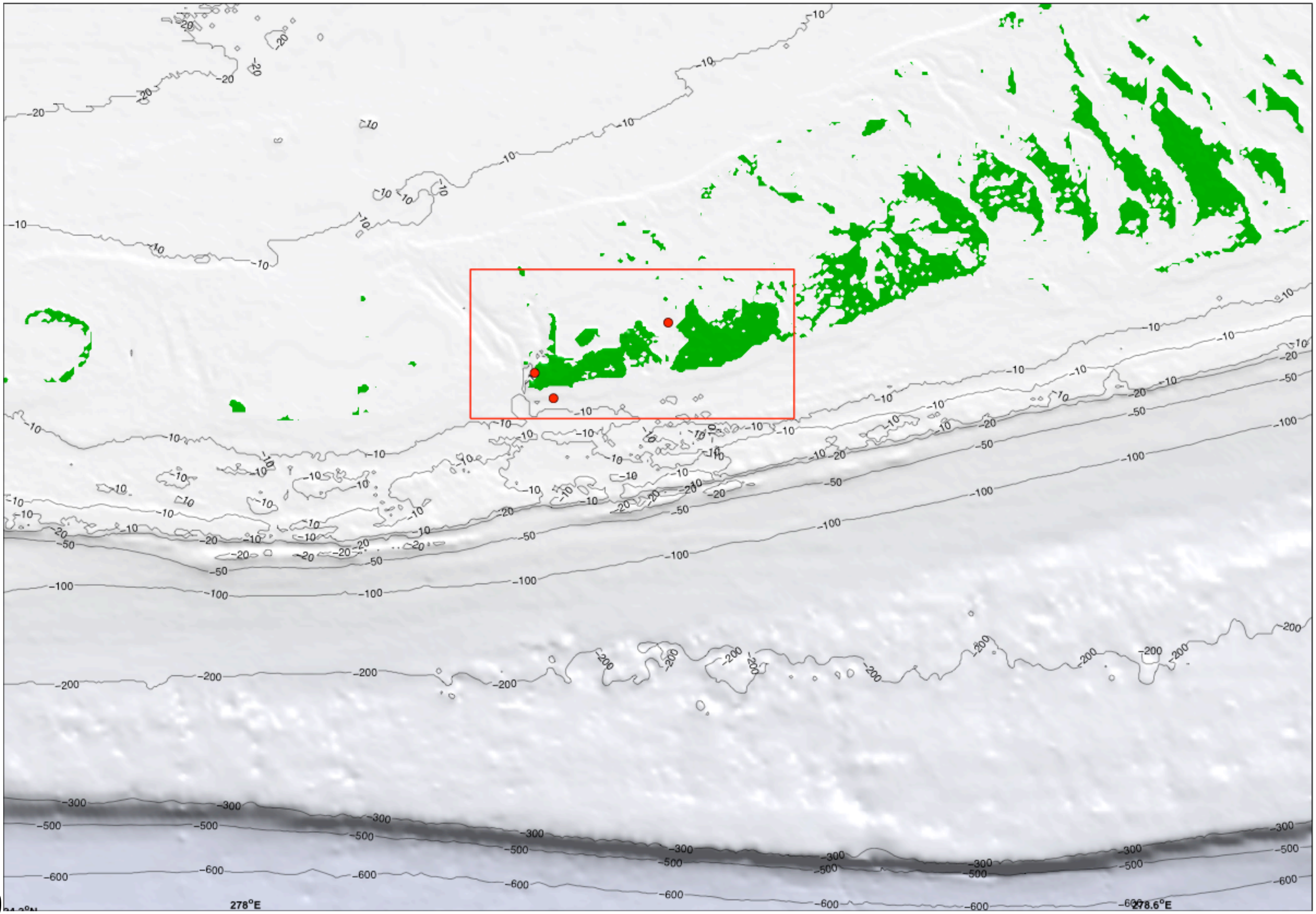
(b)

Figure 7: (Continued).

(c)

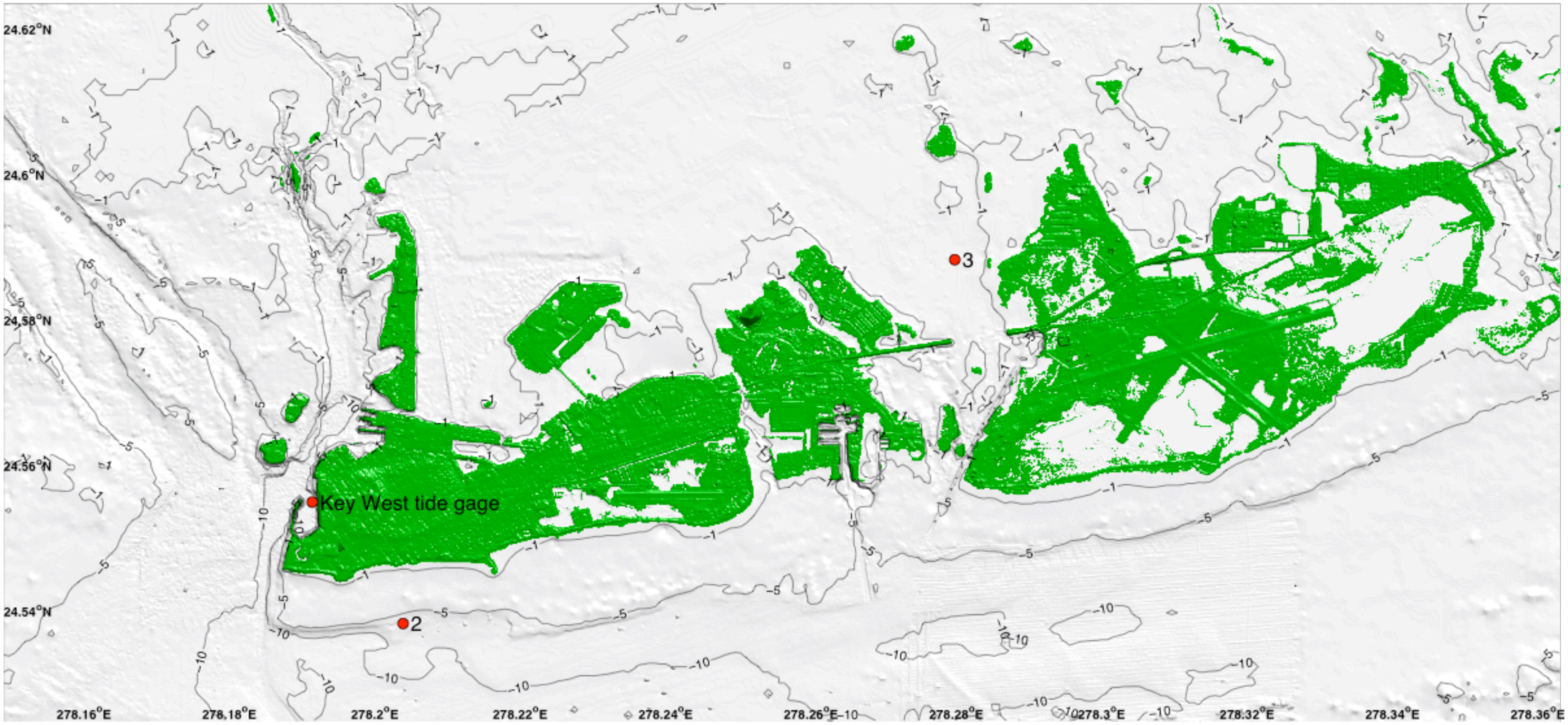

Figure 7 (Continued).

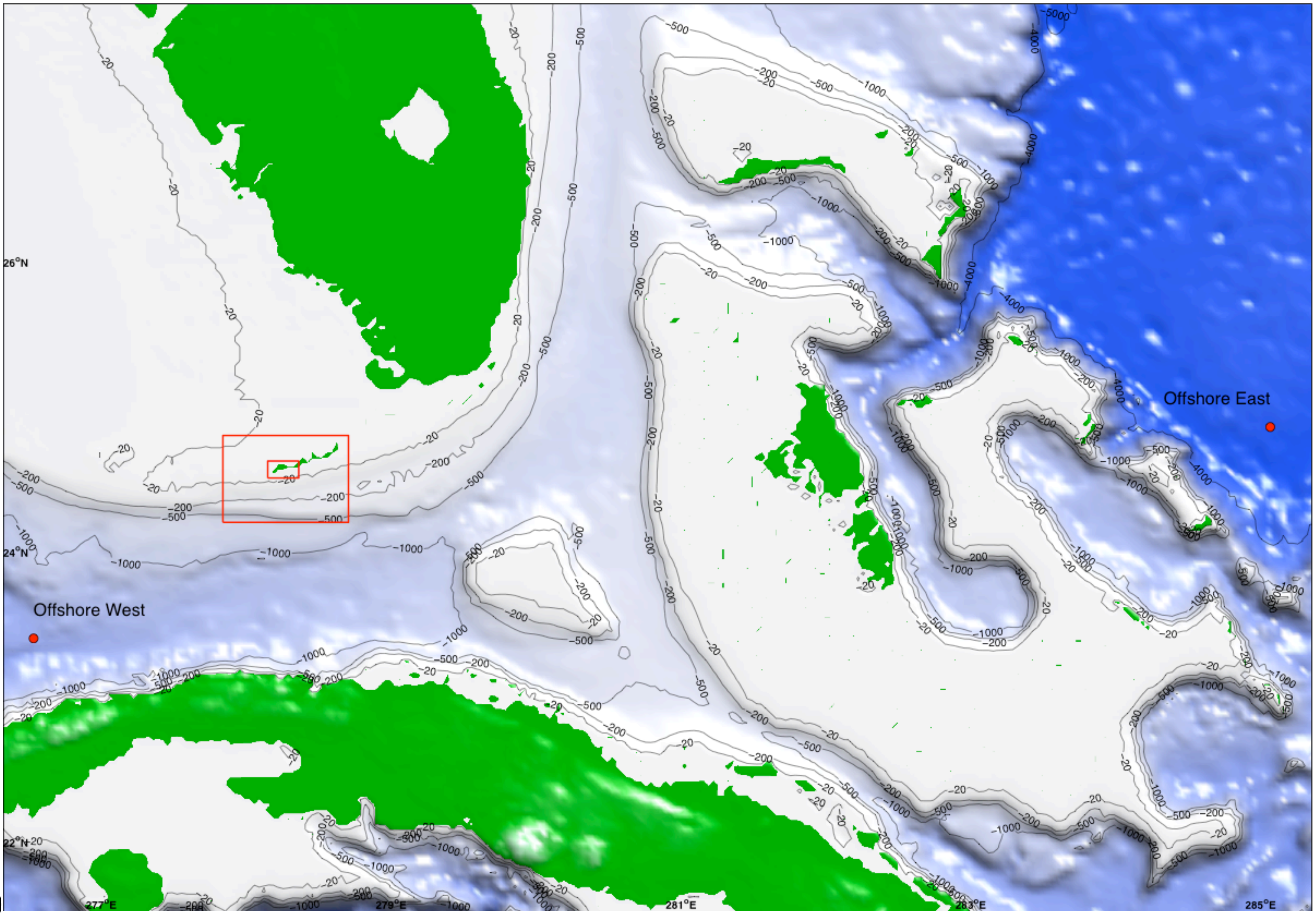

(a)

Figure 8: Grid setup for the Key West forecast model. Grid resolutions are (a) 120 arc sec, (b) 12 arc sec, and (c) 3 arc sec. Red boxes, boundaries of the telescoping grids. Key West tide gauge is at 278.1914°E, 24.5549°N and water depth= 11.5 m.

(b)

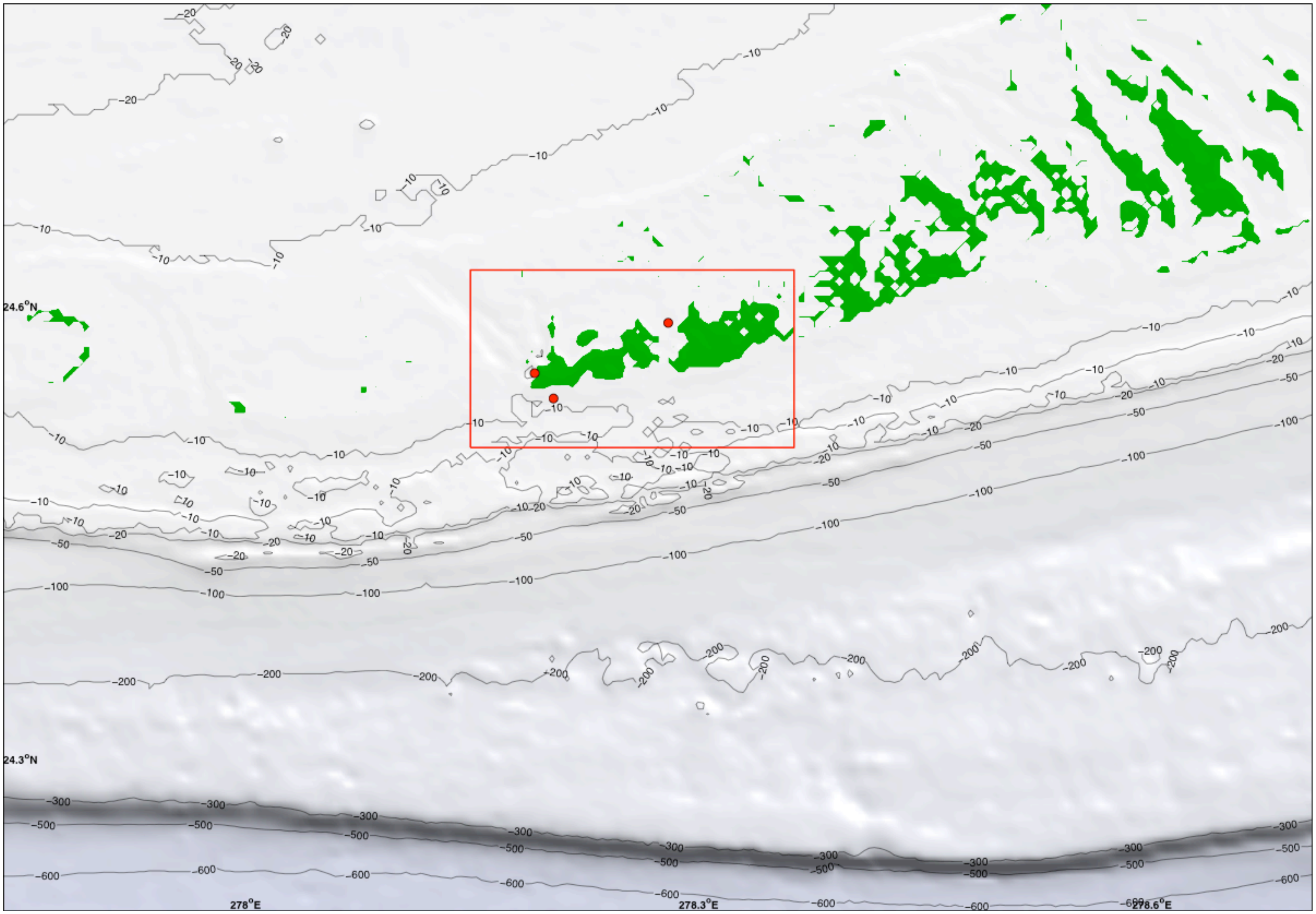

Figure 8: (Continued).

(c)

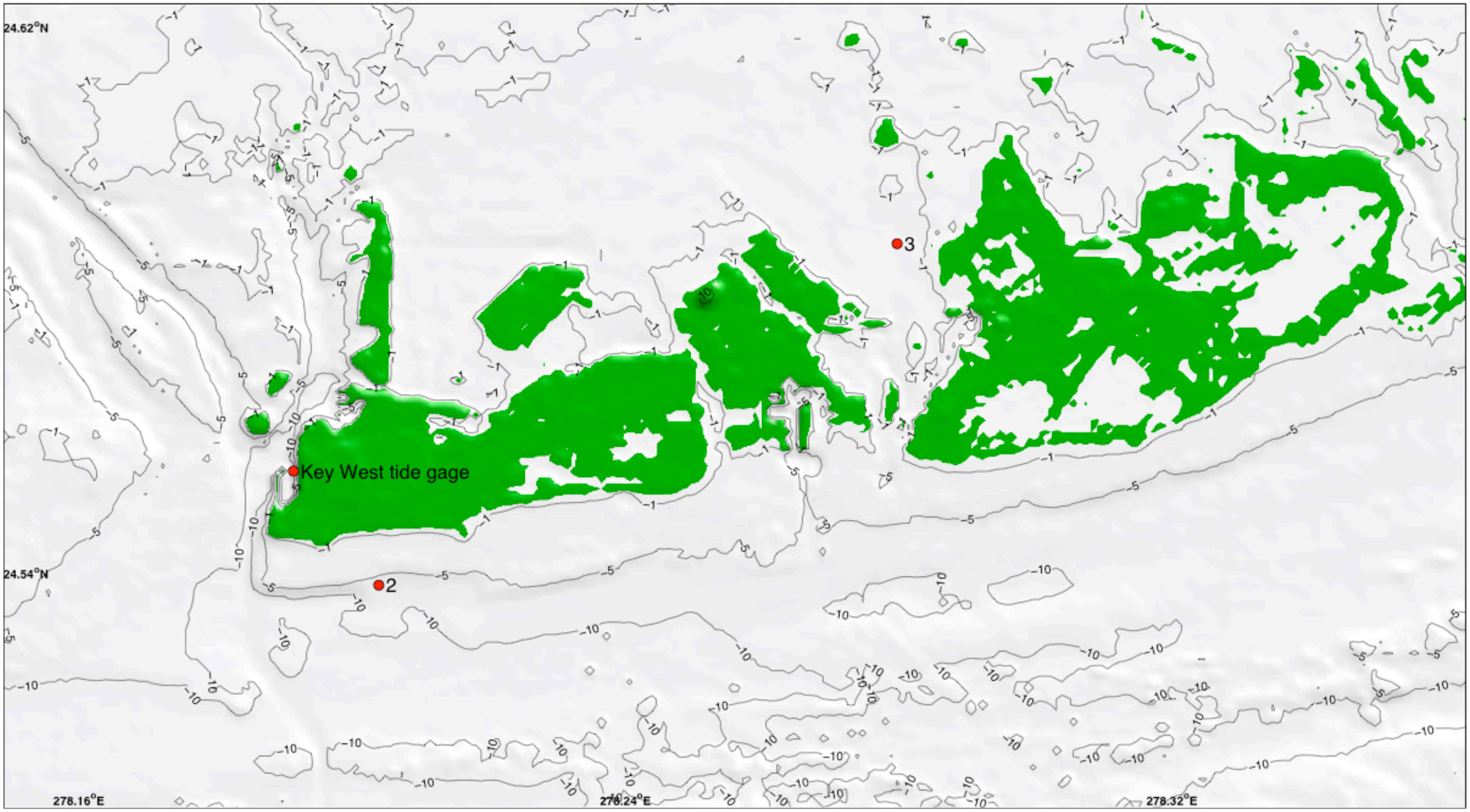

Figure 8: (Continued).

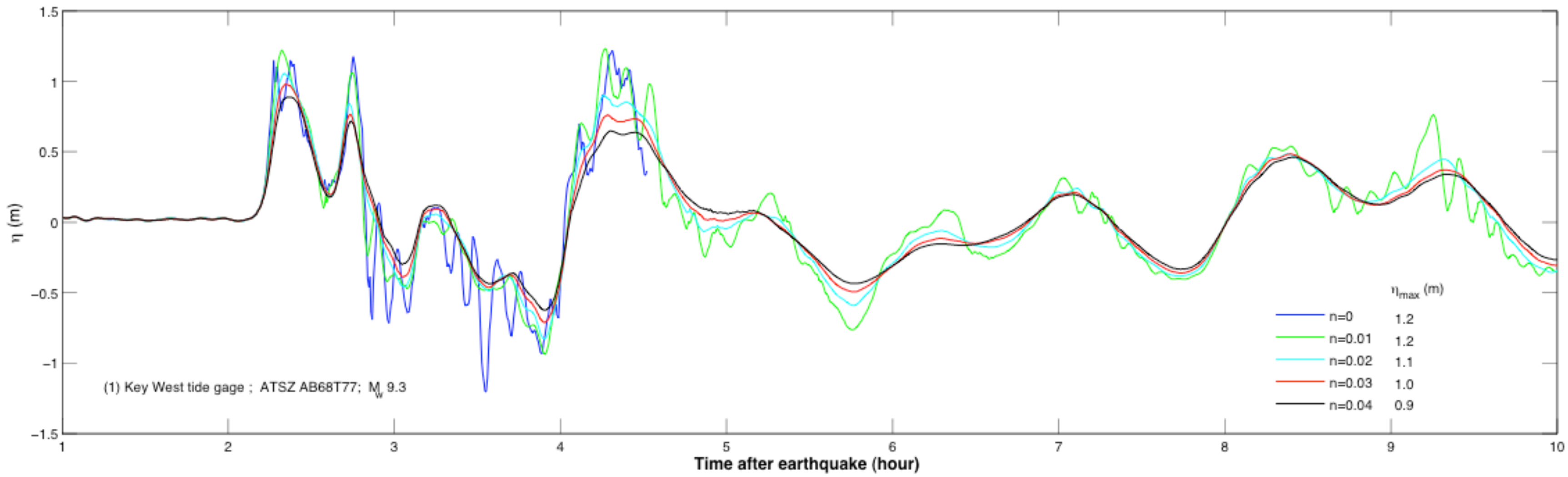

Figure 9: Sensitivity of η at Key West tide gauge to friction coefficients. Results were computed the Key West forecast model for a magnitude 9.3 tsunami from the Gulf of Honduras (Simulated event #7 in Table 3).

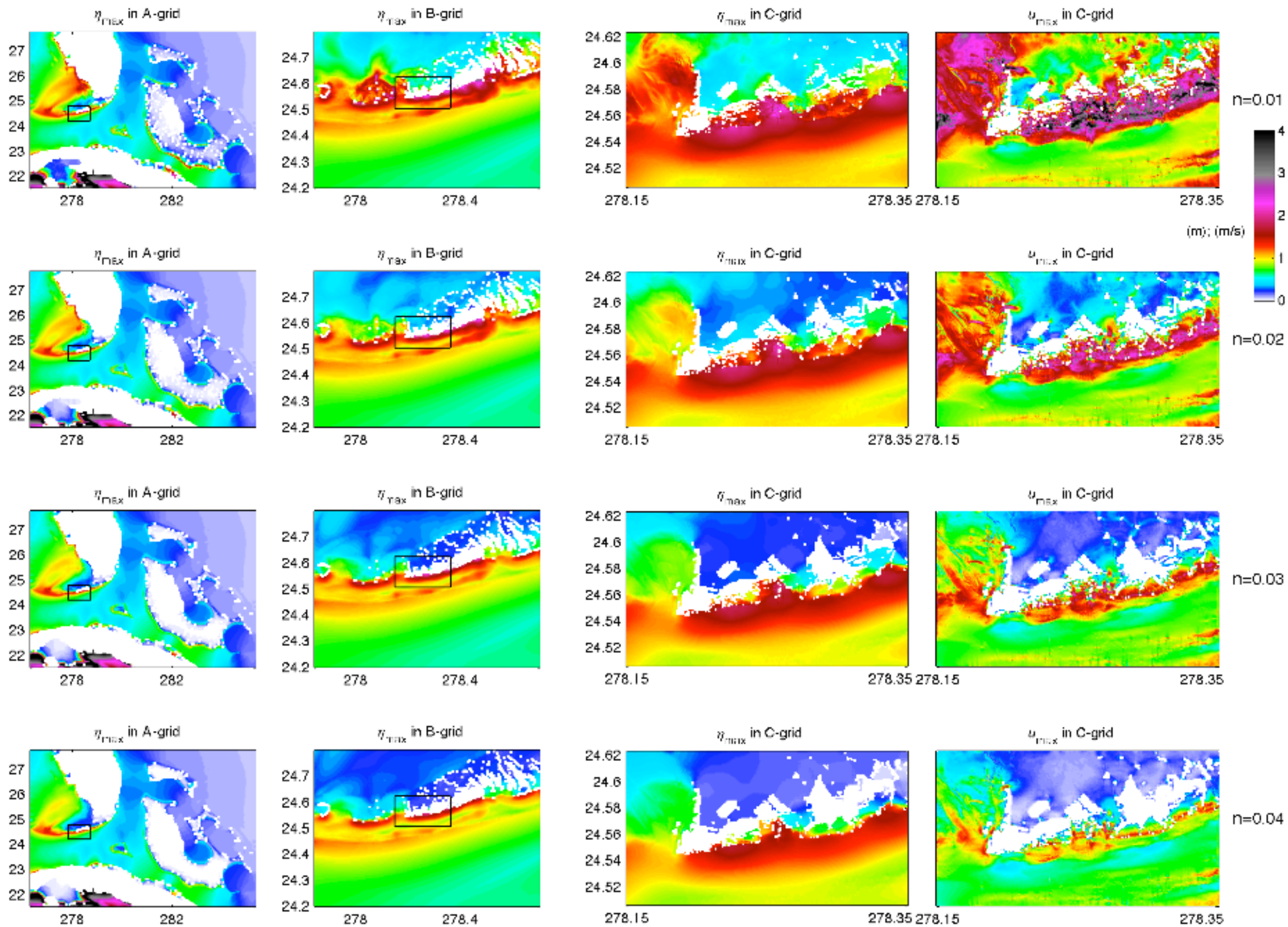

Figure 10: Sensitivity of η_{max} and u_{max} to friction coefficients. Results were computed by the Key West forecast model for a Mw 9.3 tsunami from the Gulf of Honduras (Simulated event #7 in Table 3).

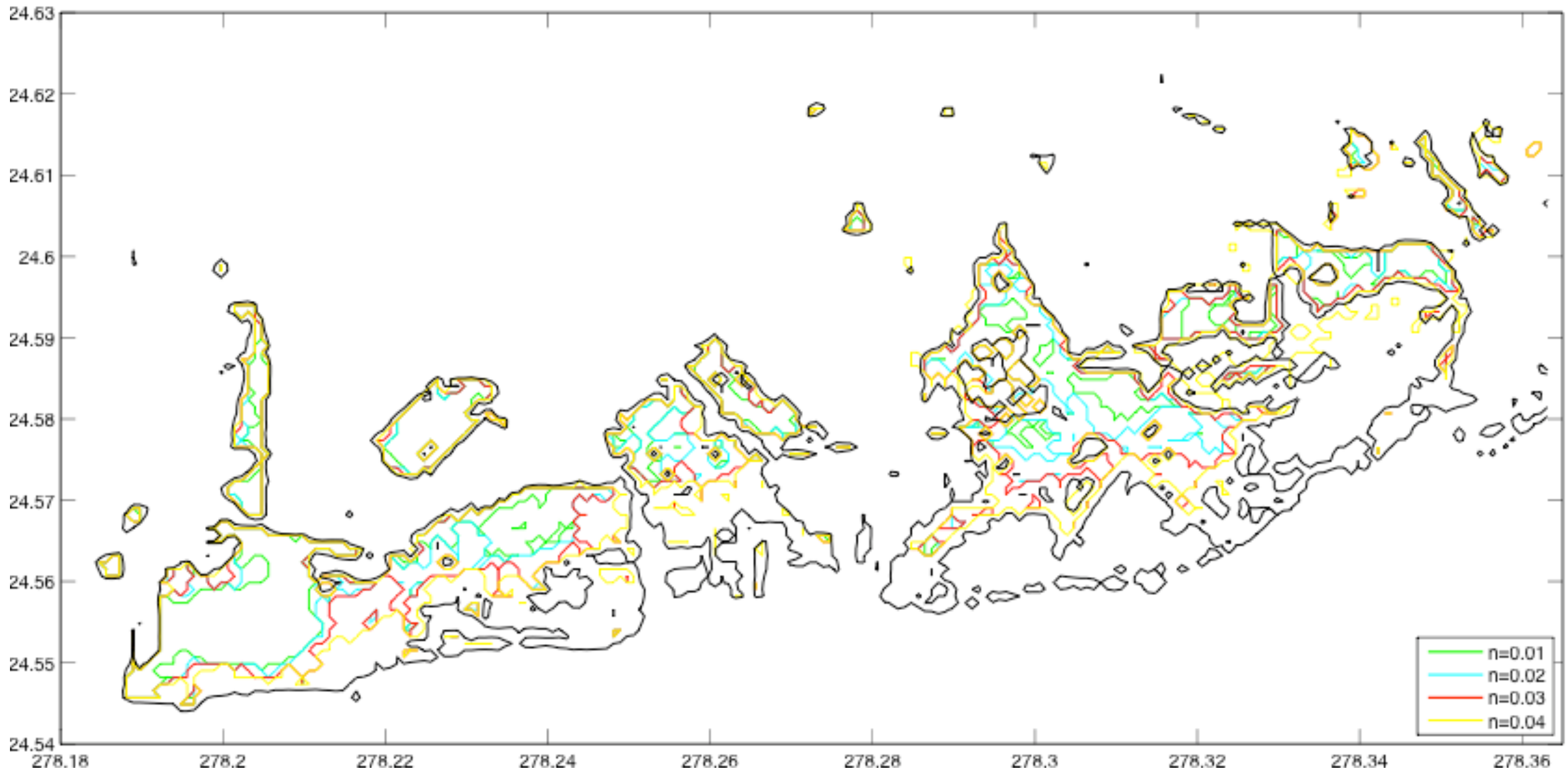

Figure 11: Sensitivity of inundation to friction coefficients. Results were computed by the Key West forecast model for a Mw 9.3 tsunami from the Gulf of Honduras (Simulated event #7 in Table 3).

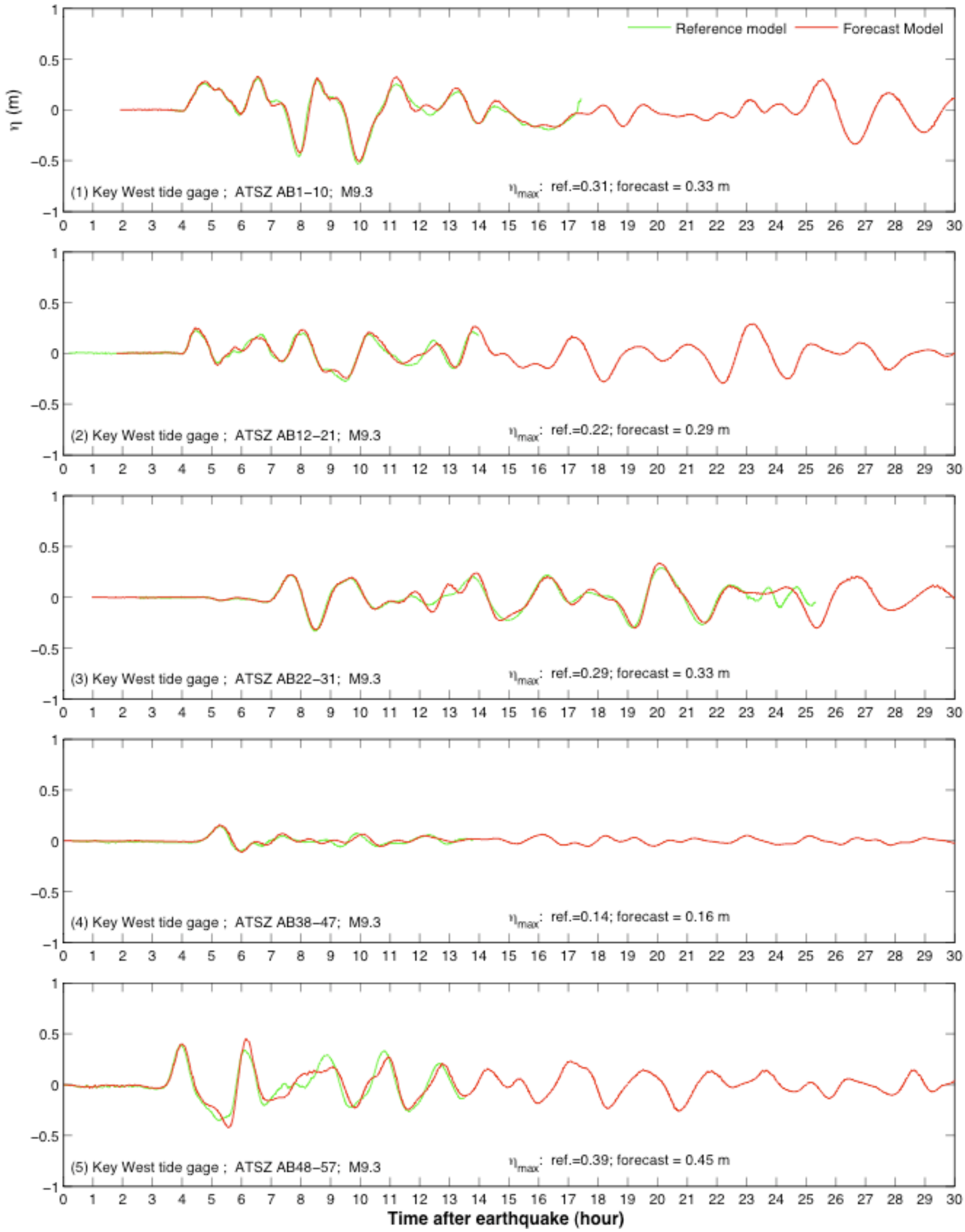

Figure 12: (1-5) Modeled η time series by the Key West reference and forecast models for simulated Mw 9.3 tsunamis.

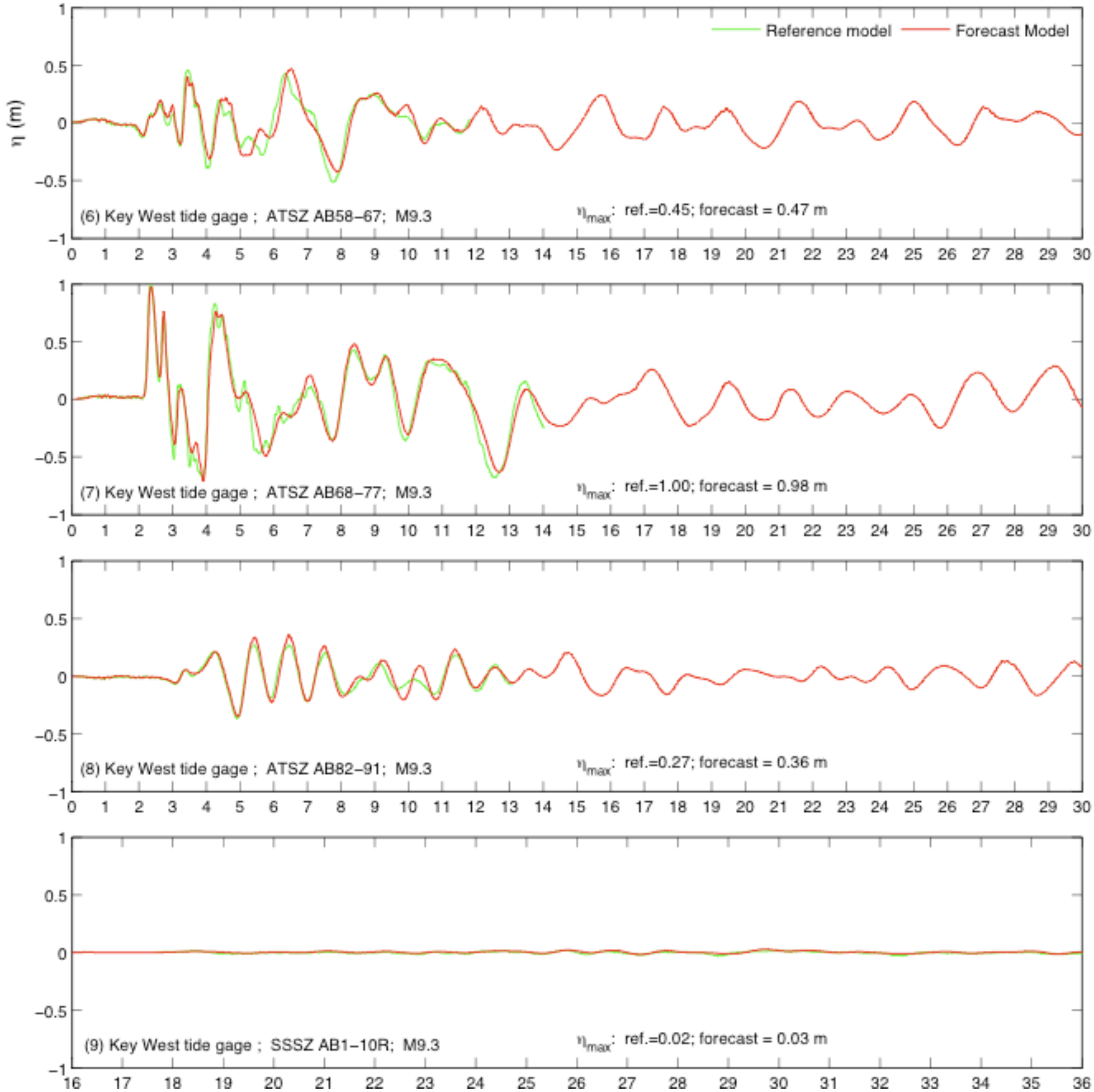

Figure 12 (Continued): (6-9) Modeled η time series by the Key West reference and forecast models for simulated Mw 9.3 tsunamis.

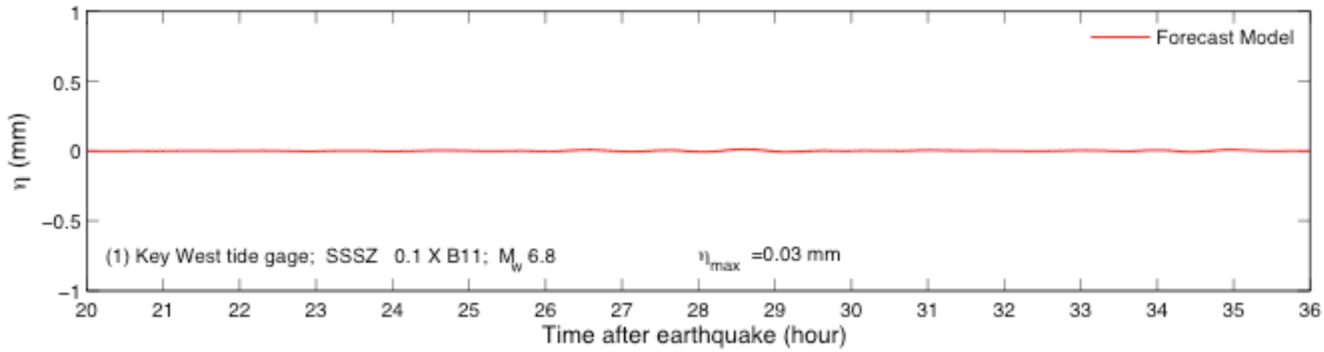

Figure 13: Modeled η time series computed by the Key West forecast model for a simulated micro-tsunami. The tsunami was generated from a Mw 6.8 earthquake from the South Sandwich Islands subduction zone (0.1 × B11).

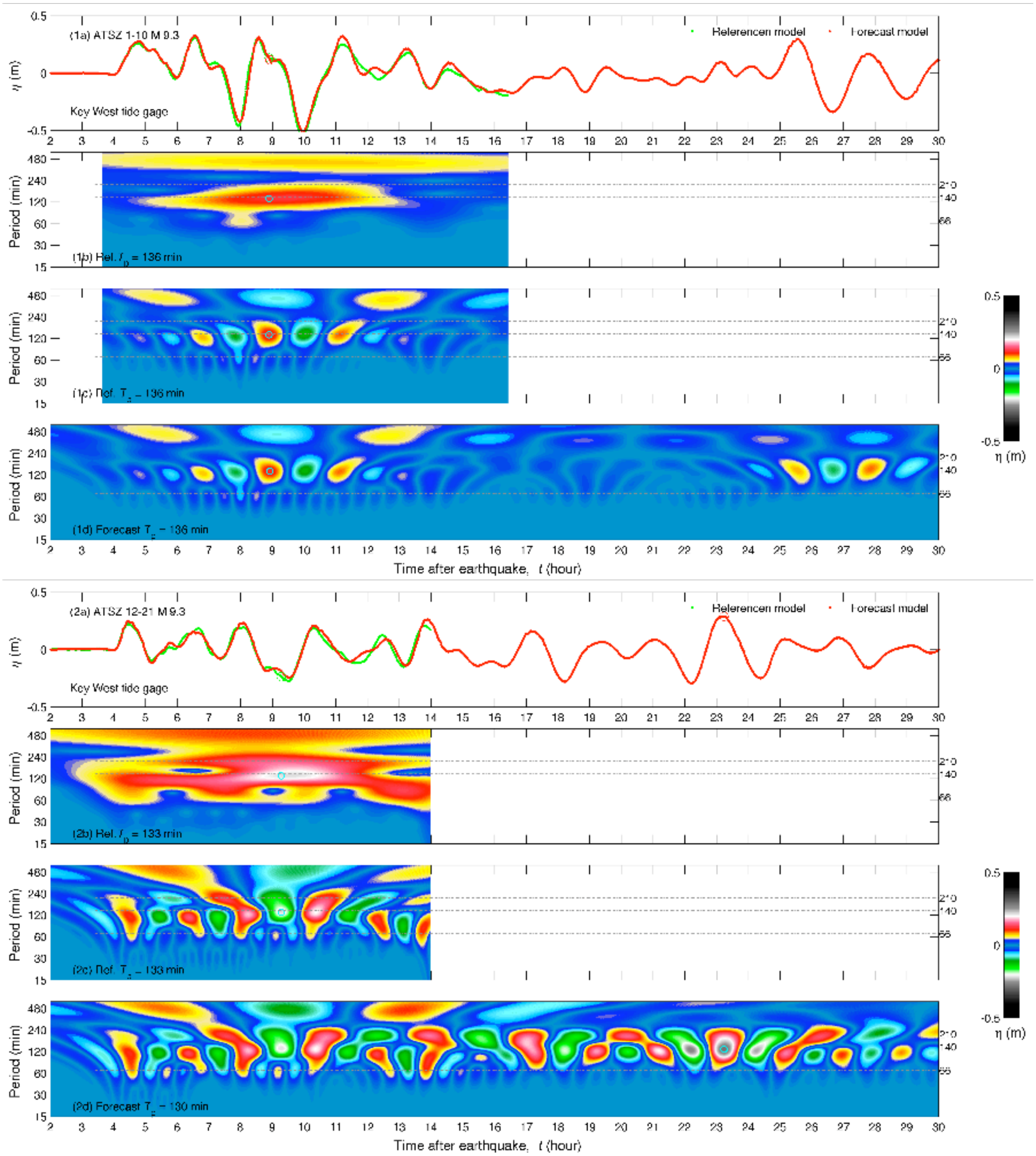

Figure 14: (1-2) (a) Modeled η time series at Key West warning point for the simulated Mw 9.3 tsunamis. (b) Wavelet–derived amplitude spectrogram for the reference model. (c and d) Real part of the spectrograms computed by the reference and forecast models.

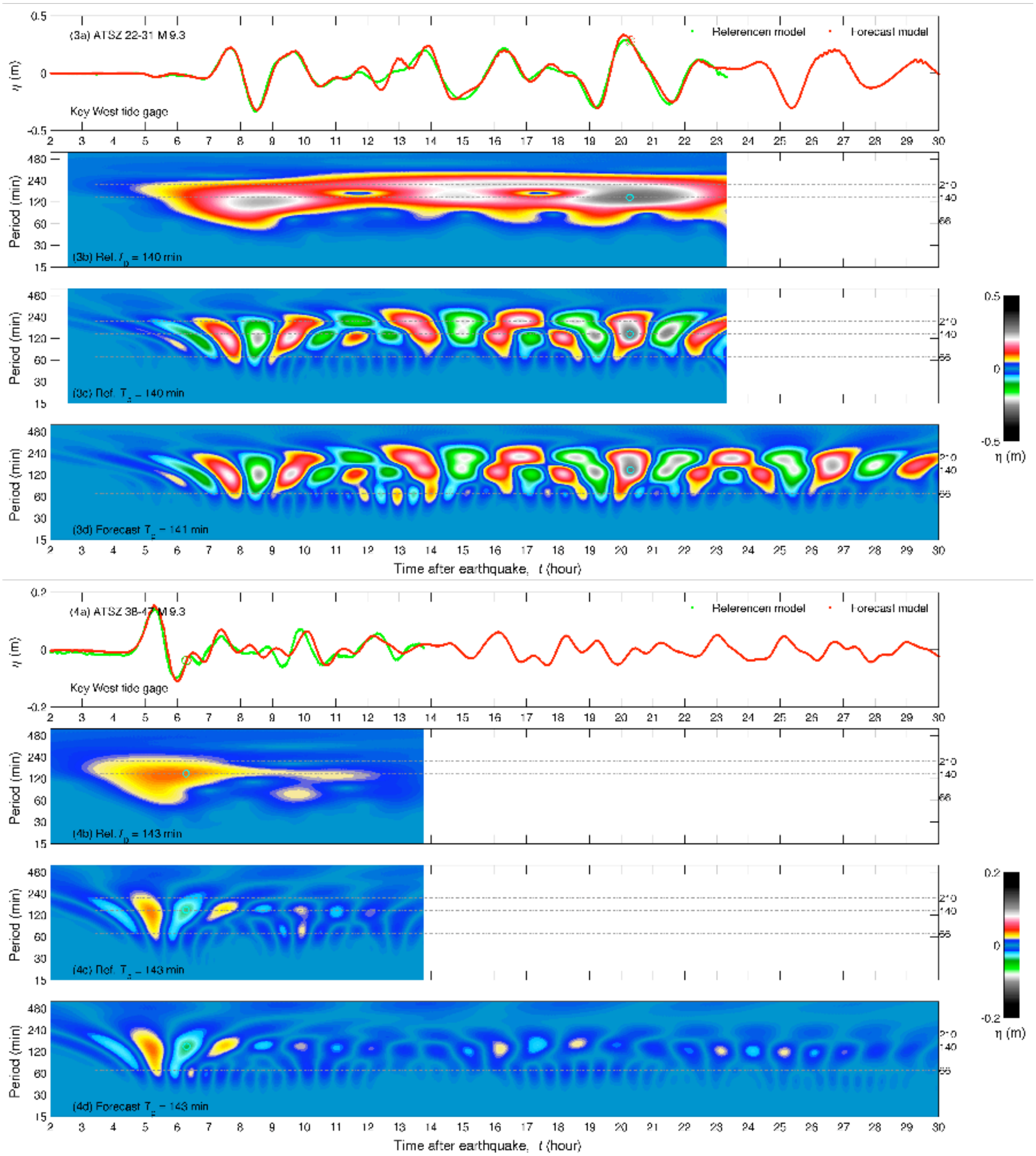

Figure 14 (Continued): (3-4) (a) Modeled η time series at Key West warning point for the simulated Mw 9.3 tsunamis. (b) Wavelet–derived amplitude spectrogram for the reference model. (c and d) Real part of the spectrograms computed by the reference and forecast models.

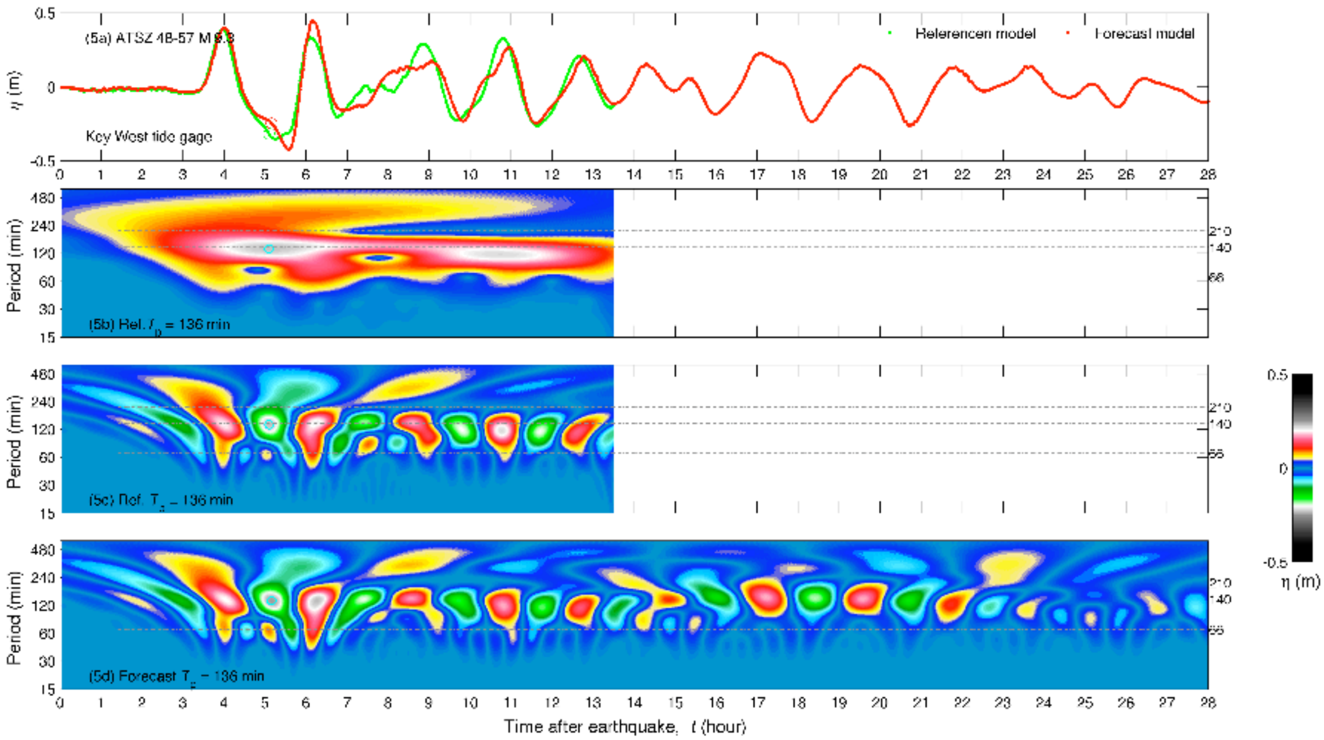

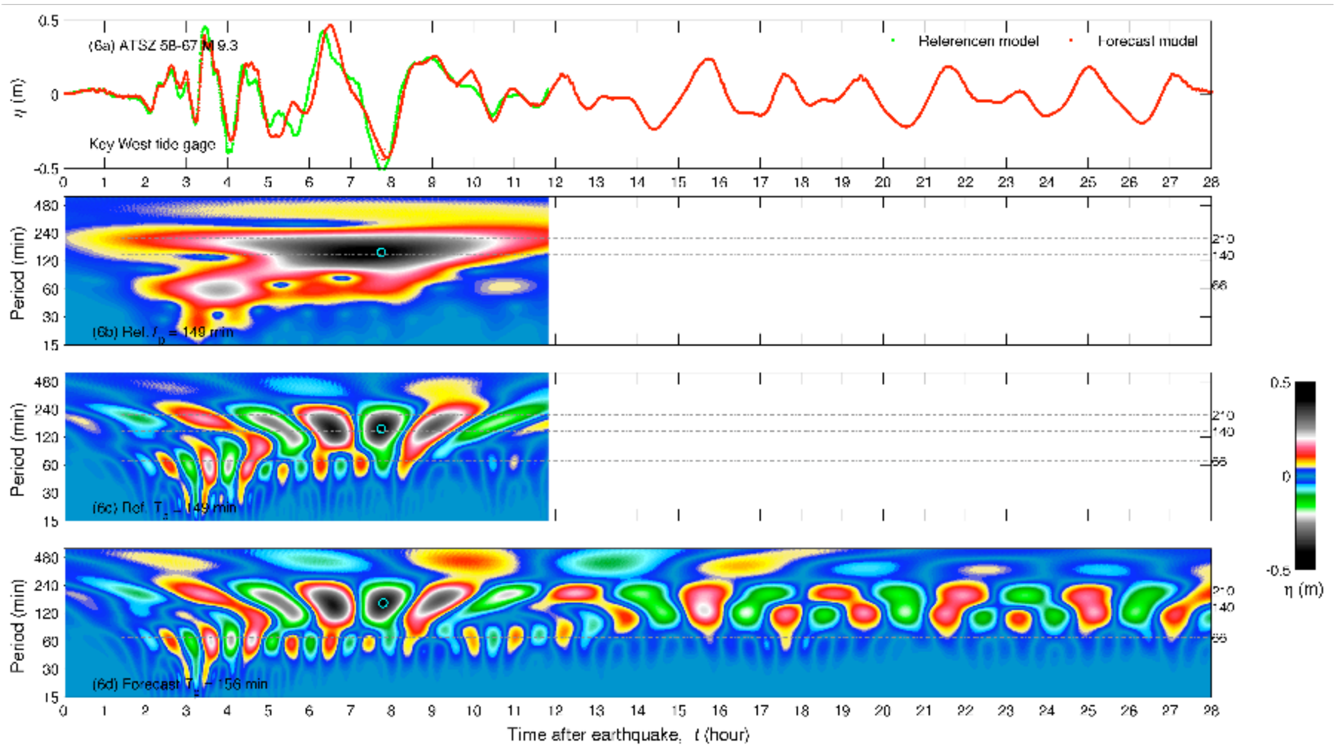

Figure 14 (Continued): (5-6) (a) Modeled η time series at Key West warning point for the simulated Mw 9.3 tsunamis. (b) Wavelet–derived amplitude spectrogram for the reference model. (c and d) Real part of the spectrograms computed by the reference and forecast models.

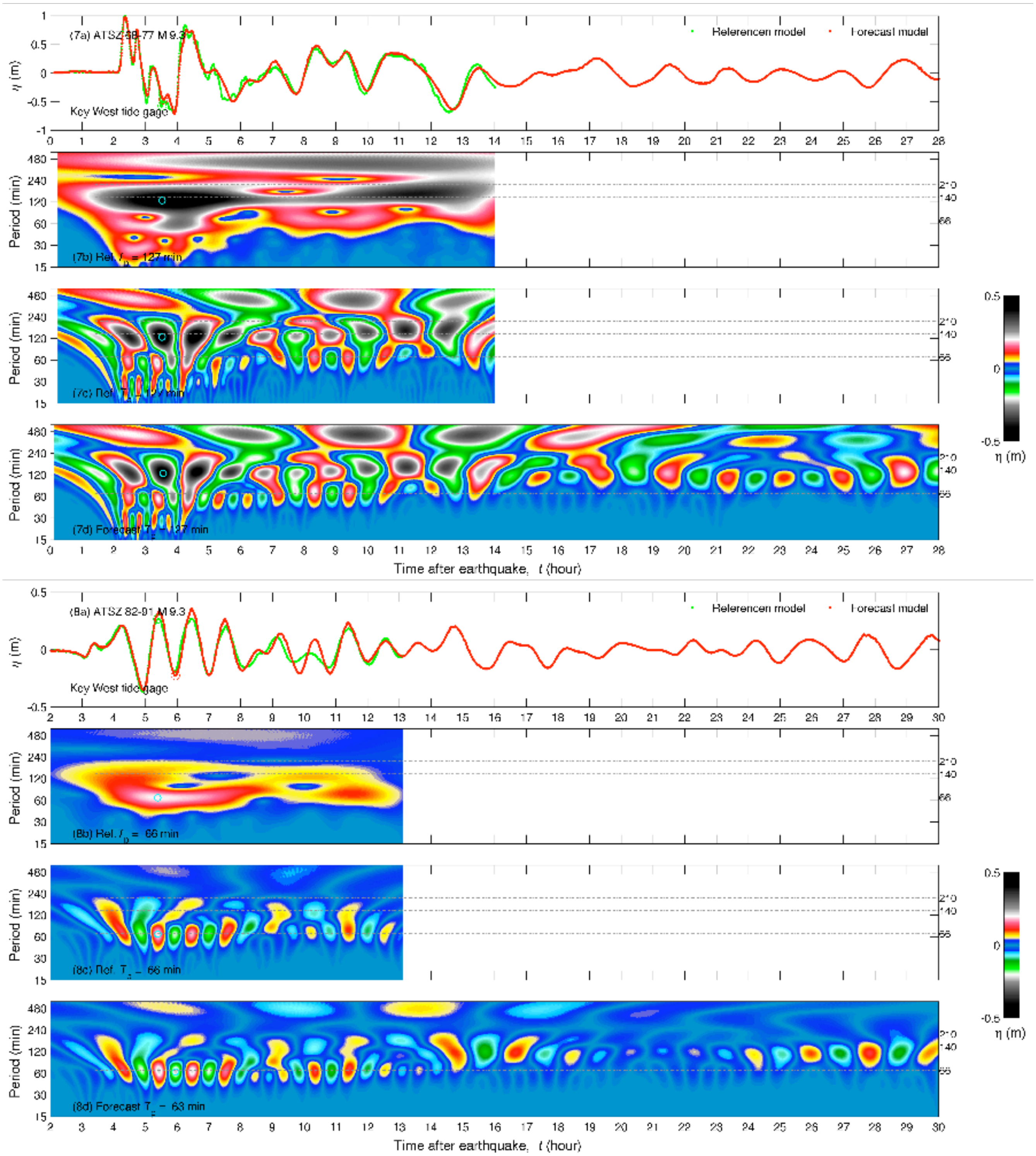

Figure 14 (Continued): (7-8) (a) Modeled η time series at Key West warning point for the simulated Mw 9.3 tsunamis. (b) Wavelet–derived amplitude spectrogram for the reference model. (c and d) Real part of the spectrograms computed by the reference and forecast models.

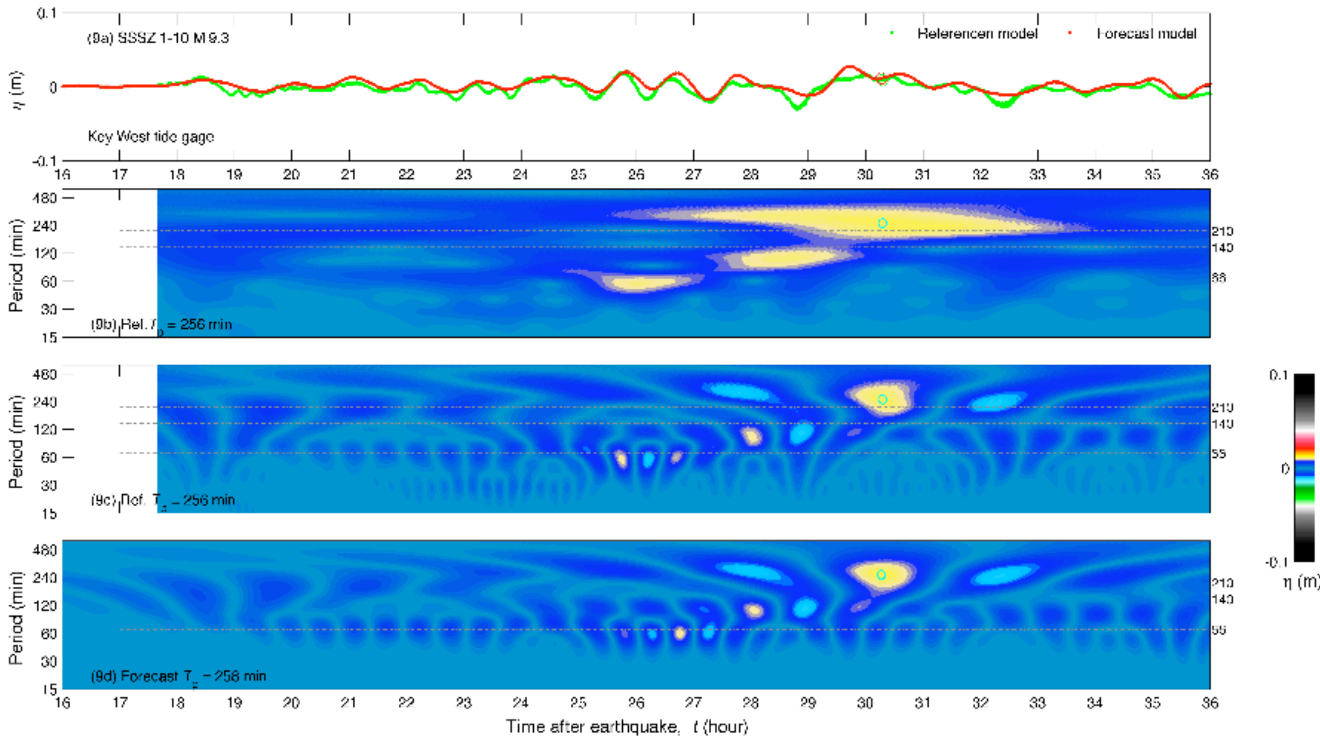

Figure 14 (Continued): (9) (a) Modeled η time series at Key West warning point for the simulated Mw 9.3 tsunamis. (b) Wavelet–derived amplitude spectrogram for the reference model. (c and d) Real part of the spectrograms computed by the reference and forecast models.

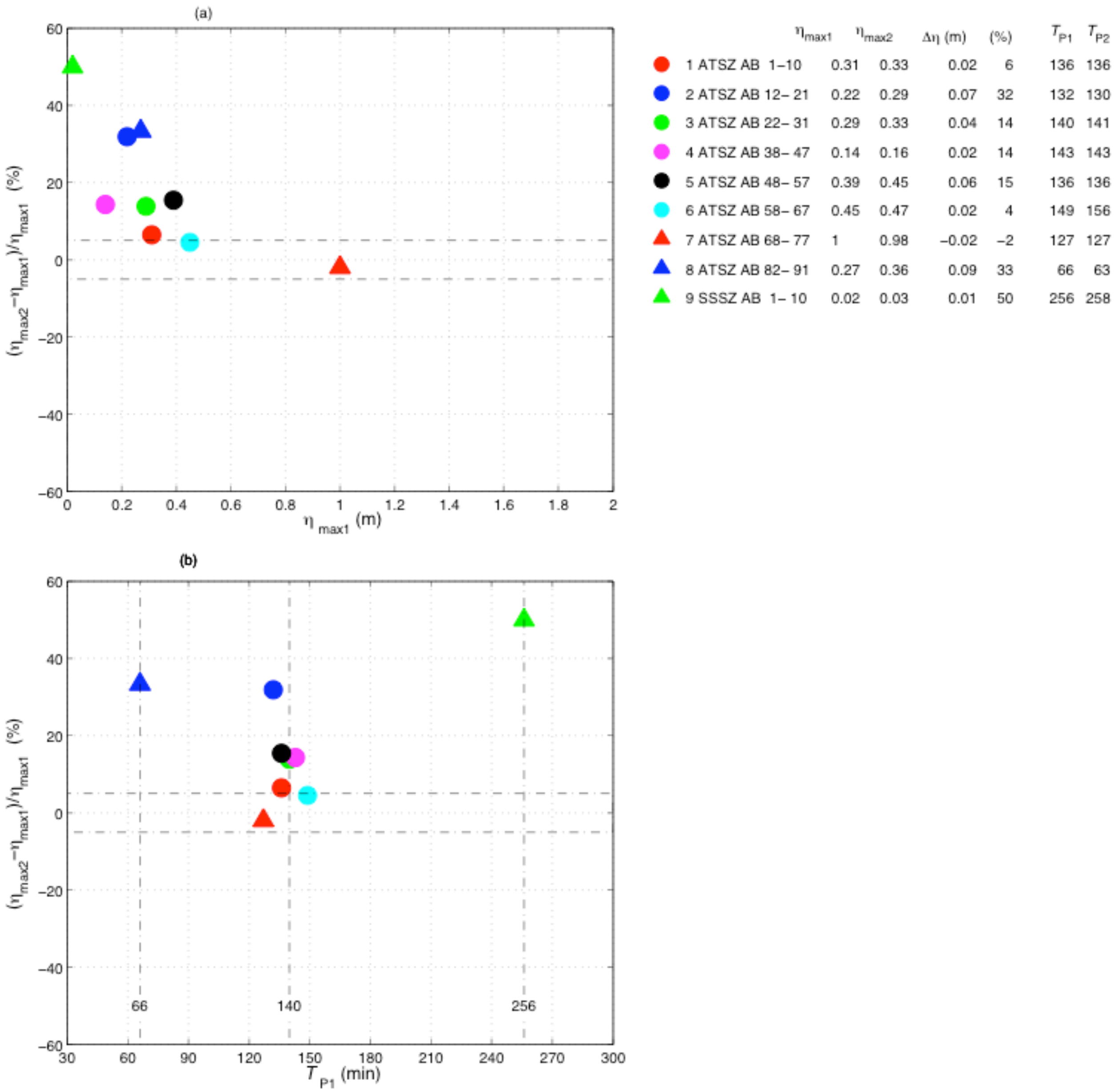

Figure 15: (a) Forecast uncertainty in the η_{max} at the Key West warning point. (b) Uncertainty vs. peak period. η_{max1} and T_{p1}, maximum water elevation and peak period at the warning point from the reference model. η_{max2} and T_{p2}, maximum water surface elevation and peak period at the warning point computed by the forecast model.

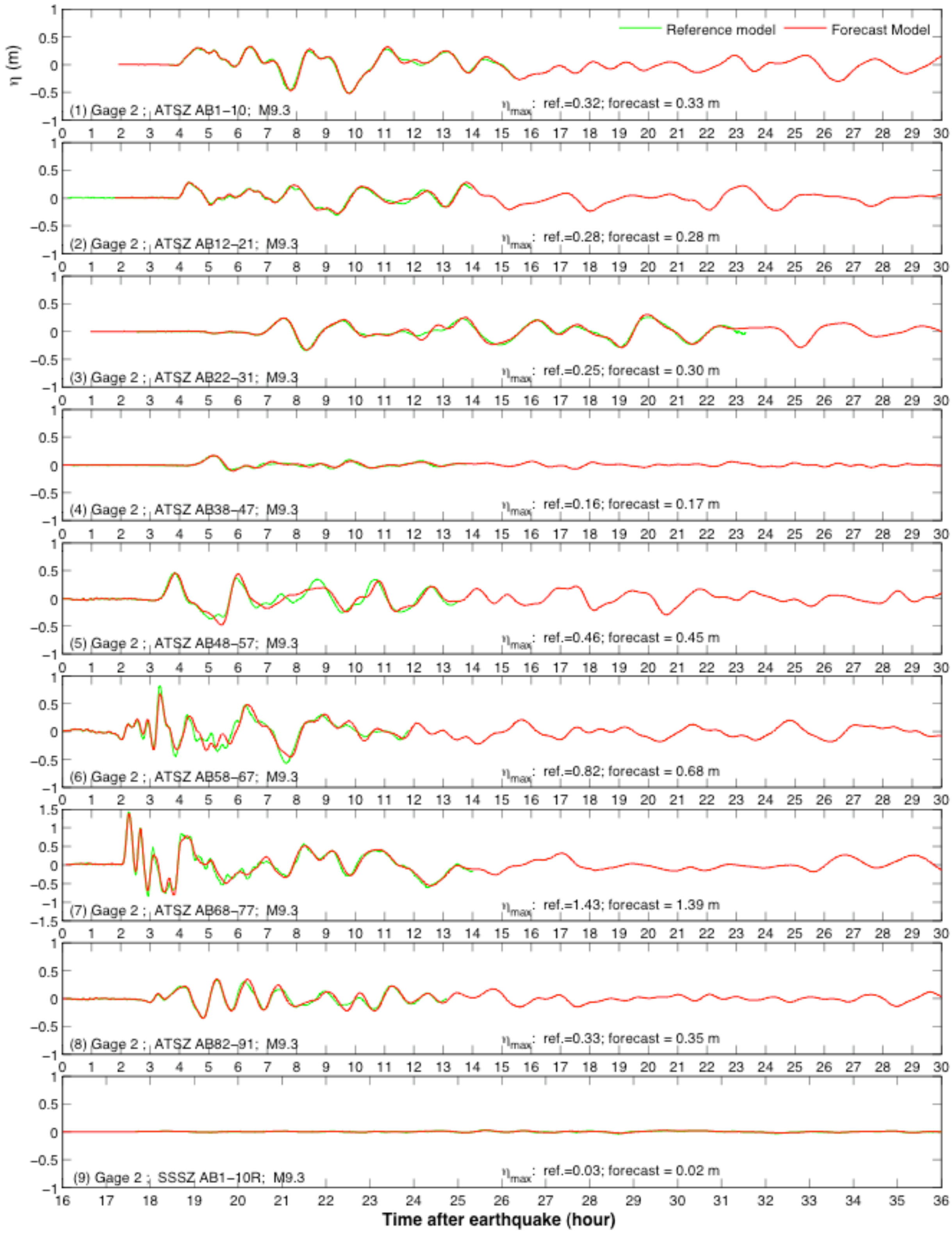

Figure 16 Modeled η time series at virtual gauge 2 by the Key West reference and forecast models fo:r simulated Mw 9.3 tsunamis.

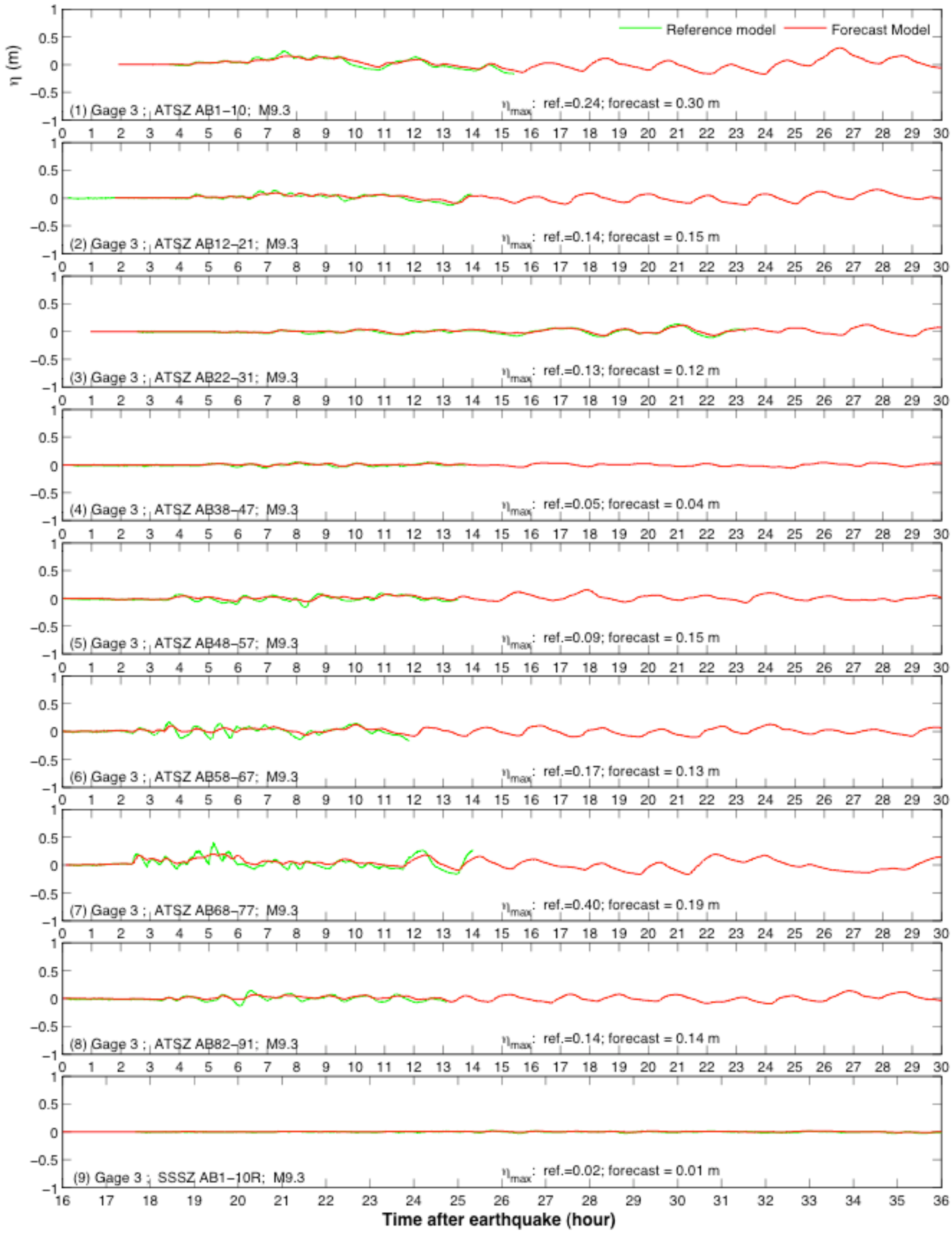

Figure 17: Modeled η time series at virtual gauge 3 by the Key West reference and forecast models for simulated Mw 9.3 tsunamis.

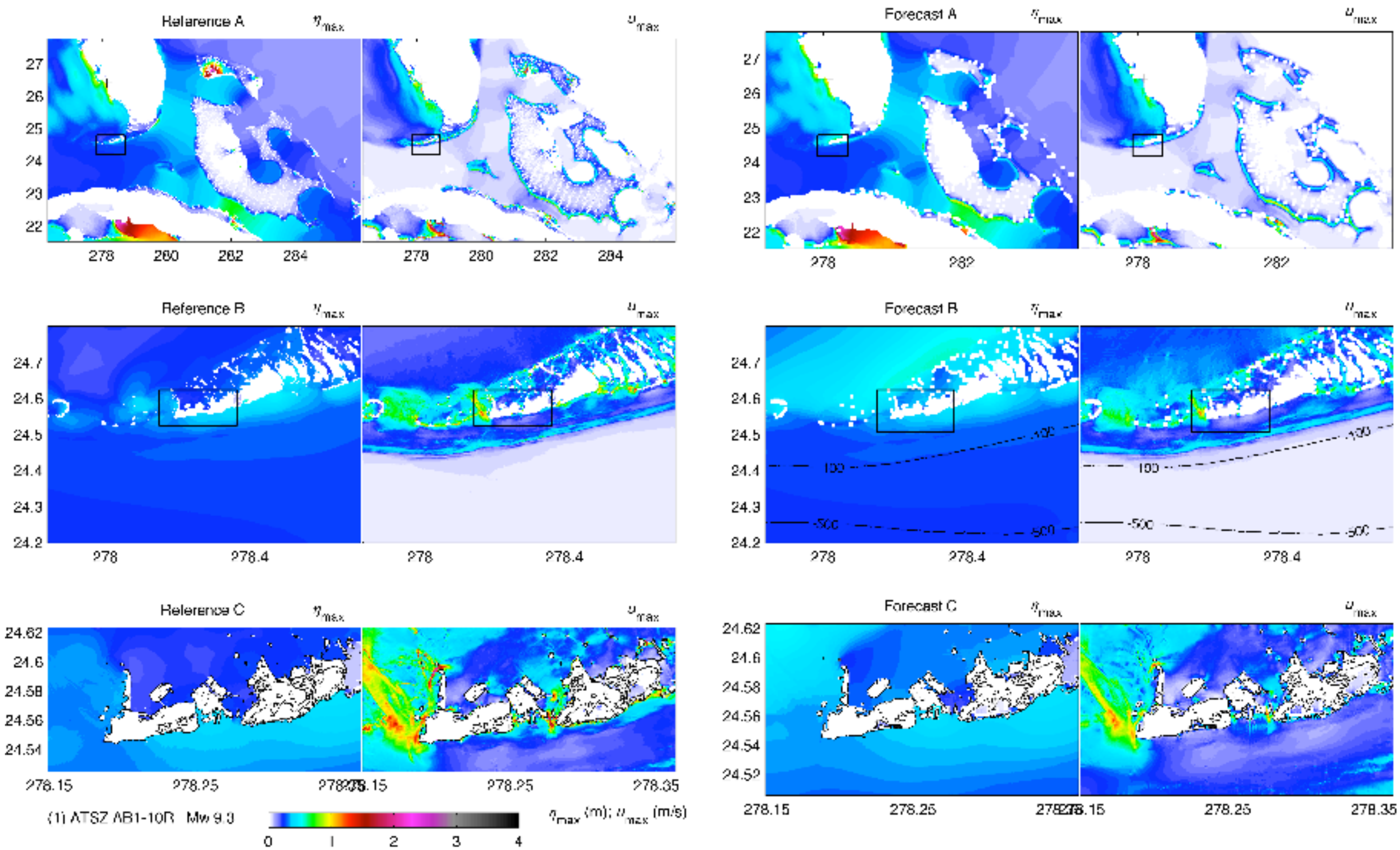

Figure 18: (1): Maximum water elevation and current computed by the Key West reference and forecast models for a simulated M 9.3 tsunami originated from subduction zones near Panama .

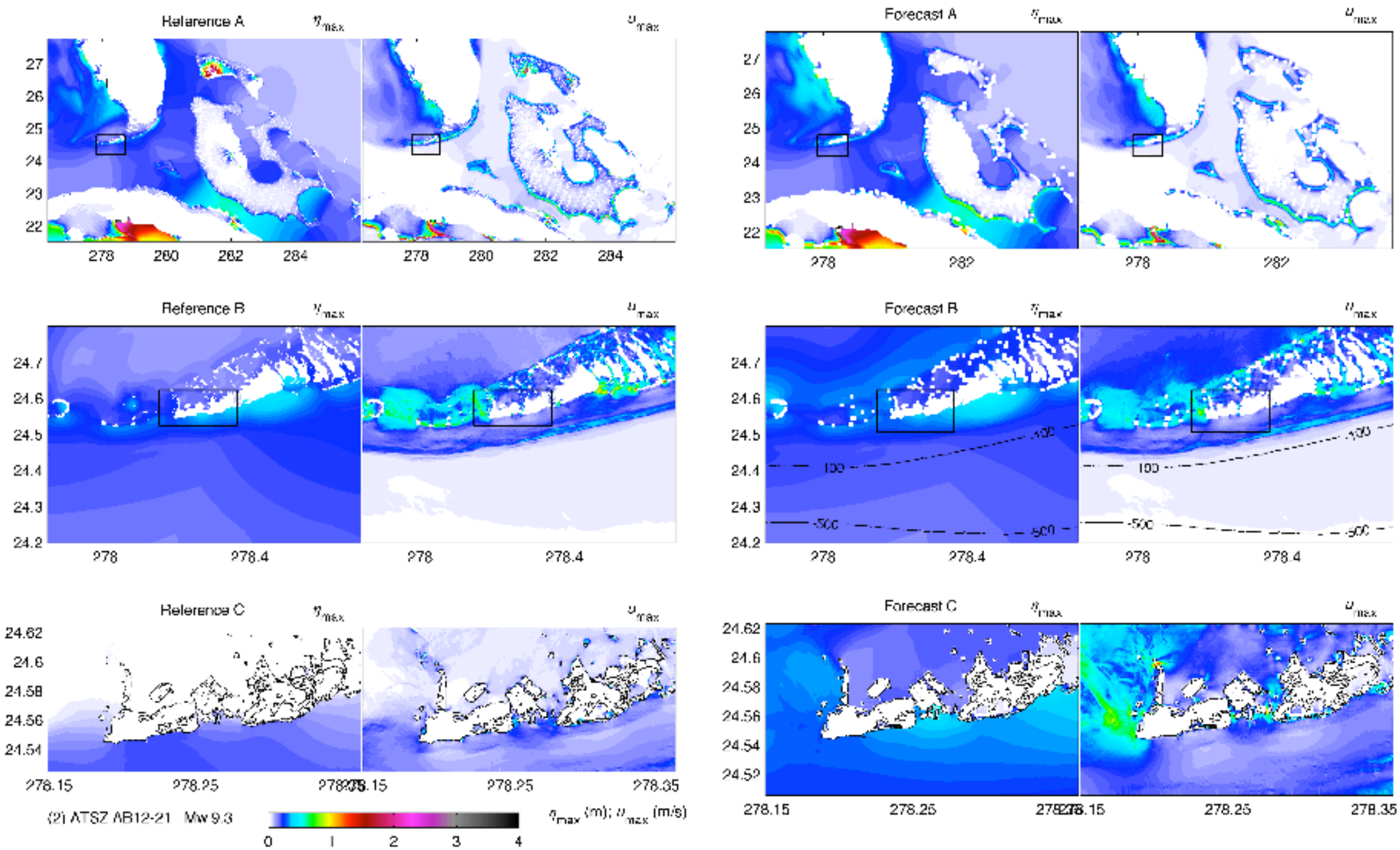

Figure 18 (Continued): (2) Maximum water elevation and current computed by the Key West reference and forecast models for a simulated Mw 9.3 tsunami originated from subduction zones near Colombia.

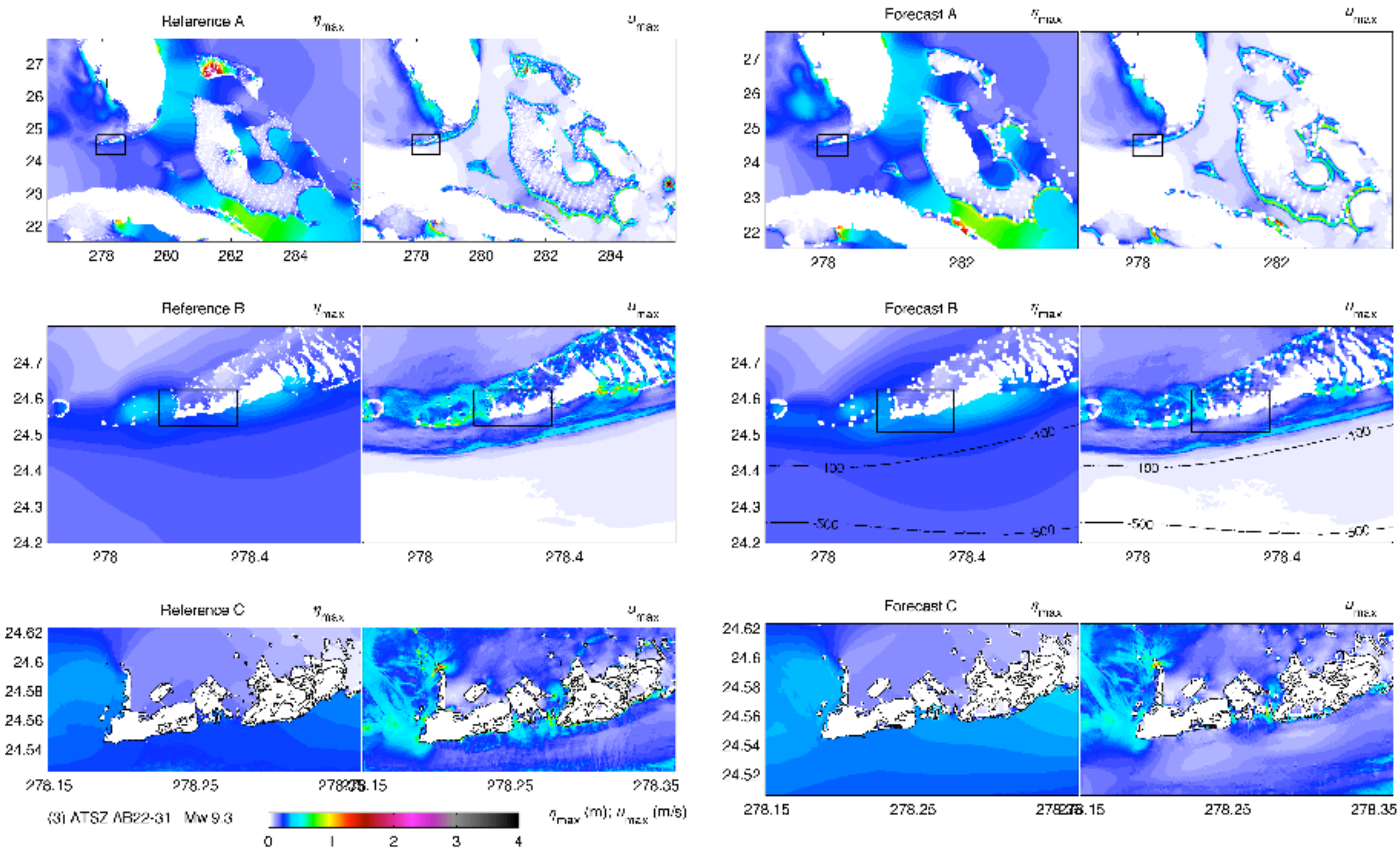

Figure 18 (Continued): (3) Maximum water elevation and current computed by the Key West reference and forecast models for a simulated Mw 9.3 tsunami originated from subduction zones near Venezuela.

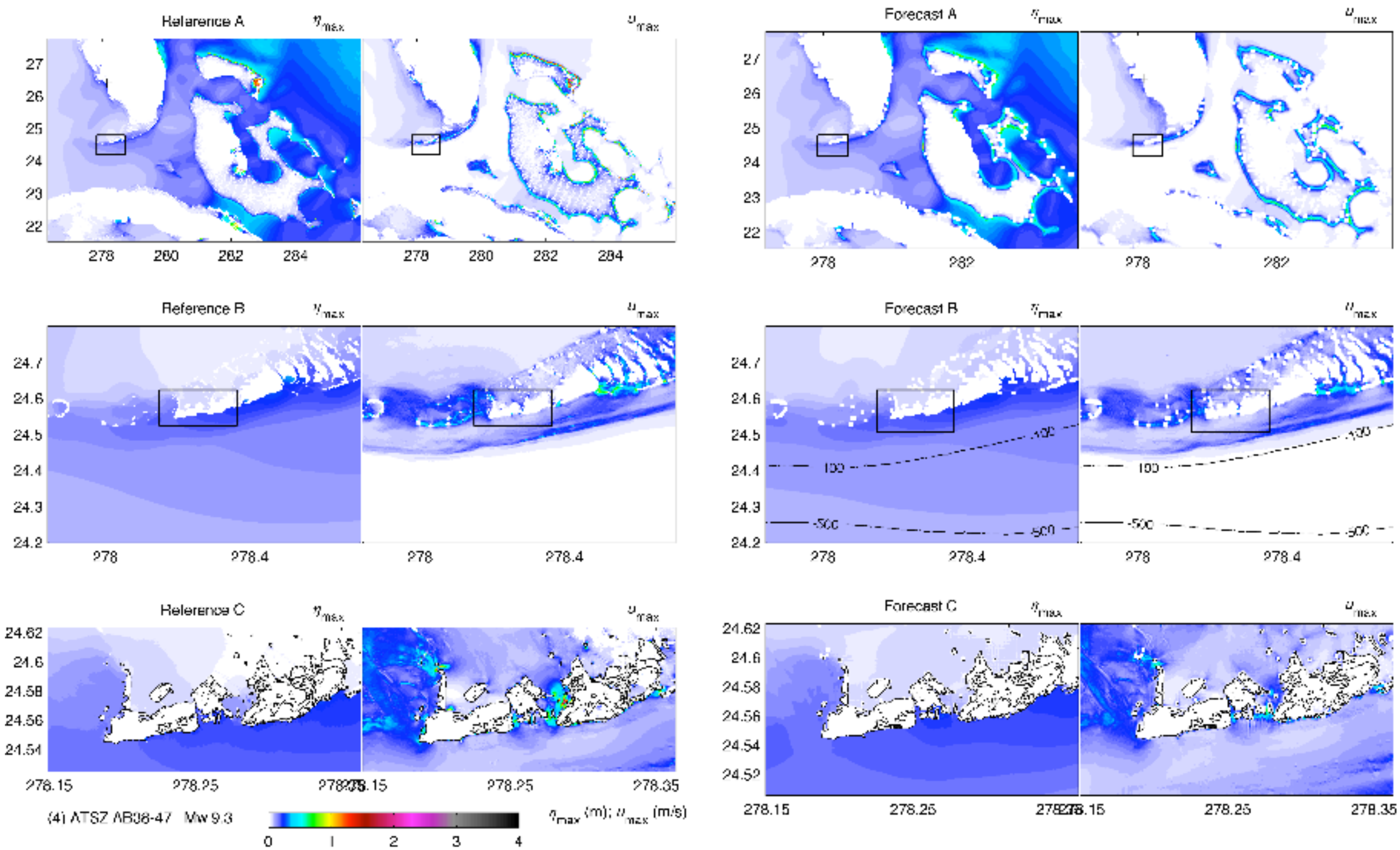

Figure 18 (Continued): (4) Maximum water elevation and current computed by the Key West reference and forecast models for a simulated Mw 9.3 tsunami originated from subduction zones near Dominica.

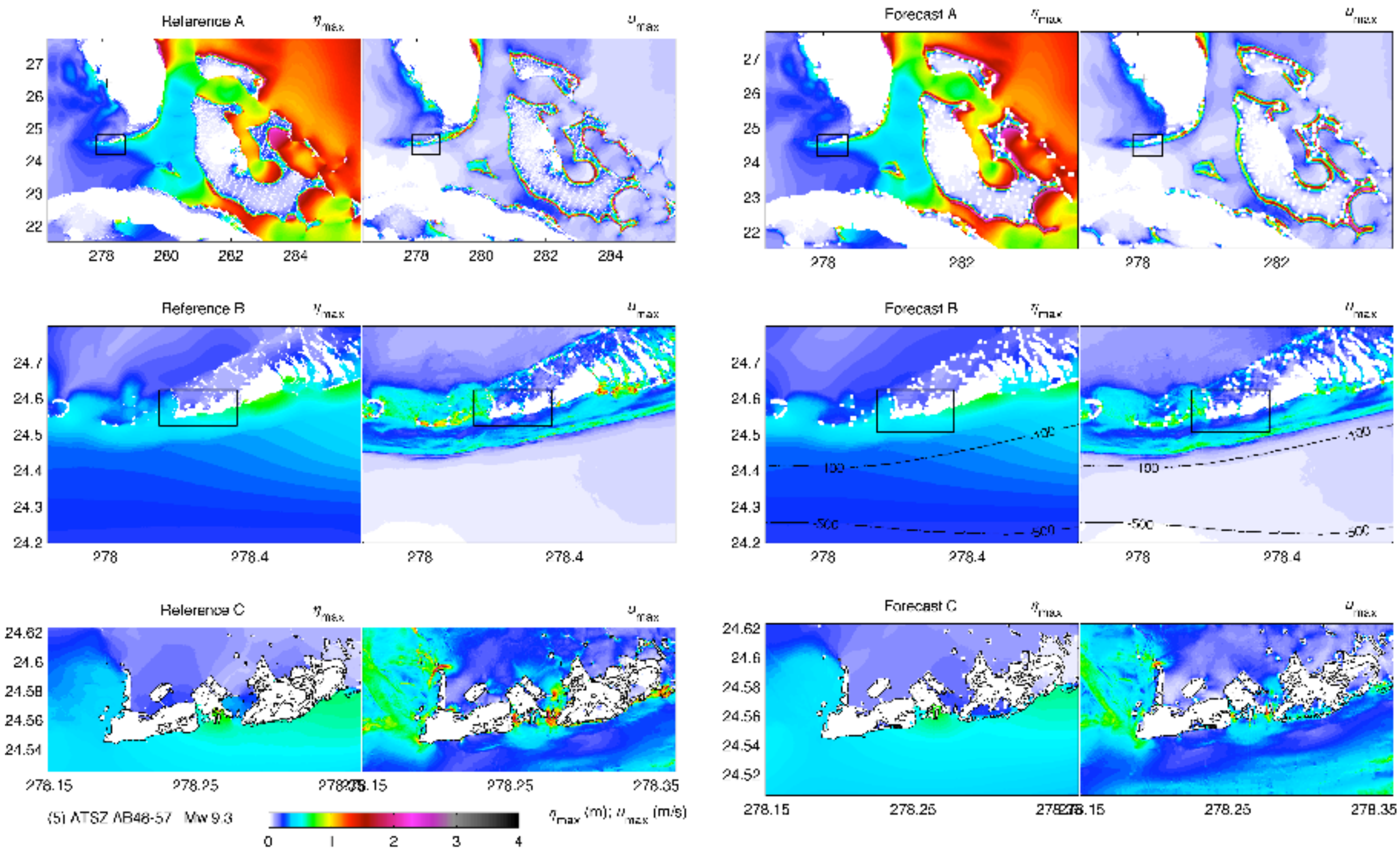

Figure 18 (Continued): (5) Maximum water elevation and current computed by the Key West reference and forecast models for a simulated Mw 9.3 tsunami originated from subduction zones near Puerto Rico.

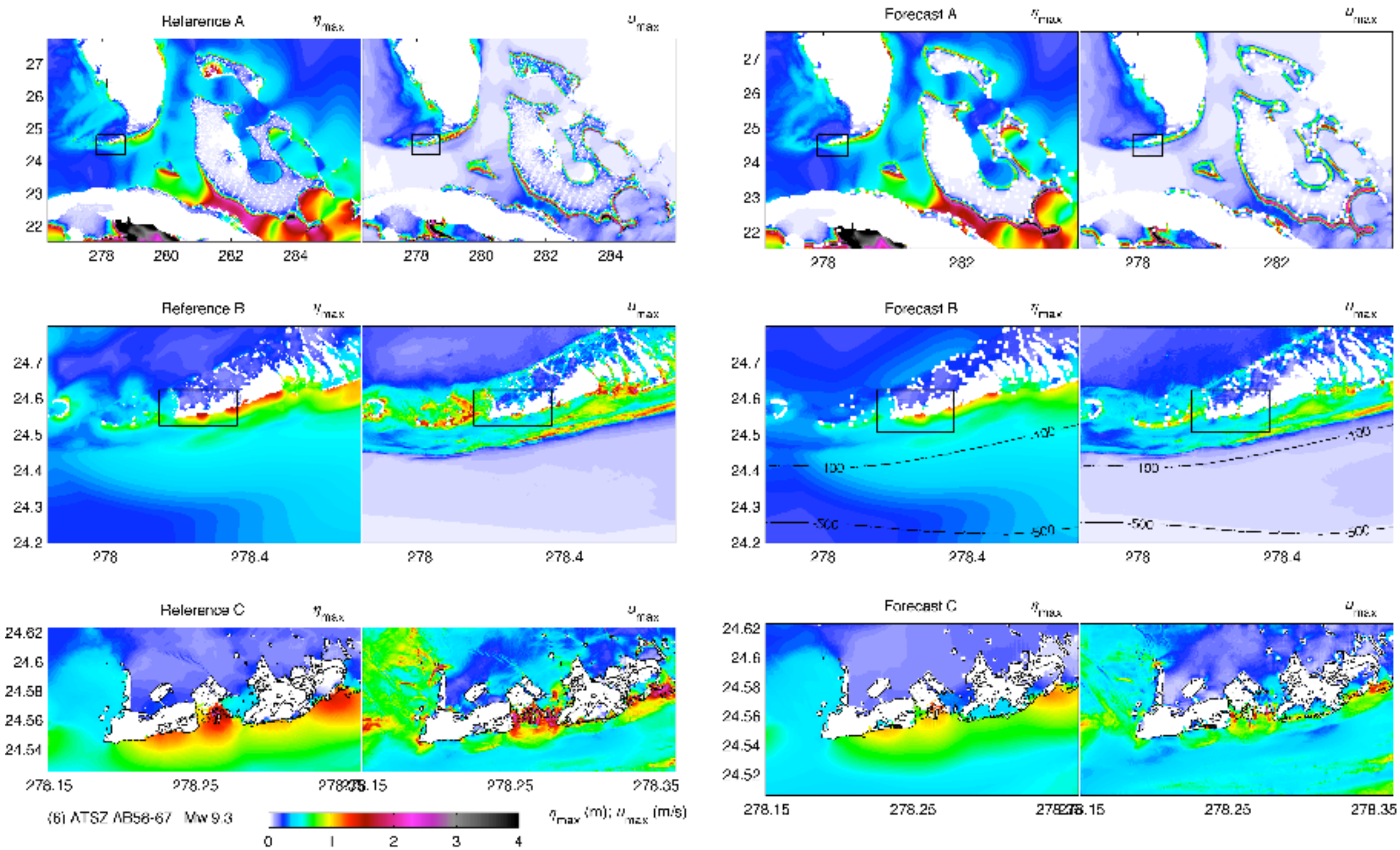

Figure 18 (Continued): (6) Maximum water elevation and current computed by the Key West reference and forecast models for a simulated Mw 9.3 tsunami originated from subduction zones near Cayman.

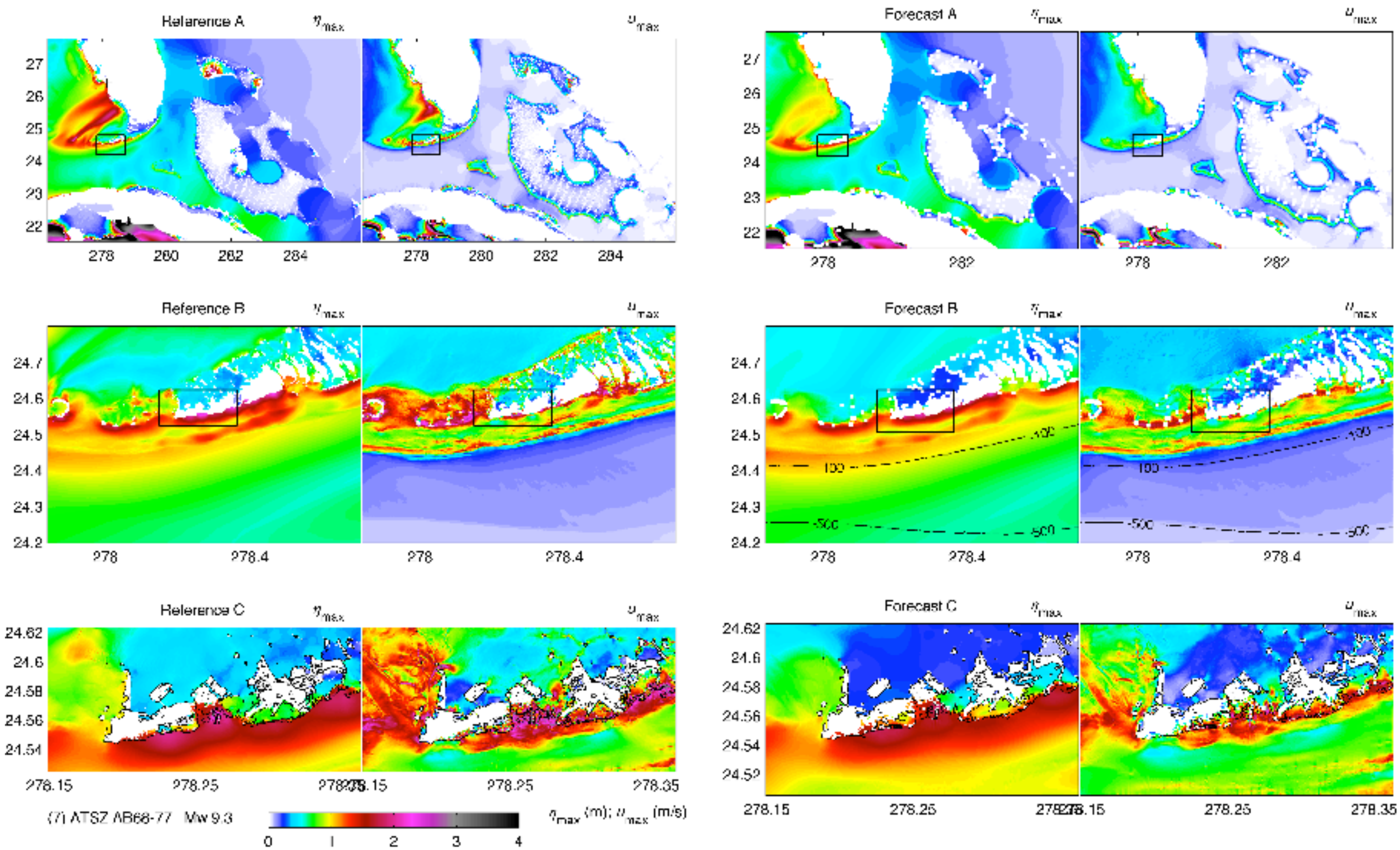

Figure 18 (Continued): (7) Maximum water elevation and current computed by the Key West reference and forecast models for a simulated Mw 9.3 tsunami originated from subduction zones near Gulf of Honduras.

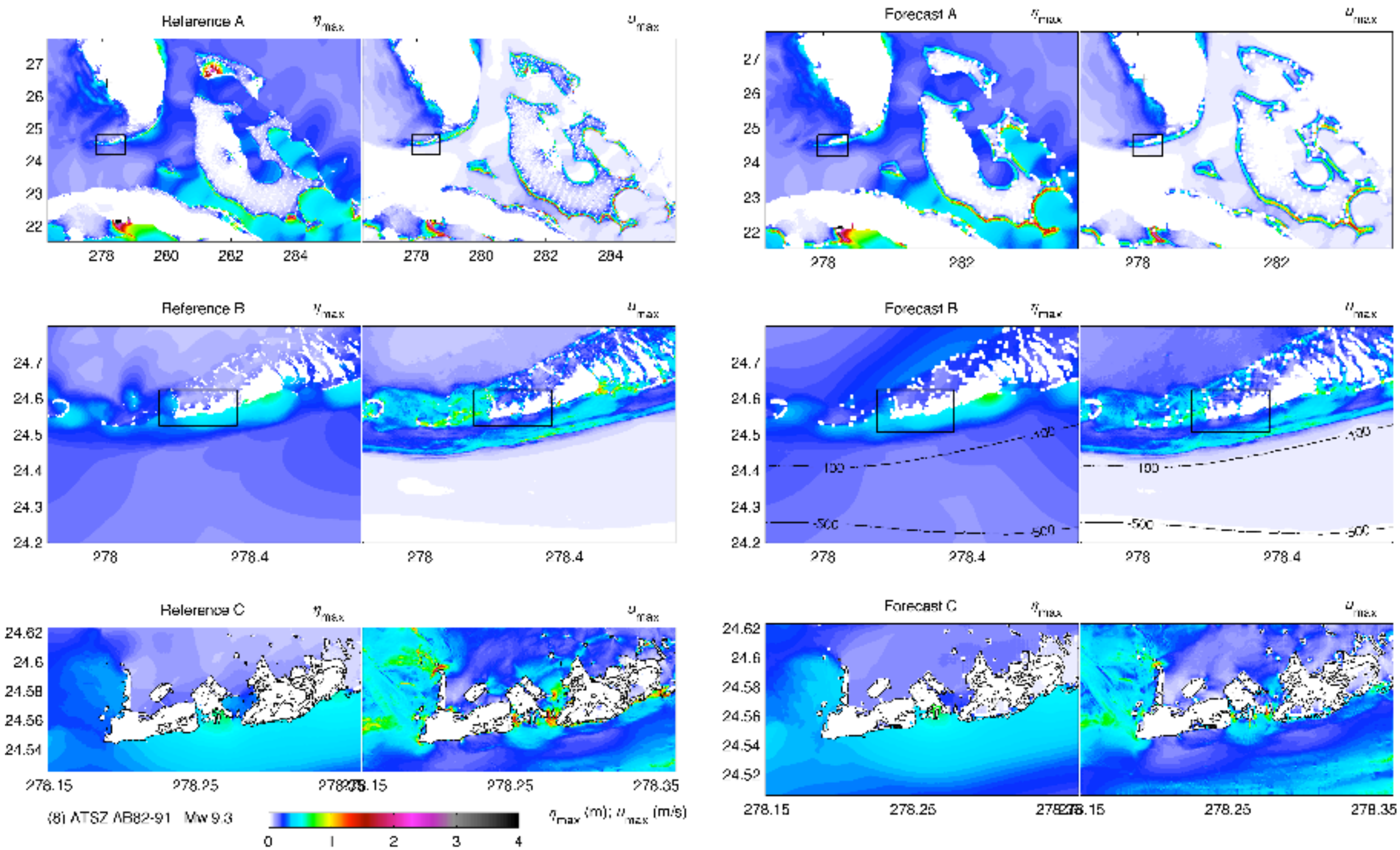

Figure 18 (Continued): (8) Maximum water elevation and current computed by the Key West reference and forecast models for a simulated Mw 9.3 tsunami originated from U.S. Virgin Islands.

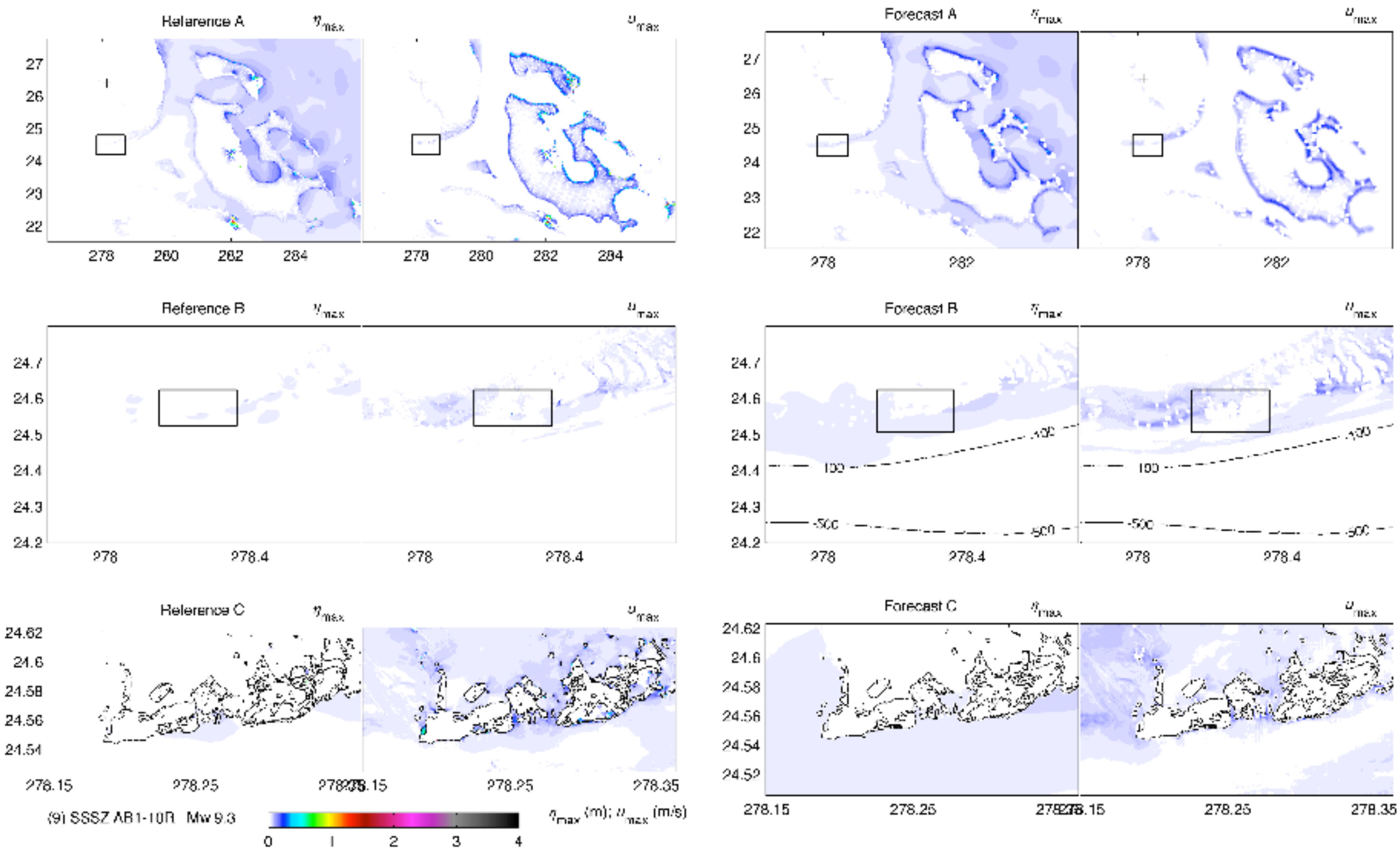

Figure 18 (Continued): (9) Maximum water elevation and current computed by the Key West reference and forecast models for a simulated Mw 9.3 tsunami originated from south Sandwich Island.

Appendix B

Propagation Database: Atlantic Ocean Unit Sources

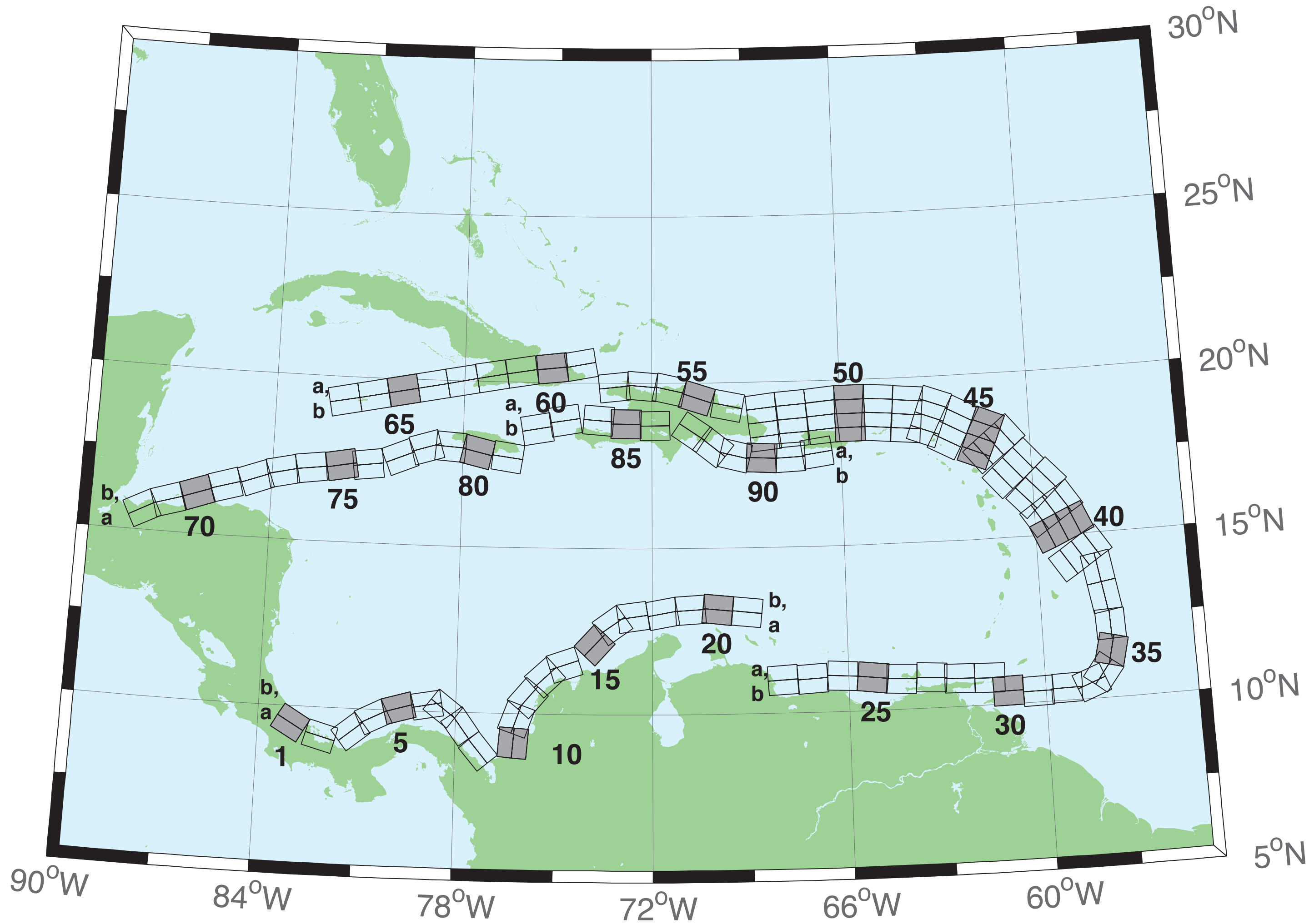

Figure B.1: Atlantic Source Zone unit sources.

Table B.1: Earthquake parameters for Atlantic Source Zone unit sources.

Segment	Description	Longitude(°E)	Latitude(°N)	Strike(°)	Dip(°)	Depth (km)
atsz–1a	Atlantic Source Zone	-83.2020	9.1449	120	27.5	28.09
atsz–1b	Atlantic Source Zone	-83.0000	9.4899	120	27.5	5
atsz–2a	Atlantic Source Zone	-82.1932	8.7408	105.1	27.5	28.09
atsz–2b	Atlantic Source Zone	-82.0880	9.1254	105.1	27.5	5
atsz–3a	Atlantic Source Zone	-80.9172	9.0103	51.31	30	30
atsz–3b	Atlantic Source Zone	-81.1636	9.3139	51.31	30	5
atsz–4a	Atlantic Source Zone	-80.3265	9.4308	63.49	30	30
atsz–4b	Atlantic Source Zone	-80.5027	9.7789	63.49	30	5
atsz–5a	Atlantic Source Zone	-79.6247	9.6961	74.44	30	30
atsz–5b	Atlantic Source Zone	-79.7307	10.0708	74.44	30	5
atsz–6a	Atlantic Source Zone	-78.8069	9.8083	79.71	30	30
atsz–6b	Atlantic Source Zone	-78.8775	10.1910	79.71	30	5
atsz–7a	Atlantic Source Zone	-78.6237	9.7963	127.2	30	30
atsz–7b	Atlantic Source Zone	-78.3845	10.1059	127.2	30	5
atsz–8a	Atlantic Source Zone	-78.1693	9.3544	143.8	30	30
atsz–8b	Atlantic Source Zone	-77.8511	9.5844	143.8	30	5
atsz–9a	Atlantic Source Zone	-77.5913	8.5989	139.9	30	30
atsz–9b	Atlantic Source Zone	-77.2900	8.8493	139.9	30	5
atsz–10a	Atlantic Source Zone	-75.8109	9.0881	4.67	17	19.62
atsz–10b	Atlantic Source Zone	-76.2445	9.1231	4.67	17	5
atsz–11a	Atlantic Source Zone	-75.7406	9.6929	19.67	17	19.62
atsz–11b	Atlantic Source Zone	-76.1511	9.8375	19.67	17	5
atsz–12a	Atlantic Source Zone	-75.4763	10.2042	40.4	17	19.62
atsz–12b	Atlantic Source Zone	-75.8089	10.4826	40.4	17	5
atsz–13a	Atlantic Source Zone	-74.9914	10.7914	47.17	17	19.62
atsz–13b	Atlantic Source Zone	-75.2890	11.1064	47.17	17	5
atsz–14a	Atlantic Source Zone	-74.5666	11.0708	71.68	17	19.62
atsz–14b	Atlantic Source Zone	-74.7043	11.4786	71.68	17	5
atsz–15a	Atlantic Source Zone	-73.4576	11.8012	42.69	17	19.62
atsz–15b	Atlantic Source Zone	-73.7805	12.0924	42.69	17	5
atsz–16a	Atlantic Source Zone	-72.9788	12.3365	54.75	17	19.62
atsz–16b	Atlantic Source Zone	-73.2329	12.6873	54.75	17	5
atsz–17a	Atlantic Source Zone	-72.5454	12.5061	81.96	17	19.62
atsz–17b	Atlantic Source Zone	-72.6071	12.9314	81.96	17	5
atsz–18a	Atlantic Source Zone	-71.6045	12.6174	79.63	17	19.62
atsz–18b	Atlantic Source Zone	-71.6839	13.0399	79.63	17	5
atsz–19a	Atlantic Source Zone	-70.7970	12.7078	86.32	17	19.62
atsz–19b	Atlantic Source Zone	-70.8253	13.1364	86.32	17	5
atsz–20a	Atlantic Source Zone	-70.0246	12.7185	95.94	17	19.62
atsz–20b	Atlantic Source Zone	-69.9789	13.1457	95.94	17	5
atsz–21a	Atlantic Source Zone	-69.1244	12.6320	95.94	17	19.62
atsz–21b	Atlantic Source Zone	-69.0788	13.0592	95.94	17	5
atsz–22a	Atlantic Source Zone	-68.0338	11.4286	266.9	15	17.94
atsz–22b	Atlantic Source Zone	-68.0102	10.9954	266.9	15	5
atsz–23a	Atlantic Source Zone	-67.1246	11.4487	266.9	15	17.94
atsz–23b	Atlantic Source Zone	-67.1010	11.0155	266.9	15	5
atsz–24a	Atlantic Source Zone	-66.1656	11.5055	273.3	15	17.94
atsz–24b	Atlantic Source Zone	-66.1911	11.0724	273.3	15	5
atsz–25a	Atlantic Source Zone	-65.2126	11.4246	276.4	15	17.94
atsz–25b	Atlantic Source Zone	-65.2616	10.9934	276.4	15	5
atsz–26a	Atlantic Source Zone	-64.3641	11.3516	272.9	15	17.94
atsz–26b	Atlantic Source Zone	-64.3862	10.9183	272.9	15	5
atsz–27a	Atlantic Source Zone	-63.4472	11.3516	272.9	15	17.94

Continued on next page

Table B.1 – continued from previous page

Segment	Description	Longitude(°E)	Latitude(°N)	Strike(°)	Dip(°)	Depth (km)
atsz–27b	Atlantic Source Zone	-63.4698	10.9183	272.9	15	5
atsz–28a	Atlantic Source Zone	-62.6104	11.2831	271.1	15	17.94
atsz–28b	Atlantic Source Zone	-62.6189	10.8493	271.1	15	5
atsz–29a	Atlantic Source Zone	-61.6826	11.2518	271.6	15	17.94
atsz–29b	Atlantic Source Zone	-61.6947	10.8181	271.6	15	5
atsz–30a	Atlantic Source Zone	-61.1569	10.8303	269	15	17.94
atsz–30b	Atlantic Source Zone	-61.1493	10.3965	269	15	5
atsz–31a	Atlantic Source Zone	-60.2529	10.7739	269	15	17.94
atsz–31b	Atlantic Source Zone	-60.2453	10.3401	269	15	5
atsz–32a	Atlantic Source Zone	-59.3510	10.8123	269	15	17.94
atsz–32b	Atlantic Source Zone	-59.3734	10.3785	269	15	5
atsz–33a	Atlantic Source Zone	-58.7592	10.8785	248.6	15	17.94
atsz–33b	Atlantic Source Zone	-58.5984	10.4745	248.6	15	5
atsz–34a	Atlantic Source Zone	-58.5699	11.0330	217.2	15	17.94
atsz–34b	Atlantic Source Zone	-58.2179	10.7710	217.2	15	5
atsz–35a	Atlantic Source Zone	-58.3549	11.5300	193.7	15	17.94
atsz–35b	Atlantic Source Zone	-57.9248	11.4274	193.7	15	5
atsz–36a	Atlantic Source Zone	-58.3432	12.1858	177.7	15	17.94
atsz–36b	Atlantic Source Zone	-57.8997	12.2036	177.7	15	5
atsz–37a	Atlantic Source Zone	-58.4490	12.9725	170.7	15	17.94
atsz–37b	Atlantic Source Zone	-58.0095	13.0424	170.7	15	5
atsz–38a	Atlantic Source Zone	-58.6079	13.8503	170.2	15	17.94
atsz–38b	Atlantic Source Zone	-58.1674	13.9240	170.2	15	5
atsz–39a	Atlantic Source Zone	-58.6667	14.3915	146.8	15	17.94
atsz–39b	Atlantic Source Zone	-58.2913	14.6287	146.8	15	5
atsz–39y	Atlantic Source Zone	-59.4168	13.9171	146.8	15	43.82
atsz–39z	Atlantic Source Zone	-59.0415	14.1543	146.8	15	30.88
atsz–40a	Atlantic Source Zone	-59.1899	15.2143	156.2	15	17.94
atsz–40b	Atlantic Source Zone	-58.7781	15.3892	156.2	15	5
atsz–40y	Atlantic Source Zone	-60.0131	14.8646	156.2	15	43.82
atsz–40z	Atlantic Source Zone	-59.6012	15.0395	156.2	15	30.88
atsz–41a	Atlantic Source Zone	-59.4723	15.7987	146.3	15	17.94
atsz–41b	Atlantic Source Zone	-59.0966	16.0392	146.3	15	5
atsz–41y	Atlantic Source Zone	-60.2229	15.3177	146.3	15	43.82
atsz–41z	Atlantic Source Zone	-59.8473	15.5582	146.3	15	30.88
atsz–42a	Atlantic Source Zone	-59.9029	16.4535	137	15	17.94
atsz–42b	Atlantic Source Zone	-59.5716	16.7494	137	15	5
atsz–42y	Atlantic Source Zone	-60.5645	15.8616	137	15	43.82
atsz–42z	Atlantic Source Zone	-60.2334	16.1575	137	15	30.88
atsz–43a	Atlantic Source Zone	-60.5996	17.0903	138.7	15	17.94
atsz–43b	Atlantic Source Zone	-60.2580	17.3766	138.7	15	5
atsz–43y	Atlantic Source Zone	-61.2818	16.5177	138.7	15	43.82
atsz–43z	Atlantic Source Zone	-60.9404	16.8040	138.7	15	30.88
atsz–44a	Atlantic Source Zone	-61.1559	17.8560	141.1	15	17.94
atsz–44b	Atlantic Source Zone	-60.8008	18.1286	141.1	15	5
atsz–44y	Atlantic Source Zone	-61.8651	17.3108	141.1	15	43.82
atsz–44z	Atlantic Source Zone	-61.5102	17.5834	141.1	15	30.88
atsz–45a	Atlantic Source Zone	-61.5491	18.0566	112.8	15	17.94
atsz–45b	Atlantic Source Zone	-61.3716	18.4564	112.8	15	5
atsz–45y	Atlantic Source Zone	-61.9037	17.2569	112.8	15	43.82
atsz–45z	Atlantic Source Zone	-61.7260	17.6567	112.8	15	30.88
atsz–46a	Atlantic Source Zone	-62.4217	18.4149	117.9	15	17.94
atsz–46b	Atlantic Source Zone	-62.2075	18.7985	117.9	15	5
atsz–46y	Atlantic Source Zone	-62.8493	17.6477	117.9	15	43.82
atsz–46z	Atlantic Source Zone	-62.6352	18.0313	117.9	15	30.88

Continued on next page

Table B.1 – continued from previous page

Segment	Description	Longitude(°E)	Latitude(°N)	Strike(°)	Dip(°)	Depth (km)
atsz–47a	Atlantic Source Zone	-63.1649	18.7844	110.5	20	22.1
atsz–47b	Atlantic Source Zone	-63.0087	19.1798	110.5	20	5
atsz–47y	Atlantic Source Zone	-63.4770	17.9936	110.5	20	56.3
atsz–47z	Atlantic Source Zone	-63.3205	18.3890	110.5	20	39.2
atsz–48a	Atlantic Source Zone	-63.8800	18.8870	95.37	20	22.1
atsz–48b	Atlantic Source Zone	-63.8382	19.3072	95.37	20	5
atsz–48y	Atlantic Source Zone	-63.9643	18.0465	95.37	20	56.3
atsz–48z	Atlantic Source Zone	-63.9216	18.4667	95.37	20	39.2
atsz–49a	Atlantic Source Zone	-64.8153	18.9650	94.34	20	22.1
atsz–49b	Atlantic Source Zone	-64.7814	19.3859	94.34	20	5
atsz–49y	Atlantic Source Zone	-64.8840	18.1233	94.34	20	56.3
atsz–49z	Atlantic Source Zone	-64.8492	18.5442	94.34	20	39.2
atsz–50a	Atlantic Source Zone	-65.6921	18.9848	89.59	20	22.1
atsz–50b	Atlantic Source Zone	-65.6953	19.4069	89.59	20	5
atsz–50y	Atlantic Source Zone	-65.6874	18.1407	89.59	20	56.3
atsz–50z	Atlantic Source Zone	-65.6887	18.5628	89.59	20	39.2
atsz–51a	Atlantic Source Zone	-66.5742	18.9484	84.98	20	22.1
atsz–51b	Atlantic Source Zone	-66.6133	19.3688	84.98	20	5
atsz–51y	Atlantic Source Zone	-66.4977	18.1076	84.98	20	56.3
atsz–51z	Atlantic Source Zone	-66.5353	18.5280	84.98	20	39.2
atsz–52a	Atlantic Source Zone	-67.5412	18.8738	85.87	20	22.1
atsz–52b	Atlantic Source Zone	-67.5734	19.2948	85.87	20	5
atsz–52y	Atlantic Source Zone	-67.4781	18.0319	85.87	20	56.3
atsz–52z	Atlantic Source Zone	-67.5090	18.4529	85.87	20	39.2
atsz–53a	Atlantic Source Zone	-68.4547	18.7853	83.64	20	22.1
atsz–53b	Atlantic Source Zone	-68.5042	19.2048	83.64	20	5
atsz–53y	Atlantic Source Zone	-68.3575	17.9463	83.64	20	56.3
atsz–53z	Atlantic Source Zone	-68.4055	18.3658	83.64	20	39.2
atsz–54a	Atlantic Source Zone	-69.6740	18.8841	101.5	20	22.1
atsz–54b	Atlantic Source Zone	-69.5846	19.2976	101.5	20	5
atsz–55a	Atlantic Source Zone	-70.7045	19.1376	108.2	20	22.1
atsz–55b	Atlantic Source Zone	-70.5647	19.5386	108.2	20	5
atsz–56a	Atlantic Source Zone	-71.5368	19.3853	102.6	20	22.1
atsz–56b	Atlantic Source Zone	-71.4386	19.7971	102.6	20	5
atsz–57a	Atlantic Source Zone	-72.3535	19.4838	94.2	20	22.1
atsz–57b	Atlantic Source Zone	-72.3206	19.9047	94.2	20	5
atsz–58a	Atlantic Source Zone	-73.1580	19.4498	84.34	20	22.1
atsz–58b	Atlantic Source Zone	-73.2022	19.8698	84.34	20	5
atsz–59a	Atlantic Source Zone	-74.3567	20.9620	259.7	20	22.1
atsz–59b	Atlantic Source Zone	-74.2764	20.5467	259.7	20	5
atsz–60a	Atlantic Source Zone	-75.2386	20.8622	264.2	15	17.94
atsz–60b	Atlantic Source Zone	-75.1917	20.4306	264.2	15	5
atsz–61a	Atlantic Source Zone	-76.2383	20.7425	260.7	15	17.94
atsz–61b	Atlantic Source Zone	-76.1635	20.3144	260.7	15	5
atsz–62a	Atlantic Source Zone	-77.2021	20.5910	259.9	15	17.94
atsz–62b	Atlantic Source Zone	-77.1214	20.1638	259.9	15	5
atsz–63a	Atlantic Source Zone	-78.1540	20.4189	259	15	17.94
atsz–63b	Atlantic Source Zone	-78.0661	19.9930	259	15	5
atsz–64a	Atlantic Source Zone	-79.0959	20.2498	259.2	15	17.94
atsz–64b	Atlantic Source Zone	-79.0098	19.8236	259.2	15	5
atsz–65a	Atlantic Source Zone	-80.0393	20.0773	258.9	15	17.94
atsz–65b	Atlantic Source Zone	-79.9502	19.6516	258.9	15	5
atsz–66a	Atlantic Source Zone	-80.9675	19.8993	258.6	15	17.94
atsz–66b	Atlantic Source Zone	-80.8766	19.4740	258.6	15	5
atsz–67a	Atlantic Source Zone	-81.9065	19.7214	258.5	15	17.94

Continued on next page

Table B.1 – continued from previous page

Segment	Description	Longitude(°E)	Latitude(°N)	Strike(°)	Dip(°)	Depth (km)
atsz–67b	Atlantic Source Zone	-81.8149	19.2962	258.5	15	5
atsz–68a	Atlantic Source Zone	-87.8003	15.2509	62.69	15	17.94
atsz–68b	Atlantic Source Zone	-88.0070	15.6364	62.69	15	5
atsz–69a	Atlantic Source Zone	-87.0824	15.5331	72.73	15	17.94
atsz–69b	Atlantic Source Zone	-87.2163	15.9474	72.73	15	5
atsz–70a	Atlantic Source Zone	-86.1622	15.8274	70.64	15	17.94
atsz–70b	Atlantic Source Zone	-86.3120	16.2367	70.64	15	5
atsz–71a	Atlantic Source Zone	-85.3117	16.1052	73.7	15	17.94
atsz–71b	Atlantic Source Zone	-85.4387	16.5216	73.7	15	5
atsz–72a	Atlantic Source Zone	-84.3470	16.3820	69.66	15	17.94
atsz–72b	Atlantic Source Zone	-84.5045	16.7888	69.66	15	5
atsz–73a	Atlantic Source Zone	-83.5657	16.6196	77.36	15	17.94
atsz–73b	Atlantic Source Zone	-83.6650	17.0429	77.36	15	5
atsz–74a	Atlantic Source Zone	-82.7104	16.7695	82.35	15	17.94
atsz–74b	Atlantic Source Zone	-82.7709	17.1995	82.35	15	5
atsz–75a	Atlantic Source Zone	-81.7297	16.9003	79.86	15	17.94
atsz–75b	Atlantic Source Zone	-81.8097	17.3274	79.86	15	5
atsz–76a	Atlantic Source Zone	-80.9196	16.9495	82.95	15	17.94
atsz–76b	Atlantic Source Zone	-80.9754	17.3801	82.95	15	5
atsz–77a	Atlantic Source Zone	-79.8086	17.2357	67.95	15	17.94
atsz–77b	Atlantic Source Zone	-79.9795	17.6378	67.95	15	5
atsz–78a	Atlantic Source Zone	-79.0245	17.5415	73.61	15	17.94
atsz–78b	Atlantic Source Zone	-79.1532	17.9577	73.61	15	5
atsz–79a	Atlantic Source Zone	-78.4122	17.5689	94.07	15	17.94
atsz–79b	Atlantic Source Zone	-78.3798	18.0017	94.07	15	5
atsz–80a	Atlantic Source Zone	-77.6403	17.4391	103.3	15	17.94
atsz–80b	Atlantic Source Zone	-77.5352	17.8613	103.3	15	5
atsz–81a	Atlantic Source Zone	-76.6376	17.2984	98.21	15	17.94
atsz–81b	Atlantic Source Zone	-76.5726	17.7278	98.21	15	5
atsz–82a	Atlantic Source Zone	-75.7299	19.0217	260.1	15	17.94
atsz–82b	Atlantic Source Zone	-75.6516	18.5942	260.1	15	5
atsz–83a	Atlantic Source Zone	-74.8351	19.2911	260.8	15	17.94
atsz–83b	Atlantic Source Zone	-74.7621	18.8628	260.8	15	5
atsz–84a	Atlantic Source Zone	-73.6639	19.2991	274.8	15	17.94
atsz–84b	Atlantic Source Zone	-73.7026	18.8668	274.8	15	5
atsz–85a	Atlantic Source Zone	-72.8198	19.2019	270.6	15	17.94
atsz–85b	Atlantic Source Zone	-72.8246	18.7681	270.6	15	5
atsz–86a	Atlantic Source Zone	-71.9143	19.1477	269.1	15	17.94
atsz–86b	Atlantic Source Zone	-71.9068	18.7139	269.1	15	5
atsz–87a	Atlantic Source Zone	-70.4738	18.8821	304.5	15	17.94
atsz–87b	Atlantic Source Zone	-70.7329	18.5245	304.5	15	5
atsz–88a	Atlantic Source Zone	-69.7710	18.3902	308.9	15	17.94
atsz–88b	Atlantic Source Zone	-70.0547	18.0504	308.4	15	5
atsz–89a	Atlantic Source Zone	-69.2635	18.2099	283.9	15	17.94
atsz–89b	Atlantic Source Zone	-69.3728	17.7887	283.9	15	5
atsz–90a	Atlantic Source Zone	-68.5059	18.1443	272.9	15	17.94
atsz–90b	Atlantic Source Zone	-68.5284	17.7110	272.9	15	5
atsz–91a	Atlantic Source Zone	-67.6428	18.1438	267.8	15	17.94
atsz–91b	Atlantic Source Zone	-67.6256	17.7103	267.8	15	5
atsz–92a	Atlantic Source Zone	-66.8261	18.2536	262	15	17.94
atsz–92b	Atlantic Source Zone	-66.7627	17.8240	262	15	5

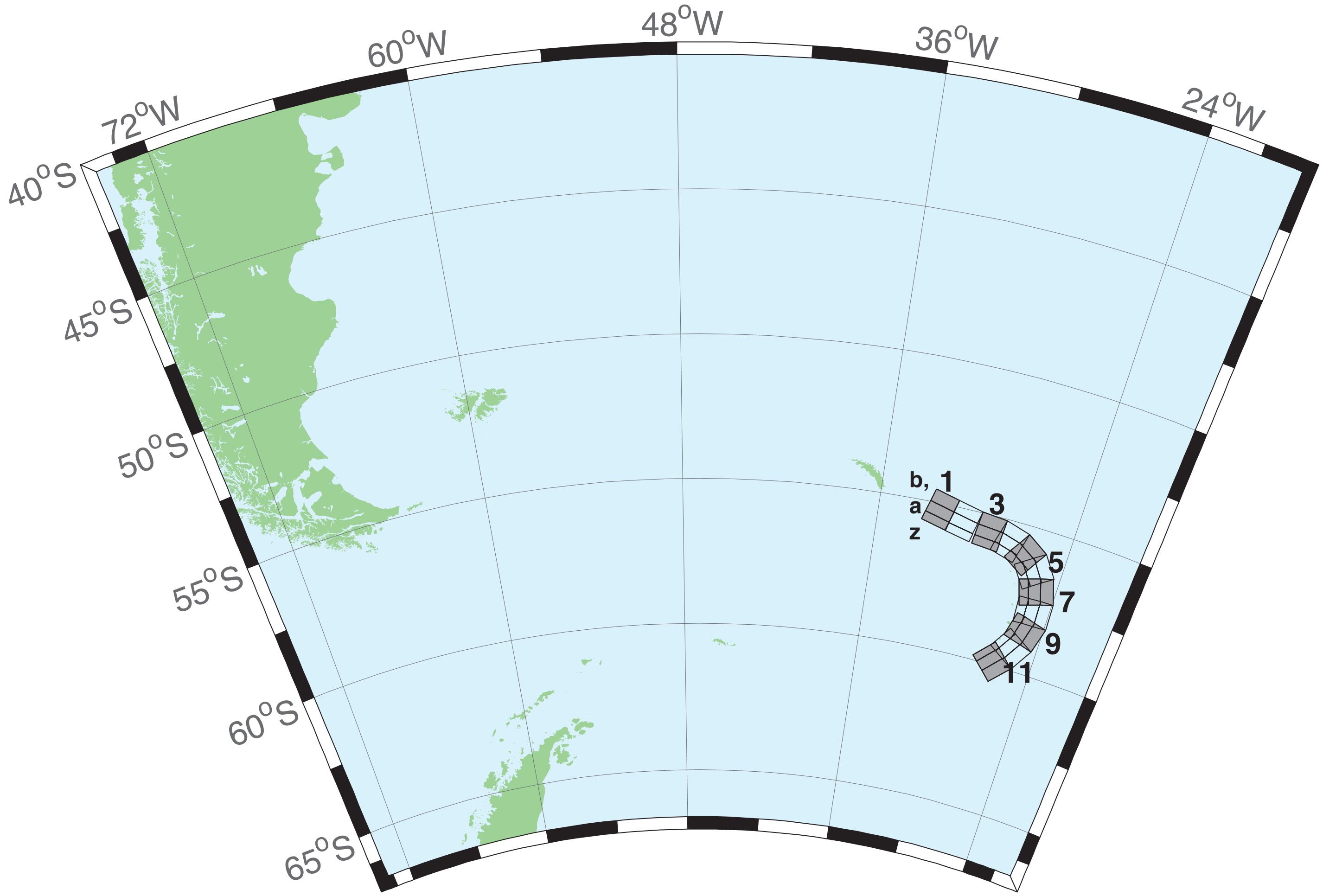

Figure B.2: South Sandwich Islands Subduction Zone.

Table B.2: Earthquake parameters for South Sandwich Islands Subduction Zone unit sources.

Segment	Description	Longitude(°E)	Latitude(°N)	Strike(°)	Dip(°)	Depth (km)	
sssz–1a	South Sandwich Islands Subduction Zone	-32.3713	-55.4655	104.7	28.53	17.51	
sssz–1b	South Sandwich Islands Subduction Zone	-32.1953	-55.0832	104.7	9.957	8.866	
sssz–1z	South Sandwich Islands Subduction Zone	-32.5091	-55.7624	104.7	46.99	41.39	
sssz–2a	South Sandwich Islands Subduction Zone	-30.8028	-55.6842	102.4	28.53	17.51	
sssz–2b	South Sandwich Islands Subduction Zone	-30.6524	-55.2982	102.4	9.957	8.866	
sssz–2z	South Sandwich Islands Subduction Zone	-30.9206	-55.9839	102.4	46.99	41.39	
sssz–3a	South Sandwich Islands Subduction Zone	-29.0824	-55.8403	95.53	28.53	17.51	
sssz–3b	South Sandwich Islands Subduction Zone	-29.0149	-55.4468	95.53	9.957	8.866	
sssz–3z	South Sandwich Islands Subduction Zone	-29.1353	-56.1458	95.53	46.99	41.39	
sssz–4a	South Sandwich Islands Subduction Zone	-27.8128	-55.9796	106.1	28.53	17.51	
sssz–4b	South Sandwich Islands Subduction Zone	-27.6174	-55.5999	106.1	9.957	8.866	
sssz–4z	South Sandwich Islands Subduction Zone	-27.9659	-56.2744	106.1	46.99	41.39	
sssz–5a	South Sandwich Islands Subduction Zone	-26.7928	-56.2481	123.1	28.53	17.51	
sssz–5b	South Sandwich Islands Subduction Zone	-26.4059	-55.9170	123.1	9.957	8.866	
sssz–5z	South Sandwich Islands Subduction Zone	-27.0955	-56.5052	123.1	46.99	41.39	
sssz–6a	South Sandwich Islands Subduction Zone	-26.1317	-56.6466	145.6	23.28	16.11	
sssz–6b	South Sandwich Islands Subduction Zone	-25.5131	-56.4133	145.6	9.09	8.228	
sssz–6z	South Sandwich Islands Subduction Zone	-26.5920	-56.8194	145.6	47.15	35.87	
sssz–7a	South Sandwich Islands Subduction Zone	-25.6787	-57.2162	162.9	21.21	14.23	
sssz–7b	South Sandwich Islands Subduction Zone	-24.9394	-57.0932	162.9	7.596	7.626	
sssz–7z	South Sandwich Islands Subduction Zone	-26.2493	-57.3109	162.9	44.16	32.32	
sssz–8a	South Sandwich Islands Subduction Zone	-25.5161	-57.8712	178.2	20.33	15.91	
sssz–8b	South Sandwich Islands Subduction Zone	-24.7233	-57.8580	178.2	8.449	8.562	
sssz–8z	South Sandwich Islands Subduction Zone	-26.1280	-57.8813	178.2	43.65	33.28	
sssz–9a	South Sandwich Islands Subduction Zone	-25.6657	-58.5053	195.4	25.76	15.71	
sssz–9b	South Sandwich Islands Subduction Zone	-24.9168	-58.6127	195.4	8.254	8.537	
sssz–9z	South Sandwich Islands Subduction Zone	-26.1799	-58.4313	195.4	51.69	37.44	
sssz–10a	South Sandwich Islands Subduction Zone	-26.1563	-59.1048	212.5	32.82	15.65	
sssz–10b	South Sandwich Islands Subduction Zone	-25.5335	-59.3080	212.5	10.45	6.581	
sssz–10z	South Sandwich Islands Subduction Zone	-26.5817	-58.9653	212.5	54.77	42.75	
sssz–11a	South Sandwich Islands Subduction Zone	-27.0794	-59.6799	224.2	33.67	15.75	
sssz–11b	South Sandwich Islands Subduction Zone	-26.5460	-59.9412	224.2	11.32	5.927	
sssz–11z	South Sandwich Islands Subduction Zone	-27.4245	-59.5098	224.2	57.19	43.46	

Appendix C SIFT Testing Report

Key West, Florida

Lindsey Wright
Liujuan Tang

1.0 PURPOSE

Forecast models are tested with synthetic tsunami events covering a range of tsunami source locations and magnitudes. Testing is also done with selected historical tsunami events when available.

The purpose of forecast model testing is three-fold. The first objective is to assure that the results obtained with the NOAA's tsunami forecast system software, which has been released to the Tsunami Warning Centers for operational use, are consistent with those obtained by the researcher during the development of the forecast model. The second objective is to test the forecast model for consistency, accuracy, time efficiency, and quality of results over a range of possible tsunami locations and magnitudes. The third objective is to identify bugs and issues in need of resolution by the researcher who developed the Forecast Model or by the forecast system software development team before the next version release to NOAA's two Tsunami Warning Centers.

Local hardware and software applications, and tools familiar to the researcher(s), are used to run the Method of Splitting Tsunamis (MOST) model during the forecast model development. The test results presented in this report lend confidence that the model performs as developed and produces the same results when initiated within the forecast system application in an operational setting as those produced by the researcher during the forecast model development. The test results assure those who rely on the Savannah tsunami forecast model that consistent results are produced irrespective of system.

2.0 TESTING PROCEDURE

The general procedure for forecast model testing is to run a set of synthetic tsunami scenarios and a selected set of historical tsunami events through the forecast system application and compare the results with those obtained by the researcher during the forecast model development and presented in the Tsunami Forecast Model Report. Specific steps taken to test the model include:

1. Identification of testing scenarios, including the standard set of synthetic events, appropriate historical events, and customized synthetic scenarios that may have been used by the researcher(s) in developing the forecast model.
2. Creation of new events to represent customized synthetic scenarios used by the researcher(s) in developing the forecast model, if any.
3. Submission of test model runs with the forecast system, and export of the results from A, B, and C grids, along with time series.
4. Recording applicable metadata, including the specific forecast system version used for testing.
5. Examination of forecast model results for instabilities in both time series and plot results.
6. Comparison of forecast model results obtained through the forecast system with those obtained during the forecast model development.
7. Summarization of results with specific mention of quality, consistency, and time efficiency.
8. Reporting of issues identified to modeler and forecast system software development team.
9. Retesting the forecast models in the forecast system when reported issues have been addressed or explained.

Synthetic model runs were tested on a DELL PowerEdge R510 computer equipped with two Xeon E5670 processors at 2.93 GHz, each with 12 MBytes of cache and 32GB memory. The processors are hex core and support hyperthreading, resulting in the computer performing as a 24 processor core machine. Additionally, the testing computer supports 10 Gigabit Ethernet for fast network connections. This computer configuration is similar or the same as the configurations of the computers installed at the Tsunami Warning Centers so the compute times should only vary slightly.

3.0 Results

The Key West forecast model was tested with SIFT version 3.2. The same version of propagation database was used during model development.

The Key West, Florida forecast model was tested with three synthetic scenarios. Test results from the forecast system and comparisons with the results obtained during the forecast model development are shown numerically in Table C1 and graphically in Figures C1 to C3. The results show that the minimum and maximum amplitudes and time series obtained from the forecast system agree with those obtained during the forecast model development, and that the forecast model is stable and robust, with consistent and high quality results across geographically distributed tsunami sources. The model run time (wall clock time) was less than 8.9 minutes for 14.9 hours of simulation time, and less than 2.36 minutes for 4.0 hours. This run time is within the 10 minute run time for 4 hours of simulation time and satisfies run time requirements.

A suite of three synthetic events was run on the Key West forecast model. The modeled scenarios were stable for all cases run with no inconsistencies or ringing. The largest modeled height was 45 centimeters (cm) from the Atlantic (ATSZ 48-57) source zone. The smallest signal of 2 cm was recorded at the far field South Sandwich (SSSZ 1-10) source zone and was 0.8 cm less than the maximum during development. Comparisons between the development cases and the forecast system output were consistent in shape and amplitude for all cases run. The Key West reference point used for the forecast model development is the same as what is deployed in the forecast system, so the results can be considered valid for the three cases studied.

Table C1. Table of maximum and minimum amplitudes (cm) at the Key West, Florida warning point for synthetic and historical events tested using SIFT 3.2 and obtained during development.

Scenario Name	Source Zone	Tsunami Source	α [m]	SIFT Max (cm)	Development Max (cm)	SIFT Min (cm)	Development Min (cm)
Mega-tsunami Scenarios							
ATSZ 38-47	Atlantic	A38-A47, B38-B47	25	15.5	16	-11.1	-11
ATSZ 48-57	Atlantic	A48-A57, B48-B57	25	44.8	45	-42.1	-42
SSSZ 1-10	South Sandwich	A1-A10, B1-B10	25	2.0	2.8	-1.7	-1.8

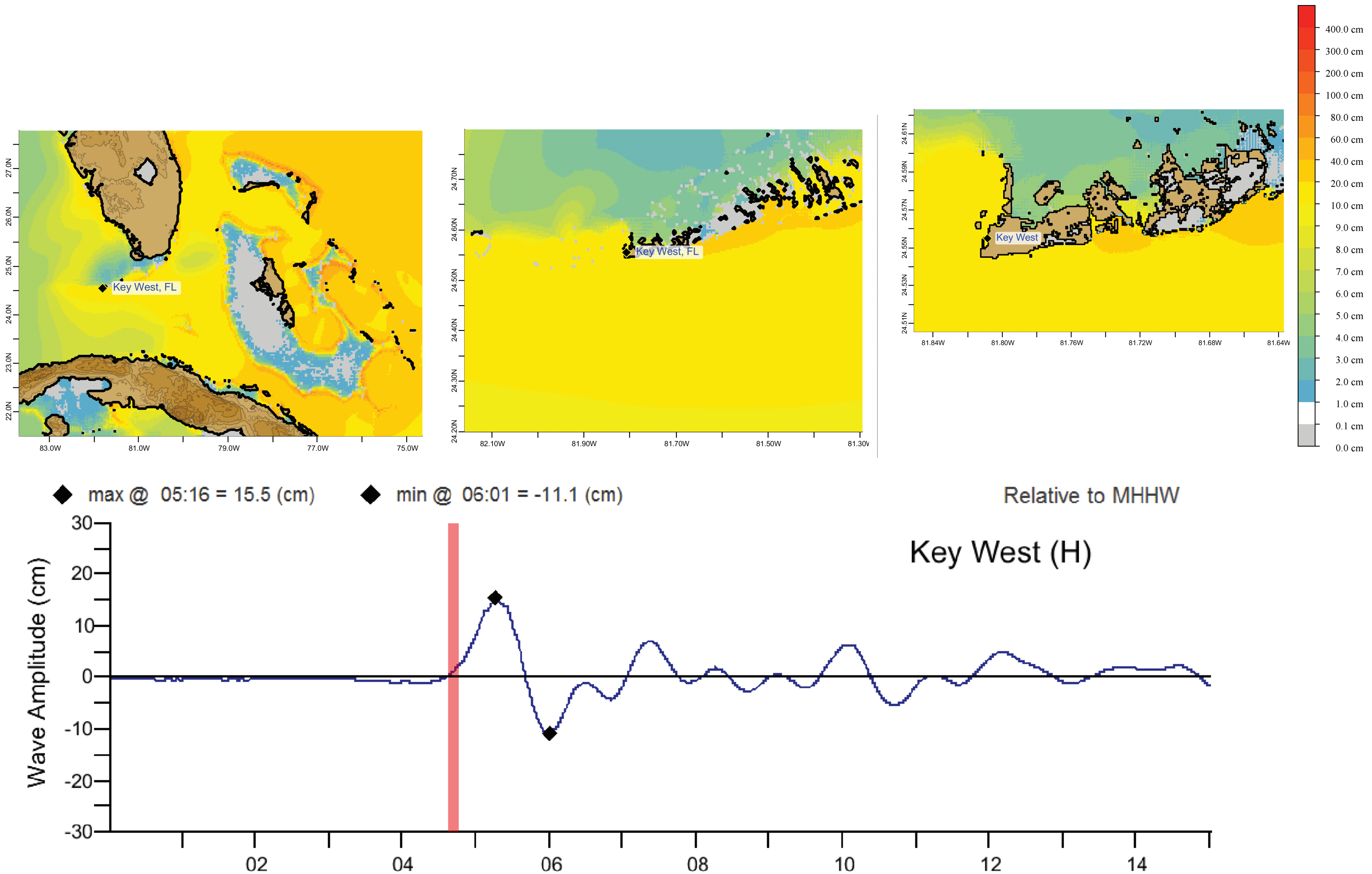

Figure C1: Response of the Key West forecast model to synthetic scenario ATSZ 38-47 (alpha=25). Maximum sea surface elevation for (a) A-grid, (b) B-grid, (c) C-grid. (d) Sea surface elevation time series at the C-grid warning point.

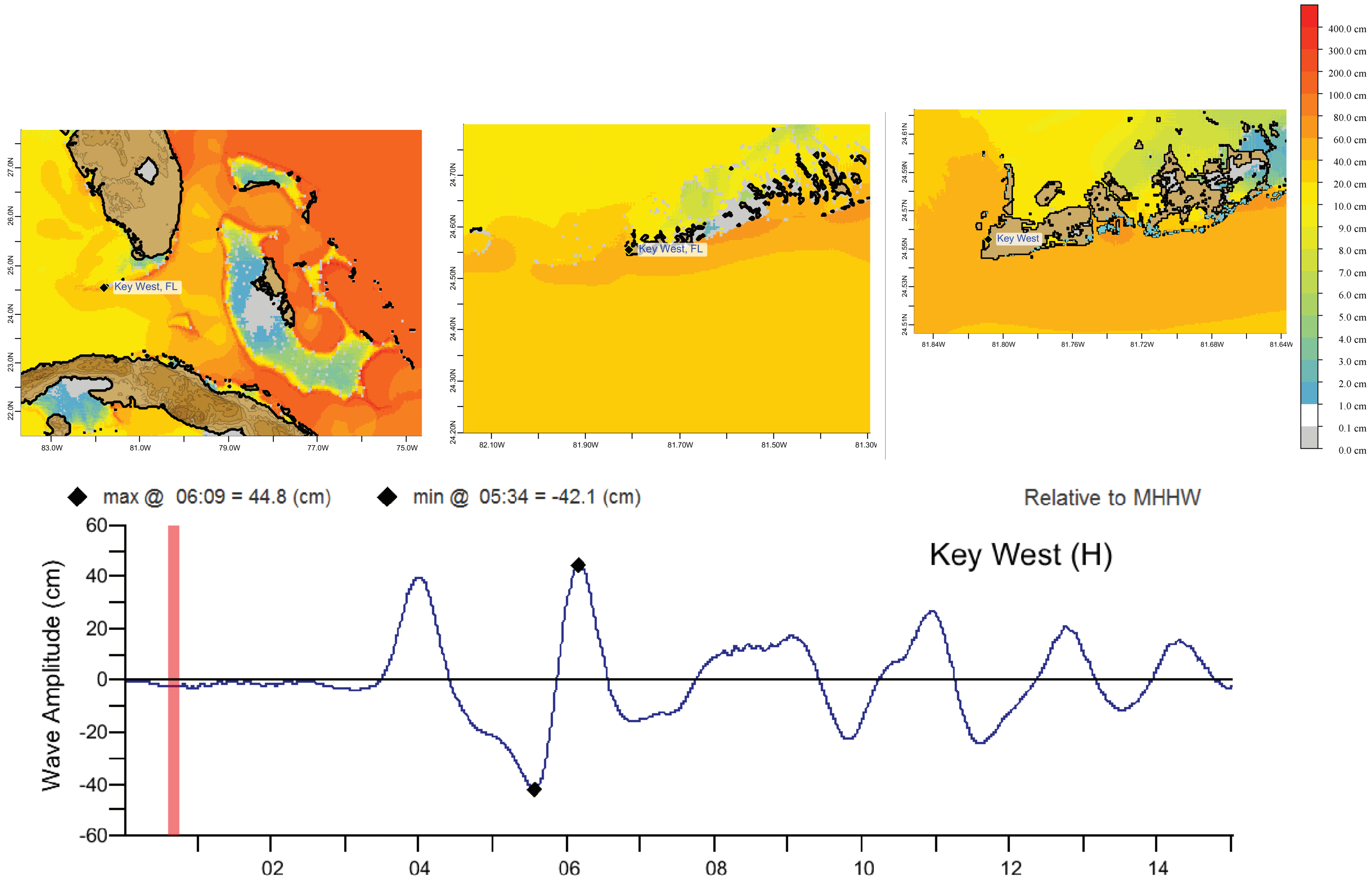

Figure C2: Response of the Key West forecast model to synthetic scenario ATSZ 48-57 (alpha=25). Maximum sea surface elevation for (a) A-grid, (b) B-grid, (c) C-grid. (d) Sea surface elevation time series at the C-grid warning point.

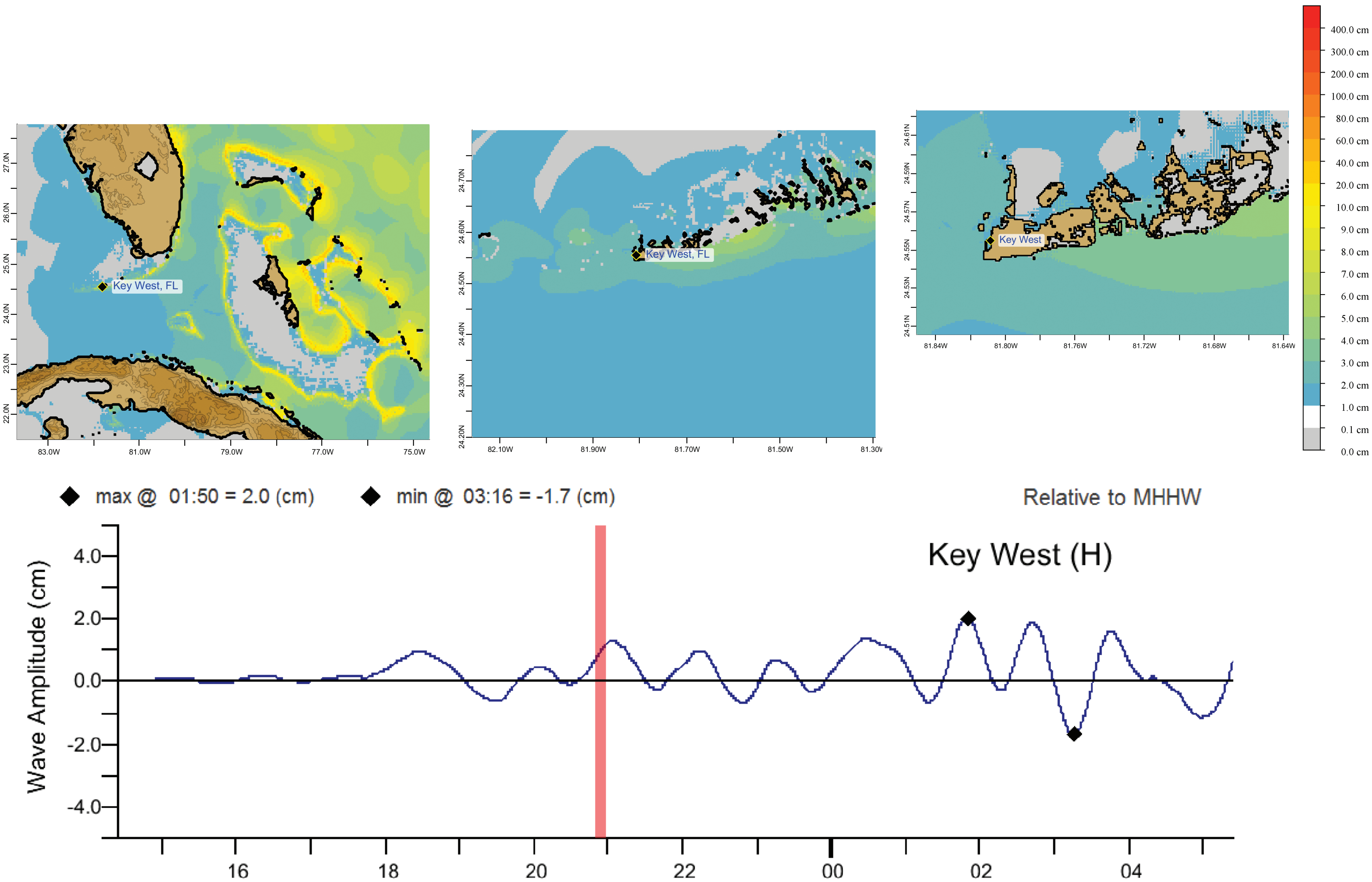

Figure C3: Response of the Key West forecast model to synthetic scenario SSSZ 1-10 (alpha=25). Maximum sea surface elevation for (a) A-grid, (b) B-grid, (c) C-grid. (d) Sea surface elevation time series at the C-grid warning point.